INTERMEDIATE- TO DEEP-WATER CIRCULATION CHANGES ON SHORT AND LONG TIME SCALES

A Dissertation

by

DANIEL PATRICK MURPHY

Submitted to the Office of Graduate Studies of
Texas A&M University
in partial fulfillment of the requirements for the degree of

DOCTOR OF PHILOSOPHY

May 2010

Major Subject: Oceanography

INTERMEDIATE- TO DEEP-WATER CIRCULATION CHANGES ON SHORT AND LONG TIME SCALES

A Dissertation

by

DANIEL PATRICK MURPHY

Submitted to the Office of Graduate Studies of
Texas A&M University
in partial fulfillment of the requirements for the degree of

DOCTOR OF PHILOSOPHY

Approved by:

Chair of Committee,	Deborah J. Thomas
Committee Members,	Alejandro Orsi
	Mitchell W. Lyle
	Franco Marcantonio
Head of Department,	Piers Chapman

May 2010

Major Subject: Oceanography

ABSTRACT

Intermediate- to Deep-Water Circulation Changes on Short and Long Time Scales.

(May 2010)

Daniel Patrick Murphy, B.S., Hawai'i Pacific University;

M.S., University of California, Santa Barbara

Chair of Advisory Committee: Dr. Deborah Thomas

Oceanic circulation remains one of the poorly understood elements of the global climate system, despite its importance to planetary heat redistribution and carbon cycling. The nature of deep-water formation and circulation in ancient oceans are even more poorly constrained. In order to understand climate dynamics of past and future climates we must have a better understanding of the role of deep-ocean circulation.

In this dissertation I investigated changes in intermediate- to deep-water circulation in three different ocean basins during two different geologic eras. The first study focused on the late Pleistocene (~25 – 60 ka) California margin to investigate the role of intermediate water circulation in abrupt climate fluctuations. The other two studies investigated deep-water circulation during the Late Cretaceous (~70 – 100 Ma) greenhouse interval, to determine if deep waters formed in the southern Indian or Atlantic basins.

The above studies employed neodymium isotopes preserved in biogenic apatite (fish teeth and bones) and foraminiferal calcite to reconstruct the provenance of

intermediate- to deep-water masses. Here I present data from two sites located at intermediate depths on the late Pleistocene California margin as well as seven Deep Sea Drilling Project and Ocean Drilling Program Cretaceous aged sites; four in the South Atlantic Ocean, and three in the Indian Ocean.

The new Pleistocene data rule out changes in the source of intermediate waters to the California margin, thus the recorded changes in seafloor oxygenation were caused by changes in sea surface productivity. In the Cretaceous, the spread of deep waters formed in the high-latitude South Atlantic was hindered by tectonic barriers until the mid Campanian when the subduction of Rio Grande Rise allowed for the continuous flow of deep waters from the Southern Ocean into the North Atlantic. The deep Cretaceous Indian Ocean was filled with deep waters formed in the high-latitude Indian Ocean, until being replaced with waters sourced in the Pacific from the late Cenomanian to early Campanian before a return to southern Indian-sourced waters for the remainder of the study interval.

For Jonna

Patience has never known fewer limits

ACKNOWLEDGEMENTS

I would like to thank everyone in the Department of Oceanography at Texas A&M University (TAMU). The faculty and staff, graduate students, and even the occasional undergraduate made the experience one to remember.

The biggest thanks go to my advisor, Debbie Thomas, who believed I could make it, even when I didn't. I learned more from her than I think either of us expected (or even realize right now), and I like to think that we learned together. The rest of my committee (Mitch Lyle, Franco Marcantonio, and Alex Orsi) provided valuable conversation, without which I am not sure I would have figured out any of the following dissertation. I owe them thanks for their advice and guidance throughout my time here.

A special thank you goes to Stella Woodard and Niall Slowey, for hundreds of hours of conversations that may not have made it into this dissertation, but contributed to my understanding of the world into which my work fits. For discussions as varied as changing lunar orbits, the kinetics of iron in anaerobic seas, and why it will all be okay, thank you.

I didn't get here on my own, and many people helped me along the way. In no particular order, thank you to: Drew Coleman at University of North Carolina-Chapel Hill for allowing me use of his lab when I was just getting started, Brent Miller at TAMU for seemingly constant guidance and trouble shooting, Jim Kennett at University of California-Santa Barbara for helping me through my masters, and Karen Thompson for helping me wrangle Jim.

Finally, thank you to my parents for supporting my career path when I didn't know what it was. I could not have done it if it were not for your support and your pride. I hope I continue to make you proud. My sisters may not understand why I would want to continue in school, and were always there to try to take me down a few pegs, but they always tried to be interested and it was appreciated. My wife, Jonna, has proven that nothing is more supportive than love; and she never ran out of support. From caring for our child while pregnant during my two months at sea last summer, to making me sloppy joes and tater tots for dinner on my rough days, you always did everything you could to help. I owe you eternal thanks. Last, but not least, my kids Autumn and Isaac may not know or care what I do, but getting to see them at the end of everyday is the best feeling anyone can have, and made me want to be my best. One day you guys may read this (probably not) and I want you to know how much I appreciate and love you everyday.

NOMENCLATURE

Units

Å	Angstroms
Ka / Ma	Thousand years ago / Million years ago
Kyr / Myr	Thousand years / Million years
mbsf	meters below sea floor
ppm	parts per million
ppt	parts per thousand
psu	practical salinity units

Elements

Nd	Neodymium
Sm	Samarium
Sr	Strontium
REE	Rare Earth Element

Water masses

AABW	Antarctic Bottom Water
AAIW	Antarctic Intermediate Water
CDW	Circumpolar Deep Water
NADW	North Atlantic Deep Water
NPIW	North Pacific Intermediate Water
SCW	Southern Component Water

SPMW	South Pacific Mode Water
WSBW	Warm Saline Bottom Water

Miscellaneous

CAG	Central Atlantic Gateway
DSDP	Deep Sea Drilling Project
IODP	Integrated Ocean Drilling Program
LIP	Large Igneous Province
MIS	Marine Isotope Stage
OAE	Oceanic Anoxic Event
ODP	Ocean Drilling Program
SST	Sea Surface Temperature

TABLE OF CONTENTS

CHAPTER Page

LIST OF FIGURES

FIGURE Page

LIST OF TABLES

CHAPTER I

INTRODUCTION TO INTERMEDIATE- TO DEEP-WATER CIRCULATION CHANGES ON SHORT AND LONG TIME SCALES

Ocean circulation plays a crucial role in modulating the Earth's climate. Our current lack of understanding of changes in density-driven circulation in the past inhibit our ability to project future changes. The following three chapters detail studies on changes in oceanic circulation on different time scales (few hundred year resolution, few hundred thousand year resolution) in different ocean basins (Pacific, South Atlantic, Indian Oceans) during different intervals of geologic time (late Pliestocene, Late Cretaceous). This chapter introduces the background behind all three studies and establishes the method used throughout.

1. Introduction

Global climate is controlled directly by the uneven distribution of solar radiation. The temperature gradient between the tropics and the polar regions dictates the pattern and intensity of global wind fields and also impacts the characteristics of the surface ocean. Salinity in the ocean is largely controlled by the precipitation distribution, with lower salinities in the equatorial regions and more saline subtropics.

This dissertation follows the style of Quaternary Science Reviews.

On a rocky planet without oceans or an atmosphere, the tropics would be extremely warm and the poles extremely cold with a sharp temperature gradient by latitude. However, the meridional temperature gradient is moderated through redistribution of heat from the tropical regions to the high latitudes in part by surface ocean circulation, with an oceanic contribution of ~20-50% (Carissimo et al., 1985; Trenberth and Caron, 2001). For example, poleward flowing western boundary currents carry warm, tropical waters to the high latitudes where heat is released to the atmosphere. The cooled waters then flow back to the equator as eastern boundary currents where they in turn absorb more heat in the tropics to renew the cycle.

1.1. Thermohaline circulation

In addition to surface ocean circulation, the flow of deep-waters also contributes to the redistribution of tropical heat. Surface water sinking draws warm surface waters across the Polar Front, allowing tropically derived waters transported by Gulf Stream/North Atlantic Drift to flow to higher latitudes and hence release more heat to the atmosphere than they would have been able to in normal gyre circulation. Generally speaking, warm and relatively saline surface waters sourced in the Caribbean are transported to the North Atlantic where they cool, become denser and sink to depth as North Atlantic Deep Water (NADW). This water-mass flows southward along the bottom of the North Atlantic until it encounters the colder, denser Antarctic Bottom Water (AABW). NADW is then forced upward over AABW and incorporated into the Antarctic Circumpolar Current where it is mixed with AABW and becomes part of

Circumpolar Deep Water (CDW) before flowing north into both the deep Indian and Pacific basins.

Thermohaline circulation is also the only mechanism by which the abyssal ocean is ventilated. In poorly ventilated basins, carbon is more efficiently buried and removed from the actively exchanging reservoirs of the global carbon cycle, whereas well-ventilated basins result in quicker oxidation of organic carbon, returning the carbon to the ocean/atmosphere. This process has a strong control on whether the oceans are a net source or sink of atmospheric carbon, which has been suggested as an explanation for natural variations in atmospheric CO_2 over the last several glacial cycles.

1.2. The world during Marine Isotope Stage 3

Oceanic and atmospheric boundary conditions were different during the time interval identified in foraminiferal oxygen isotope records as Marine Isotope Stage 3 (MIS 3; ~25-60 ka), though the paleogeographic locations of the continents were the same as today. The existence of large continental ice sheets in the Northern Hemisphere depressed sea level 60 meters below the modern level (e.g. Linsley, 1996; Waelbroeck et al., 2002; Arz et al., 2007; Rohling et al., 2008). This caused the exposure of the Sunda Shelf in Indonesia, the narrowing of the Florida Straits (a primary gateway of the Gulf Stream upon its exit from the Gulf of Mexico), the isolation of a number of basins with shallow sills from the ocean (e.g. Cariaco Basin), among other effects. Deep-water production in the North Atlantic diminished, creating a Glacial North Atlantic Intermediate Water rather than NADW. Worldwide, sea surface temperatures were lower and global winds were stronger.

Throughout MIS 3 climate was inherently unstable (e.g. Dansgaard et al., 1993; Kennett and Venz, 1995). Between ~25-60 ka there were 15 abrupt climatic oscillations, each lasting from <100 years to >3000 years (Dansgaard et al., 1993). In the Greenland ice cores, these events are referred to as Dansgaard/Oeschger cycles; in the marine realm they are referred to as stadial/interstadial cycles. The stadial/interstadial changes occurred globally, with changes ranging from temperature and precipitation to phytoplanktonic productivity (e.g. Dansgaard et al., 1993; Kennett and Venz, 1995; Wang et al., 2001; Pospelova et al., 2006).

In the subtropical eastern North Pacific, interstadials are characterized by increases in sea surface temperature (Kennett and Venz, 1995; Hendy and Kennett, 1999) and primary productivity (Ortiz et al., 2004; Pospelova et al., 2006) as well as diminished dissolved oxygen levels at intermediate water depths (~500 – 1000 m) on the continental margins (Behl and Kennett, 1996; Cannariato et al., 1999). Stadials, on the other hand, are characterized by cooler SSTs, lower primary productivity and greater oxygen concentrations at intermediate depths on the seafloor.

To explain the changes in seafloor oxygenation along the California margin, two competing hypotheses emerged. One hypothesis invokes increased primary productivity at the sea surface reducing oxygen levels at the seafloor via oxidation of organic matter during interstadials (e.g. Ortiz et al., 2004). The second hypothesis calls for a change in intermediate water circulation, in which a younger, relatively oxygen-rich stadial water mass is replaced with an older, less oxygenated water mass during the interstadials (Behl

and Kennett, 1996; Hendy and Kennett, 2003). Distinguishing between these two hypotheses is the subject of Chapter II.

The relative role of surface water productivity versus intermediate water ventilation has important implications for global climate. If seafloor oxygenation levels were primarily controlled by changes in phytoplankton productivity, then changes in California margin productivity would be tightly coupled to global climate change. If instead, changes in intermediate water circulation controlled seafloor oxygenation, the changes also would likely have impacted heat balance in the Pacific linking such changes to global climate.

1.3. The world of the mid-Late Cretaceous (Cenomanian-Campanian)

The tectonic configuration of the oceans during the mid-Late Cretaceous (~70-100 Ma) was different from today (Figure 1 – 1). By 100 Ma, Gondwana and Laurasia had separated, forming a circum-equatorial oceanic passage. Within the Indian and Atlantic this equatorial body is referred to as the Tethyan Seaway. The North American margin rifted from the African margin during the Late Jurassic , forming the North Atlantic (e.g. Barron et al., 1981; Scotese, 1991), though North America remained attached to Greenland and Scandanavia north of ~46°N (Hay et al., 1999). Iberia began rifting from Newfoundland in the late Jurassic, and seafloor spreading began near the Aptian/Albian boundary (112.0 Ma; Tucholke and Sibuet, 2007). A narrow (<200 km) epicontinental seaway between Norway and Greenland connected surface waters between the North Atlantic and the Arctic (Hay et al., 1999; Mutterlose et al., 2003), though Gradstein et al. (1999) suggested a mid-bathyal connection to the North Atlantic by the Campanian. The

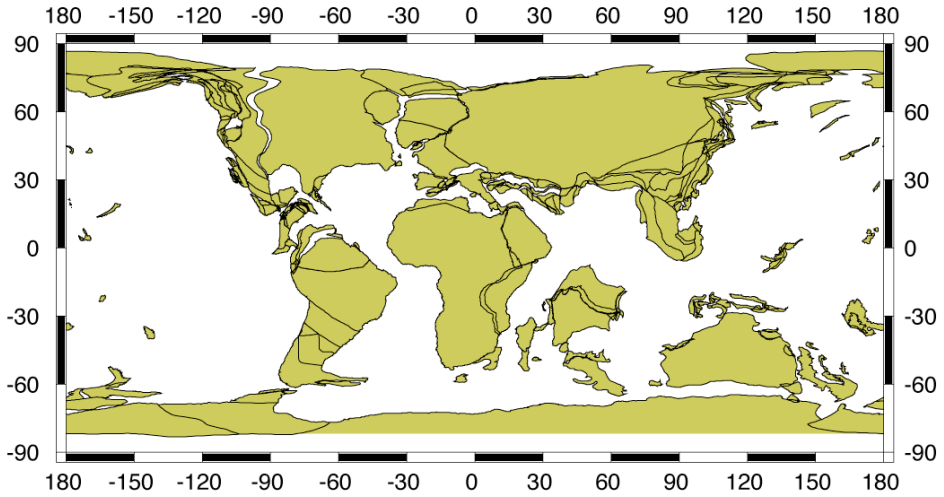

75.0 Ma Reconstruction

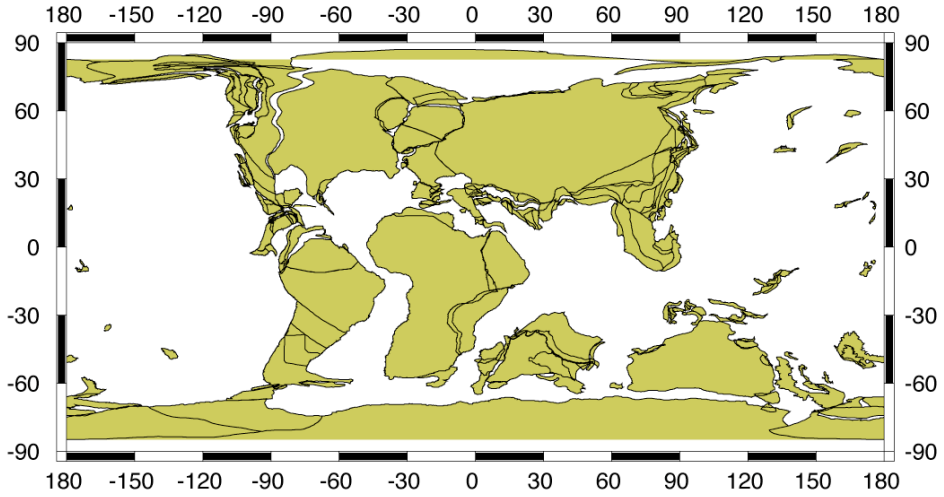

95.0 Ma Reconstruction

Figure 1-1. Paleogeographic reconstructions (Ocean Drilling Stratigraphic Network; http://www.odsn.de) of the late Campanian (~75Ma) and late Cenomanian (~95Ma). Boundaries are continental boundaries, not coastal boundaries.

Labrador Sea began rifting during the Aptian, and may have been open to upper bathyal depths by the Campanian (Hay et al., 1999). Opening of the South Atlantic completely separated Africa and South America, though it was a shallow and narrow ocean (Hay et al., 1999). Africa had separated from Antarctica, but a land bridge between Antarctica and Africa existed via the Kerguelen/India/Madagascar land mass (Hay et al., 1999). Australia and South America remained attached to Antarctica, preventing circumpolar circulation (e.g. Barron et al., 1981; Scotese, 1991; Hay et al., 1999).

Over the following ~30 Myr the South Atlantic widened, and the North Atlantic ocean began opening in the north as Greenland began separating from North America. India, Madagascar, and Kerguelen separated as India moved north toward Asia. The Drake and Tasmanian Passages remain closed through the Late Cretaceous.

The Cretaceous is referred to as a greenhouse climate interval, and the Turonian (89.3 – 93.5 Ma) was the warmest interval of the last 100 Myr of Earth's history. Atmospheric carbon dioxide levels during this interval were likely ~2-5 times higher than modern (e.g. Freeman and Hayes, 1992; Ekart et al., 1999; Royer et al., 2004; Berner, 2006). Sea surface temperatures were higher than any other time during the Mesozoic and Cenozoic, with tropical temperatures approaching 36°C (e.g. Pearson et al., 2001; Norris et al., 2002; Wilson et al., 2002). High latitude sea surface temperatures (SSTs) were correspondingly warm, with estimates ranging from ~20 – 32°C in the South Atlantic and South Indian (Huber et al., 1995; Huber and Hodell, 1996), although these high temperatures are questioned (Price et al., 1996). Deep-water temperatures reached 9°C – 12°C (Huber et al., 2002). Correspondingly, sea-ice

formation could not have formed in these conditions, prohibiting the high-latitude salinity increase caused by brine rejection as in the modern Southern Ocean.

The diminished meridional gradient is the "paradox" of the Cretaceous. The lower gradient implies more efficient movement of heat from the tropics to the poles, but would at the same time lead to decreased atmospheric and oceanic circulation. This led to proposals as varied as doubling density-driven ocean circulation (e.g. Barron et al., 1995) to enhanced polar heat transport via latent heat transport in the atmosphere (e.g. Hay and DeConto, 1999; Ufnar et al., 2004) to explain the paradox.

Despite lower than modern global salinity during the Late Cretaceous (Hay et al., 2006), the South Atlantic is inferred to have been much more saline than the modern basin (e.g. Brady et al., 1998; Hay and DeConto, 1999). During the Cretaceous, the Amazon River flowed to the Pacific Ocean and the Congo flowed to the Indian Ocean (Emery and Uchupi, 1984). With no major inputs of fresh water, the South Atlantic salinity gradients were probably similar to modern marginal seas such as the Red or Mediterranean Seas. Surface salinities of 39.5 psu in Angola Basin (Brady et al., 1998) illustrate this fact.

The paleogeographic and hydrographic boundary conditions that existed during the mid- to Late Cretaceous likely impacted the manner in which the deep ocean basins were ventilated. The majority of the Cretaceous sedimentary record indicates that the deep oceans were well ventilated, with the exception of the Oceanic Anoxic Events (OAEs; discussed below), thus oxygenated waters must have circulated at depth. This may have occurred via thermohaline circulation analogous to the modern system. However the

extreme warmth of Cretaceous deep waters led to the proposal of "halothermal circulation" (Brass et al., 1982), in which the densest waters formed by evaporation in low latitudes. Sinking of warm and saline waters in the Mediterranean and Red Seas contributes to the ventilation of the modern oceans at intermediate water depths.

However, during the Cretaceous, the existence of warm, saline deep waters may have been more significant, with possible convection in the northern South Atlantic (Brass et al., 1982). During the Cenomanian, the South Atlantic basin reached 3,000 km at its widest (Barron et al., 1981; Scotese, 1991; Hay et al., 1999), and as discussed above the surface waters were likely much more saline than the modern. This combination of a relatively restricted basin with saline surface waters suggests that convection of warm and saline waters was plausible.

Each circulation mode (thermohaline or halothermal; thermally driven or salinity driven, respectively) has a distinct impact on the global heat budget. The formation of deep-water in the high latitudes draws warm tropical waters to the poles where heat can be released to the atmosphere. The formation of deep-water in the tropics via halothermal circulation does not contribute to movement of surface waters or their heat to the poles. Before we can begin to understand the role of deep-ocean circulation in climate dynamics of the Cretaceous and other greenhouse intervals, we must first determine the mechanism by which deep-water formed.

In addition to contributing to our understanding of warm climate dynamics, establishing the mode of deep-ocean circulation during the Cretaceous will help test hypotheses proposed to explain the Oceanic Anoxic Events. While the global oceans

were well ventilated for most of the Cretaceous, three episodes of widespread oceanic anoxia - the Oceanic Anoxic Events (OAEs) - occurred. OAEs are characterized by laminated black shales rich in organic carbon, and are found throughout the ocean basins and inferred to have extended through the entire water column. One mechanism proposed to explain widespread anoxic conditions is that the deep oceans became stagnant through slowed deep-water circulation (e.g. Zimmerman et al., 1987). Slowed advection of deep waters would have diminished the rate of ventilation at the seafloor, enhancing the preservation of organic matter. Clearly we must first establish the mode of deep-ocean circulation before we can test this proposed mechanism.

To address the issue of how the deep oceans operated during the mid- to Late Cretaceous question we investigated deep-sea sediment cores from the South Atlantic (Chapter III) and Indian Oceans (Chapter IV) spanning the Cenomanian to Campanian.

2. Tracing Water Masses

2.1. Carbon isotopes

Modern water masses can be traced using conservative chemical (anthropogenic tracers) and physical (temperature, salinity) properties or semi-conservative isotopic tracers (carbon isotopes) that are retained or only slightly modified over great distances. Due to the difficulty of mixing across isopycnal boundaries, water masses tend to retain characteristics of the surface waters from which they formed. Changes to these inherited surface water characteristics occur relatively slowly via lateral mixing and water mass aging (such as the accumulation of inorganic carbon via organic matter oxidation).

In order to track the composition and circulation of ancient water masses, we must rely on proxies of ancient water mass properties recorded in the sedimentary record. Traditionally, paleoceanographers have used the ratio of ^{13}C to ^{12}C (hereafter referred to as $\delta^{13}C$; calculated as in equation 1)

$$\delta^{13}C = \left(\frac{\left({}^{13}C / {}^{12}C \right)_{Sample}}{\left({}^{13}C / {}^{12}C \right)_{Standard}} - 1 \right) \times 1000 \quad (1)$$

as a tracer of water mass aging (e.g. Curry and Lohmann, 1982). As deep water masses age, they accumulate ^{12}C from the oxidation of organic matter derived from surface waters, lowering the $\delta^{13}C$ ratio. The $\delta^{13}C$ of waters at the seafloor is recorded in the carbonate tests of benthic foraminifera, enabling reconstructions of water mass $\delta^{13}C$ at a particular location through time. Comparison of contemporaneous $\delta^{13}C$ values from numerous locations enables us to infer aspects of deep-water aging patterns.

However, geographic gradients in benthic $\delta^{13}C$ records are not uniquely determined by deep-water aging patterns, as other processes affect the carbon isotope composition of deep waters. Local surface productivity can alter the water mass signal locally (e.g. Charles et al., 1996; Rutberg and Peacock, 2006), which can be significant on productive continental margins and in restricted basins and seas. This process is different from the normal "aging" of a water mass, as the local signature does not reflect the whole water mass. In addition, changes in the global oceanic carbon budget also impact $\delta^{13}C$ values (Boyle, 1992), as can changes in local venting of hydrocarbons (Torres et al., 2003). These complications can be minimized when explaining the $\delta^{13}C$

record of a single site using other proxies and an understanding of the history of the site. However, comparing $\delta^{13}C$ records from sites of different depths, in fundamentally different settings when deep ocean circulation is almost entirely unconstrained is difficult.

Ideally we seek a tracer of ancient water masses that meets the following criteria: The tracer must 1) be relatively conservative, preserving its value without considerable vertical mixing or internal sources; 2) have a short oceanic residence time relative to oceanic mixing (i.e., less than 1500 years); 3) be recorded and preserved by a ubiquitous phase in the sedimentary record. For broad scale circulation patterns, one of the most useful tracers in this regard is the isotopic composition of neodymium.

2.2. Neodymium systematics

Neodymium (Nd) is a light Rare Earth Element (REE). Nd has seven naturally occurring stable isotopes, but the ratio $^{143}Nd/^{144}Nd$ is the most widely applied tracer of geologic and oceanographic processes. ^{143}Nd is the radiogenic daughter product of ^{147}Samarium (Sm; produced through α-decay with a half-life of 1.06×10^{11} years), and ^{144}Nd is a stable isotope. Different rocks acquire different $^{143}Nd/^{144}Nd$ values based on their age and composition. All REE are incompatible (i.e., prefer the melt phase during partial melting) but light REE such as Nd are more incompatible than the heavy REE. Thus partial melting of the mantle fractionates Nd from Sm, leading to greater Sm/Nd ratios in the mantle than those found in continental crust (e.g. DePaolo and Wasserburg, 1976).

Nd isotope ratios are typically expressed using epsilon notation [hereafter referred to as ε_{Nd}; calculated as in equation 2 where CHUR refers to Chondritic Uniform Resevoir, a standard value based on the $^{143}Nd/^{144}Nd$ of bulk Earth and has a modern value of 0.512638 (DePaolo and Wasserburg, 1976)] .

(2)
$$\varepsilon_{Nd} = \left(\frac{\left({}^{143}Nd / {}^{144}Nd \right)_{Sample}}{\left({}^{143}Nd / {}^{144}Nd \right)_{CHUR}} - 1 \right) \times 10000$$

In ancient samples, one must correct for age to account for in situ production of ^{143}Nd from ^{147}Sm in the sample (the age-corrected values are presented as $\varepsilon_{Nd(t)}$). Continental crust typically has ε_{Nd} values ranging from ~-20 – -10 whereas basaltic rocks have values between ~-2 – +14 (Piepgras and Wasserburg, 1980).

The dominant source of dissolved Nd to the oceans is weathered rock delivered by riverine input (Piepgras et al., 1979; Goldstein and Jacobsen, 1987). The type of rock weathered and drained by a given fluvial system directly controls the ε_{Nd} of the surface ocean receiving the riverine discharge. The weathering and delivery processes do not fractionate the Nd isotopes or the Sm/Nd ratio and represent an average value of all of the rocks in the river's drainage system (Goldstein and Jacobsen, 1988). This is apparent by the very radiogenic (greater $^{143}Nd/^{144}Nd$ ratio / more positive ε_{Nd}) values of the North Pacific surface waters from the weathering of younger, mantle-derived terranes as compared to the unradiogenic (lower $^{143}Nd/^{144}Nd$ ratio / more negative ε_{Nd}) values of the North Atlantic derived from weathering and drainage of old cratonic

terranes (e.g. Stordal and Wasserburg, 1986; Piepgras and Jacobsen, 1988; Amakawa et al., 2004; Lacan and Jeandel, 2005a).

Today, the ε_{Nd} of North Atlantic Deep Water (NADW) is ~ -14 (e.g. Piepgras and Wasserburg, 1987; Jeandel, 1993). NADW is the product of highly unradiogenic waters imparted with Nd by the weathering of ancient Canadian shield rocks and subsequent convection in the Labrador Sea with relatively radiogenic waters convected in the Norwegian-Greenland Sea (Goldstein and Jacobsen, 1987; Lacan and Jeandel, 2005a). In contrast, Antarctic Bottom Water is more radiogenic (ε_{Nd} ~ -7 to -9) and reflects a combination of upwelled unradiogenic NADW and radiogenic Pacific surface waters (Piepgras and Wasserburg, 1982). In the Indian Ocean, AABW flows north, carrying the Southern Hemisphere signal with it (Jeandel et al., 1998; Goldstein et al., 2007). Intermediate depths in the Indian Ocean are more radiogenic than AABW as they contain a greater proportion of Pacific surface waters due to their formation at the polar front, rather than south of it, like AABW (Jeandel et al., 1998; Amakawa et al., 2000).

In order to exploit the marine geochemical cycling of Nd as a tracer of ancient water mass composition, the seawater Nd isotopic ratio must be recorded and preserved in the geologic record. In the following three studies we utilize two different sedimentary phases as recorders of past seawater ε_{Nd}: biogenic apatite (fish teeth and bones) and benthic calcite (foraminifera).

Biogenic apatite records the Nd isotopic composition of seawater at the seafloor (e.g. Staudigel et al., 1985; Reynard et al., 1999). The small crystal structure of biogenic apatite ($Ca_5(PO_4,CO_3)_3OH$, carbonate hydroxylapatite) in living bone and teeth renders it

susceptible to early diagenetic transformation at the seafloor (Martin et al., 2005). During early diagenesis, biogenic apatite recrystallizes as flourapatite ($Ca_5(PO_4)_3F$), a thermodynamically stable mineral at seafloor temperatures. REEs and other trace metals are incorporated onto the crystal surface, and the crystal then grows around them (Armstrong et al., 2001). This process increases the amount of Nd incorporated into apatite from <20 ppm to >1000-10000 ppm (Patrick, 2006). As crystals grow, their decreased surface area to volume ratio, combined with their new structure makes them highly resistant to further alteration. Alteration can only occur during high-grade metamorphism (Person et al., 1995). As a consequence, fish debris (fossilized bones and teeth from fish) reliably record and retain ε_{Nd} values of seawater acquired at the seafloor. The high concentrations of REE in biogenic apatite permit precise analyses with small amounts of phosphatic material. However, fish debris in some locations is too rare in deep-sea sediments to generate high-resolution records.

Biogenic carbonate precipitated by foraminifera, also records the Nd isotopic composition of the waters in which it grew. The ionic radius of Nd^{3+} is 1.00Å, which is very close to the 0.99Å radius of Ca^{2+}, enables Nd to substitute into the calcite structure (Palmer, 1985). However, the charge difference makes this substitution unfavorable. Thus biogenic carbonate contains low concentrations of Nd (~0.2 - 2.7 ppm; e.g. Palmer, 1985; Vance et al., 2004; Klevenz et al., 2008; Roberts et al., 2010). Neodymium is not biologically fractionated (i.e., there is no "vital effect"), making it unnecessary to analyze monospecific populations. Benthic foraminifera record the Nd isotopic composition of waters at the seafloor, the same as coeval fish debris (Carter et al., 2007;

Klevenz et al., 2008; Murphy and Thomas, *submitted*). The abundance of foraminiferal calcite in carbonate sediments potentially allows for a more continuous record than one generated by fish debris. However, the low concentration of Nd in foraminiferal calcite requires a large mass of calcite (~10 mg) for precise analysis, and such large masses are often not available in a single sample. In addition, foraminiferal calcite is susceptible to burial diagenesis.

Changes in the Nd isotopic composition of waters in a given location may reflect a variety of processes including changes in the ε_{Nd} of the water mass source region (e.g., weathering inputs), mixing between water masses of similar densities (e.g. von Blanckenburg, 1999; Goldstein et al., 2007), particle exchange (e.g. Goldstein and Hemming, 2003) and boundary exchange (e.g. Lacan and Jeandel, 2001, 2005a; Zhang et al., 2008). Each one of these factors is accounted for in the following studies, as their effects differ by time frame and study area.

3. Prelude

The following chapters lay out three studies focused on defining changes in oceanic circulation during times of global climate change. Each study focuses on a different geographic region (California margin, South Atlantic Ocean, eastern Indian Ocean; Chapters II, III, and IV respectively), different time interval (late Pleistocene, Late Cretaceous), and different time scales (few hundred year resolution, few hundred thousand year resolution). However, they all focus on the impacts of intermediate and deep-water circulation using Nd isotope data collected from fish debris and benthic foraminifera. Chapter II has been submitted to Quaternary Science Reviews and is in

review. Chapters III and IV are being prepared for submission to Paleoceanography in the next six months.

CHAPTER II

THE ROLE OF INTERMEDIATE WATER CIRCULATION IN STADIAL-INTERSTADIAL OXYGENATION VARIATIONS ALONG THE SOUTHERN CALIFORNIA MARGIN

Changes in the source of intermediate waters to the southern California margin may have caused variations in seafloor oxygen levels on stadial-interstadial time scales. We test this hypothesis using the Nd isotopic composition of benthic foraminifera and fossil fish debris from ODP Sites 893 and 1017 to track the composition of intermediate waters across interstadials 8-14 (~37-52 ka) during Marine Isotope Stage 3. Our data indicate a Southern Ocean source for intermediate waters bathing the Southern California margin throughout the study interval, with no systematic stadial-interstadial variations in the source of those waters. Instead, changes in local/regional sea surface productivity likely caused the recorded changes in seafloor oxygenation.

1. Introduction

The millennial scale climate oscillations (stadial-interstadial events) first identified in Greenland ice cores (Dansgaard et al., 1993) during Marine Isotope Stage 3 (MIS 3; ~60 to 25 ka) are now recognized throughout the Northern Hemisphere and the tropics (e.g. Behl and Kennett, 1996; Hughen et al., 1996; Wang et al., 2001). Along the California margin (Figure 2-1) interstadial events coincided with increases in sea surface temperature (Kennett and Venz, 1995) and primary productivity (Pospelova et al., 2006), as well as a decrease in dissolved oxygen levels at the seafloor (Behl and Kennett, 1996;

Cannariato and Kennett, 1999). Stadials were characterized by sea surface temperature cooling and higher levels of dissolved oxygen at the seafloor.

Stadial – interstadial changes in seafloor oxygenation along the California margin may have resulted from changes in the supply of organic carbon to the seafloor or changes in dissolved oxygen concentrations at the seafloor due to a change in intermediate water ventilation. Based on benthic foraminiferal stable isotopes from Santa Barbara Basin Ocean Drilling Program (ODP) Site 893, Hendy and Kennett (2003) proposed that the source of intermediate waters to the California margin may have shifted from a stadial source of North Pacific Intermediate Water (NPIW) to a Southern Ocean interstadial source. Today, intermediate waters that reach the California margin are generically referred to as Southern Component Water (SCW) (Hendy and Kennett, 2003), a water mass that consists of Antarctic Intermediate Water (AAIW) and South Pacific Mode Water (SPMW) (Tsuchiya, 1981). The only occurrence of SCW in the North Pacific basin north of ~15°N, is in a boundary current along the Mexican and Californian margins, and it is detectable as far north as Oregon based on nitrogen isotope data (Kienast et al., 2002). Site 893 benthic foraminiferal $\delta^{18}O$ values are lighter during interstadials coincident with evidence for decreased dissolved O_2 (Cannariato et al., 1999), suggesting warmer intermediate-waters than during stadials. The abrupt $\delta^{18}O$ changes imply a shift to a warmer, older source of water rather than gradual warming of the same water mass (Hendy and Kennett, 2003).

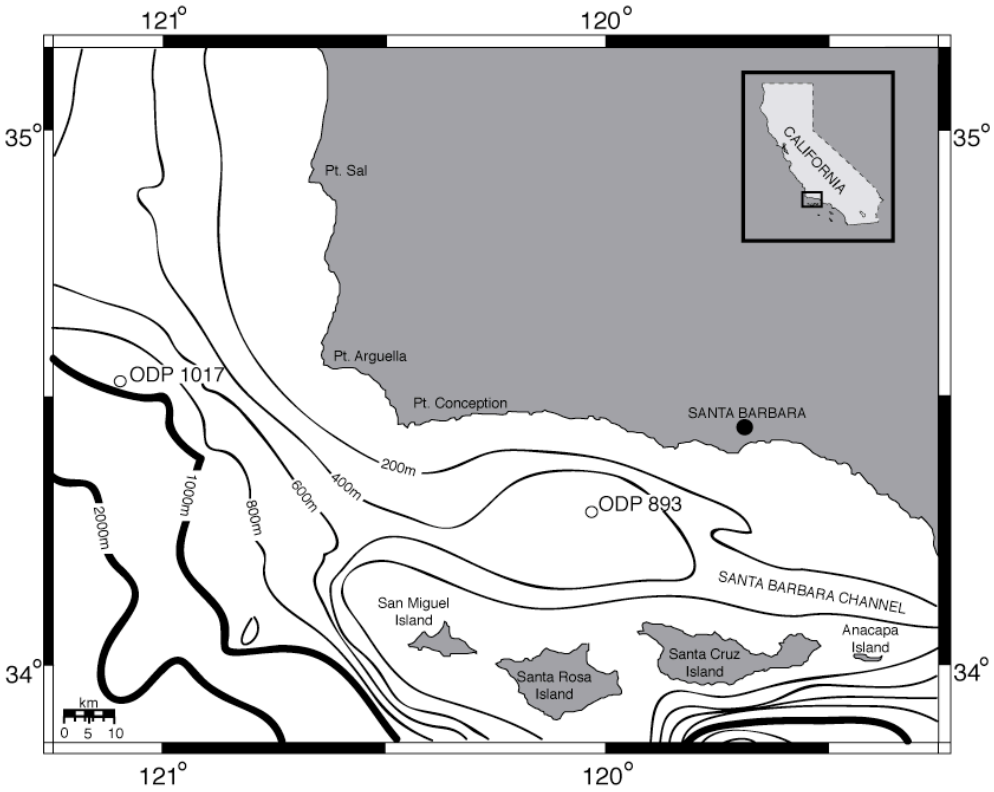

Figure 2-1. Map of study area. ODP Hole 893A is located at a depth of ~576m and Hole 1017E at ~955m. Modified from (Cannariato and Kennett, 1999).

While the hypothesis that a change in the source of intermediate waters to the California Margin potentially explains the coincident changes in temperature and seafloor oxygenation in the Santa Barbara Basin, oxygen isotope data alone are not diagnostic indicators of water mass provenance. Furthermore, other sites on the open California margin do not record the same set of stadial-interstadial changes. Analysis of ODP Site 1017 (~955 m; Figure 2-1) does not indicate coincident changes in benthic $\delta^{18}O$ and seafloor oxygenation, implying that sea surface productivity was the primary driver of the small dissolved oxygen changes recorded by benthic foraminiferal faunal assemblages (Cannariato and Kennett, 1999; Kennett et al., 2000). Evidence for nitrogen cycle changes and surface productivity fluctuations on the California margin during MIS 3 reinforce this interpretation (Kienast et al., 2002; Hendy and Pedersen, 2005).

To test the hypothesis that changes in the stadial-interstadial seafloor oxygenation in the Santa Barbara Basin were caused by changes in intermediate water provenance, and reconcile some of the inconsistencies between the Santa Barbara Basin and open California margin, we present new millennial scale Nd isotope records from ODP Holes 893A and 1017E. The modern difference between the Nd isotopic composition of NPIW (ε_{Nd} = -2 to –4) (Piepgras and Jacobsen, 1988; Vance et al., 2004; Amakawa et al., 2009) and SCW (ε_{Nd} = -7 to –9) (Lacan and Jeandel, 2001; Arsouze et al., 2007) provides a straightforward test of intermediate water provenance during MIS 3. Our data rule out any significant and systematic change in intermediate water

provenance, suggesting that sea surface productivity changes along the margin played the dominant role in controlling seafloor oxygen levels.

2. Regional Setting

ODP Site 893 is located within the Santa Barbara Basin (34°17.25'N, 120°02.20'W) at ~576 m water depth (Figure 2-1). Extremely high sedimentation rates (>120 cm/kyr) and seasonally varved sediments preserve millennial scale variations (Soutar and Crill, 1977). During the spring upwelling season, water from the oxygen minimum zone flows over the western sill, refreshing the basin (Bograd et al., 2002). ODP Site 1017 is located on the Santa Lucia Slope at a water depth of ~955 m (34°32.10'N, 121°06.43'W (Figure 2-1). The California Current flows parallel to the slope, and a persistent upwelling cell has sustained high rates of sea surface productivity over the last 60 kyr (Hendy et al., 2004). The oxygen minimum zone along the Santa Lucia Slope, from ~525 m to ~1000 m, reaches dissolved oxygen values <0.50 ml/L at 700 m (Levitus, 2001). The sedimentation rate of ~23 cm/kyr also permits high-resolution studies of millennial scale climate variability, even though the sediments are not laminated. The age models for Sites 893 and 1017 are from Hendy et al. (2002) and Hendy et al. (2004), respectively.

3. Materials and Methods

3.1 Neodymium isotopes as a tracer of water mass composition

The Nd isotopic composition of a water mass, expressed as ε_{Nd} [the $^{143}Nd/^{144}Nd$ value of a geologic sample normalized to the bulk earth (DePaolo and Wasserburg, 1976)] reflects the isotopic composition of the rocks weathering into the water mass

source region. Due to the short residence time (~1000 years) relative to oceanic mixing (~1500 years), a water mass retains the Nd isotopic composition imparted when it formed with minor predictable changes caused by processes such as boundary exchange (Lacan and Jeandel, 2005a) and mixing. Today, the ε_{Nd} value of NPIW at its source ranges from –2 to –4 (Amakawa et al., 2004), while the Southern Ocean signature is –7 to –9 (Piepgras and Wasserburg, 1982). Temporal changes in Nd isotopes can result from a change in water mass source region or a change in the composition of weathered material in the water mass formation region. However, any changes in the ε_{Nd} ratio of the source region will be too small to mask the observed differences between northern and southern hemisphere derived sources. Potential changes in the ε_{Nd} value of NPIW, for example, include the movement of its formation from the present day site in the Sea of Okhost, to south of the Aleutian Islands, resulting in a subtle change in the ε_{Nd} value. However, NPIW Nd would still be dominated by the radiogenic weathering products of the entire Pacific rim, in contrast to the relatively unradiogenic SCW signature.

3.2. Sampling and analytical methods

Fish teeth and bones preserve the Nd isotopic signature of waters bathing the seafloor (e.g. Staudigel et al., 1985; Reynard et al., 1999). However, fish debris are not sufficiently abundant in the sediments of Sites 893 and 1017 to generate high resolution records. Previous work has demonstrated that well-preserved and well-cleaned foraminifera record the Nd isotopic composition of the water in which their shells precipitated (Burton and Vance, 2000; Vance et al., 2004; Klevenz et al., 2008). The high abundance (>1500 individuals/20 cc sample) of benthic foraminifera, together with

high sedimentation rates at Site 893 and 1017, makes them ideal for this study. To determine if benthic foraminiferal species with different sedimentary depth habitats record different ε_{Nd} values, we analyzed multiple species with known depth habitats separately, along with fish debris, from the same sample (Figure 2-2). Among the benthic foraminifera analyzed, *Epistominella* sp. is epifanual, *Bolivina argentea* is deep infaunal, and *Uvigerina peregrina* as well as a sample of all other mixed benthics are mid-depth infaunal. For all samples, we picked >10 mg of foraminifera from the >150 μm fraction.

We sampled Hole 893A at a resolution of one sample every ~150-1000 years (~650 years on average for 23 samples), and Hole 1017E at one sample every~300-1200 years (1/~750 yrs on average for 18 samples). Fish debris and teeth were picked by hand from the >63μm fraction, while benthic foraminifera were picked from the >150μm fraction. Foraminifera were used for 13 of 43 analyses.

After foraminifera were selected for analyses, the chambers of each individual were opened to expose the inside of the test for cleaning. All samples (fish debris and foraminiferal calcite) underwent an oxidative/reductive cleaning stage as described in Boyle (1981) with modifications as in Vance et al. (2004). The rare earth elements were isolated using REE Spec cation exchange chemistry, and then the Nd was separated from the other rare earth elements using methyllactic acid chemistry.

Samples at UNC-Chapel Hill were run as NdO^+ using a multi-collector VG Sector 54, and at Texas A&M on the Thermo Triton thermal ionization mass spectrometer as Nd^+. The procedural blank is ~15 pg and is considered negligible.

Replicate samples run at UNC-Chapel Hill and Texas A&M University gave values within error of each other. At UNC-CH, external analytical precision based upon replicate analysis of the international standard JNdi (Tanaka et al., 2000), analyzed as an oxide, yielded 0.512111 ± 11 ppm (n=30). Replicate analysis of the JNd_i standard (n=28) on the TAMU Thermo Triton is currently 7.0 ppm (2σ) and the value is 0.51210156. Replicate analysis of the La Jolla standard (n=22) on the TAMU Triton yields a value of 0.5118459 at 6.2 ppm (2σ).

4. Results

4.1 Comparison of foraminifera and fish debris

Benthic foraminifera record the same Nd isotope value as fossil fish teeth, which are known to record the isotopic composition of waters bathing the seafloor (Figure 2-2). Thus benthic foraminifera are suitable recorders of the same seawater. Furthermore, there is no difference in the ε_{Nd} value between epifaunal and infaunal benthic foraminiferal species or fish debris, permitting analysis of mixed benthic samples.

4.2 California margin water mass composition

The ε_{Nd} of the water mass bathing Sites 893 and 1017 did not change systematically on a stadial-interstadial basis and both sites record values consistent with a Southern Ocean source (Appendix 1; Figures 2-3 and 2-4). Site 893 ε_{Nd} values were typically ~-9 throughout the study interval, with a few shifts toward more radiogenic values. During interstadial 14 ε_{Nd} values varied between –8.2 to –9.0 and then decreased to –9.2 between ~49.2-46.5 ka. ε_{Nd} values increased to -7.9 before gradually decreasing back to –9.1 across interstadial 13. The last prominent shift occurred prior to interstadial

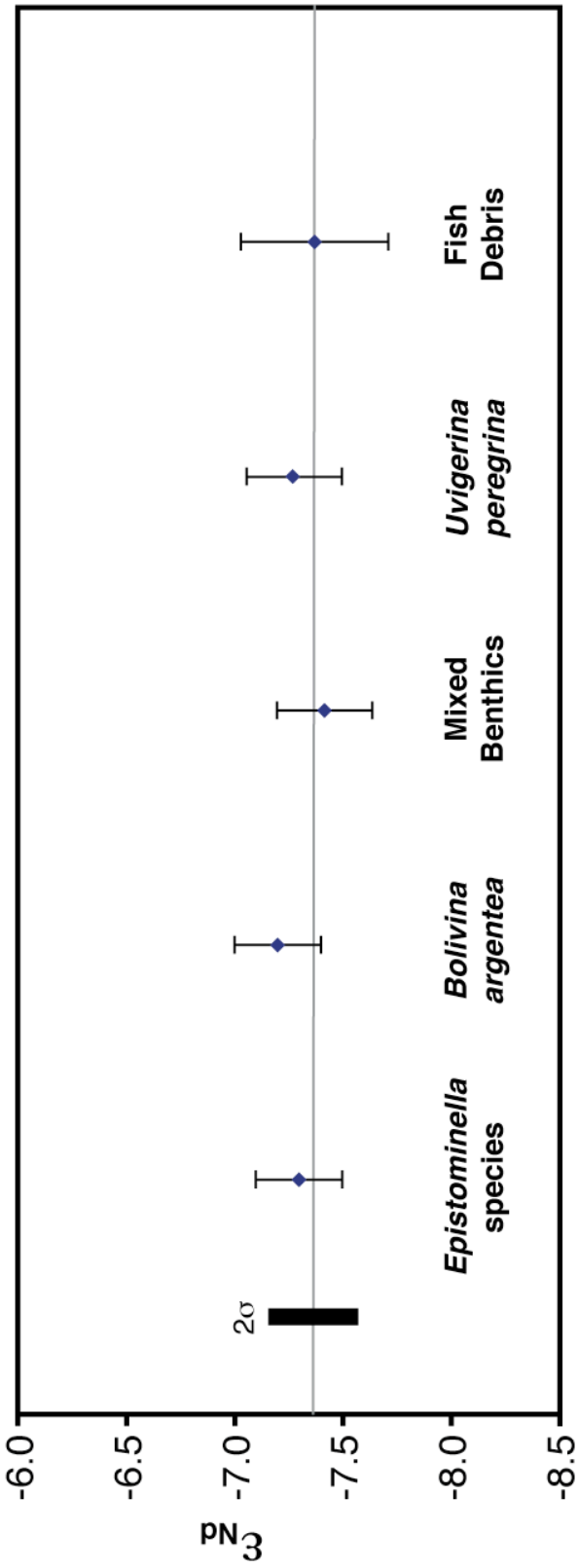

Figure 2-2. Comparison of the ε_{Nd} values of benthic foraminifera and fish debris. *Epistominella spp.* (epifauna), *B. argentea* (deep infauna), and *U. peregrina* (shallow infauna) record the same value as the sample of mixed benthic specimens and fish debris. Gray center line at -7.37 is the fish debris value from the same sample. Black bar is 2σ external reproducibility.

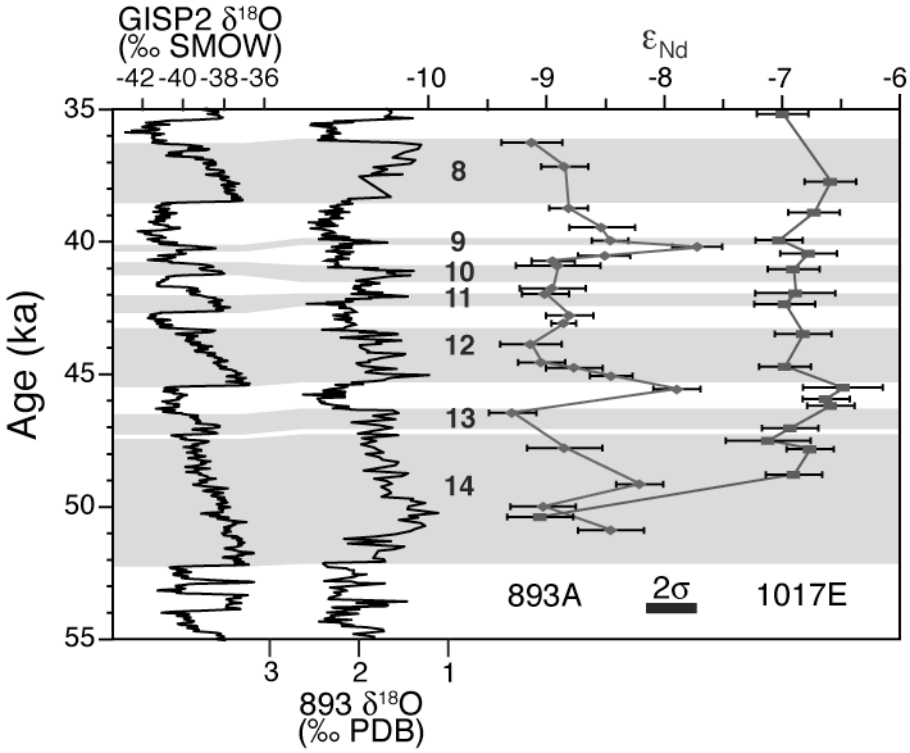

Figure 2-3. Comparison of GISP2 ice core $\delta^{18}O$ (SMOW) record (Grootes et al., 1993) with the Hole 893A $\delta^{18}O$ (PDB) record derived from the planktonic foraminifera *Neogloboquadrina pachyderma*, (a thermocline dwelling species) (Hendy and Kennett, 1999) and Nd isotopic data from ODP Holes 893A and 1017E. For reference, NPIW ε_{Nd} values are ~-2 to -4 (Vance et al., 2004; Amakawa et al., 2009). Gray shading demarcates interstadials 8-14.

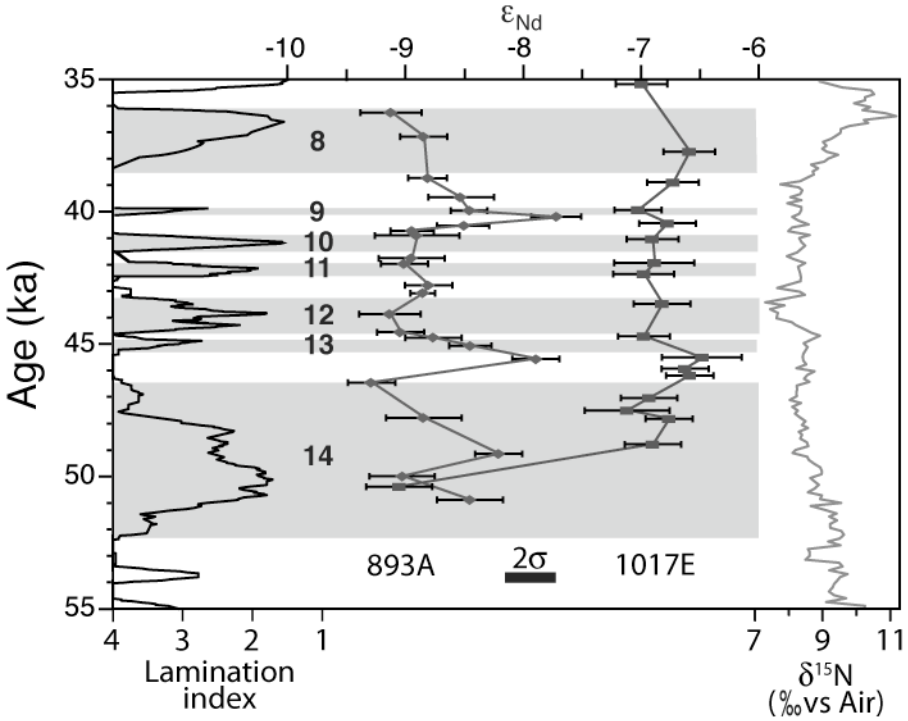

Figure 2-4. Comparison of Nd isotopic data from ODP Holes 893A and 1017E with the Hole 893A lamination index (Behl and Kennett, 1996) and the $\delta^{15}N$ record from the Chilean margin, a proxy of SCW ventilation (De Pol-Holz et al., 2007). Low values in lamination index indicate greater lamination (low oxygen); high values reflect bioturbation (relatively high oxygen). Nd error bars indicate within-run precision, and the solid bar denotes the 2σ external reproducibility. Gray shading demarcates interstadials in Site 893A based on planktonic $\delta^{18}O$ values (as shown in Figure 2-3, from Hendy and Kennett, 1999; 2003). Northern hemisphere and southern hemisphere records are shown to demonstrate the stability of the water mass source at the California margin, regardless of global climate change.

9, in which ε_{Nd} values increased to –7.7 before returning to –8.4 over the following ~400 years. Site 1017 ε_{Nd} values varied between –7.1 to –6.5 from ~50-35 ka (Figures 2-3 and 2-4). Prior to this interval a single data point at ~51 ka yielded an ε_{Nd} value of –9.0 similar to the range of values recorded at Site 893.

5. Discussion

The values and trends in the Nd isotope records from both Sites 893 and 1017 suggest that the source of intermediate waters to the California margin was the Southern Ocean. Furthermore, the composition of this water mass did not change on a stadial-interstadial basis. However, in order to unambiguously interpret these records in terms of hydrographic processes, we must rule out other factors that may have contributed to changes (or lack of change, as in the case of Site 1017) in the seafloor Nd isotopic composition. Such factors include boundary exchange and diagenesis.

Boundary exchange (Lacan and Jeandel, 2005b) involves the leaching of Nd from margin sediments into the overlying water column, potentially displacing the original seawater Nd. This process has been demonstrated at a number of locations such as Papua New Guinea (Lacan and Jeandel, 2001), the Greenland margin (Lacan and Jeandel, 2005a), and Kerguelen Plateau (Zhang et al., 2008). The latter study calculated ~20% of the Nd within the Antarctic Circumpolar Current after interaction with the Kerguelan Plateau derived from the remobilization of Nd from plateau silicates. We can rule out boundary exchange as the principal control of the Nd isotopic composition recorded at Sites 893 and 1017 because the silicates on the Californian and Mexican margin that the SCW would have interacted with are more radiogenic (-6.4 to +4.2) than

our fish debris and foraminiferal Nd (e.g. McLennan et al., 1990; Jeandel et al., 2007). Significant contributions from margin sediments thus would have imparted Nd isotope values resembling waters sourced from the North Pacific rather than the Southern Ocean.

We can also eliminate diagenesis as the dominant control of Nd composition recorded by the benthic foraminfera and fish debris. Nd associated with metabolism of particulate organic carbon or reduction of oxide minerals could over-print the water mass signal at the seafloor (Haley et al., 2004). However, along the California margin the majority of the Nd associated with surface-derived particulates would have been more radiogenic, reflecting fluvial inputs of regional weathering products, than the contemporaneous values recorded at the seafloor, and no significant deflection from values typical of the Southern Ocean is apparent in the Site 893 or 1017 data. Dissolution of oxide minerals within the sediment column could increase the pore water concentration of Nd but would likely not alter the isotopic composition because Fe-oxides record seawater values (e.g. O'Nions et al., 1978; Albarède and Goldstein, 1992). Finally, the high clay content of Sites 893 and 1017 would render vertical diffusion rates of Nd within the pore waters very slow relative to sedimentation rates at the two sites, preventing any 'smearing' of peaks.

Diagenetic or boundary exchange processes did not significantly impact the California margin seafloor Nd isotope values recorded at Sites 893 and 1017. However, there is some subtle structure evident in the Site 893 record that does not correspond with any changes in the Site 1017 data. The radiogenic shifts recorded at Site 893 (Figures 2-3 and 2-4; from ~-9 to ~-8) did not occur on a stadial-interstadial basis nor

did they follow any other record of climate change. One possible explanation for these subtle shifts is local boundary exchange in the Santa Barbara basin that did not significantly impact the record of seawater composition (otherwise Site 893 would have recorded values even more radiogenic than Site 1017). Regardless of the cause, the small ε_{Nd} shifts do not impact the primary interpretation of the new Nd isotope data, namely that the provenance of intermediate waters along the California margin remained constant on a stadial-interstadial basis.

One other aspect of the data needs to be explained before proceeding with the paleoceanographic implications of the California margin Nd isotope records. The ε_{Nd} values of each site are offset by ~2 epsilon units. The offset in absolute Nd isotope values can be explained by the difference in water depth between the two sites. Considering the lower glacial sea level during MIS 3, Site 1017 was situated at the deepest extent of SCW along the California margin (Reid, 1965). Site 1017 ε_{Nd} values were therefore affected by mixing with the water mass below. Deeper than ~1000 m, the central North Pacific has ε_{Nd} values of ~-3.6 (Amakawa et al., 2009), thus this deeper water mass imparted a more radiogenic signature to the base of the glacial SCW. Mixing between this deeper water mass and SCW with an average value of ~-9 (from Site 893) would require a mixture of 37% North Pacific Nd to create the 2 epsilon offset assuming approximately equal dissolved Nd concentrations between the two end members (Lacan and Jeandel, 2001; Vance et al., 2004). This offset is constant throughout the record, implying a constant mixing ratio.

The one exception to this offset is a single data point at ~50.7 ka recorded at Site 1017 that is similar to coeval Site 893 data. The convergence of values recorded at the two sites occurred during interstadial 14, the longest interstadial of the study interval and the most vertically expanded OMZ. An increase in SCW production may have led to a deeper boundary between SCW and Pacific deep waters during interstadial 14 than exists today. If SCW extended deeper within the water column, the mixing ratio of Pacific Nd with southern-sourced Nd at Site 1017 would decrease, causing the observed convergence of values.

The relative constancy of the Nd isotope composition of California margin intermediate waters across interstadials 8-14 effectively rules out any change in intermediate water provenance as a cause of the recorded changes in seafloor oxygenation or temperature. The difference in ε_{Nd} values between SCW and NPIW is sufficiently large to have manifested itself had a provenance change occurred, even with potential contributions from boundary exchange and allochthonous Nd.

Having ruled out a change in water mass provenance, we explore other processes to explain stadial-interstadial changes in intermediate water oxygenation: 1) changes in intermediate water ventilation from the Southern Ocean to the California margin, 2) changes in surface productivity along the flow of the water mass, and 3) changes in the rates of local productivity along the California margin.

Reconstructions of the intensity of the eastern tropical North Pacific oxygen minimum zone during the last 60 kyr suggest that SCW experienced ventilation changes along its flow path (Ganeshram et al., 2000; Hendy and Pedersen, 2006; De Pol-Holz et

al., 2007). Recall that SCW is a combination of SPMW and AAIW. SPMW is originally formed in the southwest Pacific near New Zealand (Tsuchiya, 1981), and then flows north to be incorporated into the Equatorial Undercurrent, where it is carried to the east before splitting into northward and southward flowing arms around 100°W (Fiedler and Talley, 2006). During the last glacial interval, intensified Hadley circulation may have intensified the Equatorial Undercurrent (Andreasen et al., 2001), increasing ventilation of SPMW and thereby increasing the oxygenation of SCW in the eastern tropical North Pacific (Kienast et al., 2002). An increase in SPMW production is supported by $\delta^{15}N$ changes recorded along the Chilean margin (De Pol-Holz et al., 2007) and the Gulf of Tehuantepec, Southern Mexico (Hendy and Pedersen, 2006).

However, changes in Southern Hemisphere ventilation (i.e., SPMW production) occurred in response to the timing of Antarctic events (Figure 2-4), *not* Northern Hemisphere stadial – interstadials (i.e., the oxygenation record of Sites 893 and 1017). The timing of SCW ventilation does not correlate with changes in the oxygenation on the California margin (based on foraminiferal assemblages; Cannariato and Kennett, 1999), and therefore could not have been the cause of seafloor dysoxia during interstadials.

We can also rule out the effect of productivity along the flow path of SCW that might have occurred in the equatorial upwelling region. If this were the case, one would expect increased primary productivity at all sites influenced by SCW. However, changes in seafloor oxygenation evident in sediment cores from the Gulf of Tehuantepec at 15°N (20° south of our study sites) are paced by Southern Hemisphere climate

changes (Hendy and Pedersen, 2006) and not the Northern Hemisphere stadial-interstadial events. Thus the Northern Hemisphere stadial-interstadial paced changes along the California margin must have resulted from local/regional processes.

The lack of correspondence between indicators of intermediate water ventilation and the impacts of sea surface productivity on those waters during the transit from the Southern Ocean suggests that local/regional variations in *sea surface productivity along the California margin* were the primary control on stadial-interstadial changes in seafloor oxygenation. Several lines of evidence support this conclusion. Coccolithophorid (Nederbragt et al., 2008) and dinoflagellate cyst (Pospelova et al., 2006) abundances in Santa Barbara basin sediments were higher during interstadials and the Holocene, implying greater productivity during dysoxic intervals within the basin. Studies of carbonate and opal percentage, as well as organic carbon and major and minor element analysis also confirm increased productivity over Site 1017 during interstadials (Hendy et al., 2004).

Stott et al. (2000) found that since the late 1970's, upwelling in the Santa Barbara Basin has decreased by 20 – 30%, coinciding with an increase in dissolved oxygen concentrations of 0.17 – 0.22 ml/L at the seafloor due to a decrease in sea surface productivity caused by nutrient limitation. If this relationship can be extended to stadial-interstadial changes, a shift from well-oxygenated waters to dysoxic, laminated sediments would require an increase in local upwelling of ~160% over glacial upwelling rates and the subsequent increases in local productivity in response to newly available

nutrients. This is well within the range of changes in organic carbon preservation on millennial time scales (e.g. Ortiz et al., 2004).

One complication with this explanation is that if regional productivity exclusively controlled oxygenation at the seafloor along the southern California margin, then Sites 893 and 1017 should display similar records of seafloor oxygenation changes, given their close proximity (~100 km). Although some authors attribute the difference between the two sites to the difference between a silled basin (such as Santa Barbara Basin) and the open margin (Mangelsdorf et al., 2000), oscillations in seafloor oxygenation at Site 893 are not unique to the basin. Changes in seafloor oxygenation (smaller in magnitude, but similar in behavior) have been found on the open California margin at water depths shallower than Site 1017, ruling out a silled basin effect (Dean, 2007).

A more likely explanation for the apparent difference in oxygenation changes between Sites 1017 and 893 involves the sensitivity of benthic foraminifera to changes in dissolved oxygen levels at values above a certain threshold. Benthic foraminifera used to reconstruct seafloor oxygenation are only sensitive to low levels of oxygen (<1.5 mL/L) (Kaiho, 1994), such as those seen in Site 893, but not Site 1017. An equivalent magnitude of dissolved oxygen changes likely occurred at the seafloor at Site 1017, but at oxygen concentrations above those that would affect foraminiferal assemblages (the dissolved oxygen indicators). Thus, we conclude that productivity was the most likely control on stadial-interstadial changes in seafloor oxygenation along the California margin.

6. Conclusions

Seawater Nd isotope data from ODP Sites 893 and 1017 demonstrates that a.) the intermediate waters bathing both sites originated in the Southern Ocean and b.) the source of intermediate waters to the southern California margin did not vary on a stadial-interstadial basis. Millennial-scale changes in seafloor oxygenation and organic carbon preservation were most likely controlled by local sea surface productivity on the California margin.

CHAPTER III

THE ROLE OF GATEWAYS IN DENSITY DRIVEN OCEANIC CIRCULATION IN THE LATE CRETACEOUS SOUTH ATLANTIC

Much focus has been given to changes in deep-ocean circulation during the Oceanic Anoxic Events in the Cretaceous, but little is actually known about circulation processes during the background, "normal" intervals of the Cretaceous. Low meridional thermal gradients characterize the extreme greenhouse warmth of the Late Cretaceous, and the role of ocean circulation in such climate dynamics is poorly understood. In the modern climatic regime, water sinking in the high-latitudes drives deep-ocean circulation. However, Cretaceous paleogeography and bathymetry were significantly different, and various gateways that have opened and closed complicate our understanding of deep ocean circulation during this time. Here we use neodymium isotopic data from four sites in the South Atlantic to reconstruct deep-water mass chemistry and infer Late Cretaceous circulation patterns. During the Cenomanian to early Campanian, the South Atlantic had a complex circulation pattern because the seafloor was divided into several distinct basins. Deep-water production in the proto-Southern Ocean became the primary source of deep-water within the South Atlantic during the early Campanian.

1. Introduction

The Late Cretaceous was the warmest time of the last 100 Myr (e.g. Veizer et al., 2000; Royer et al., 2004). Atmospheric carbon dioxide levels were estimated to have been 2-5 times higher than modern levels, similar to projections from the IPCC for the

next century (e.g. Royer et al., 2004; Berner, 2006; IPCC, 2007). The meridional temperature gradient during the Turonian (89.3 – 93.5 Ma) was lower than modern, with sea surface temperatures ranging from 36°C in the tropics (Norris et al., 2002; Wilson et al., 2002) to 20°C in the high-latitude South Atlantic (Huber et al., 1995).

The redistribution of heat is one of the most important consequences of oceanic circulation of surface and deep waters. Today, the poleward movement of heat from the tropics warms the high-latitudes through the release of heat to the atmosphere, moderating the global meridional thermal gradient. Deep-water production in the modern oceans occurs via the cooling and sinking of surface waters at high latitudes in the Atlantic and Southern Oceans.

However, the extreme warmth of the Cretaceous oceans led to the proposal of 'halothermal circulation', in which deep-water formation occurred in low latitude locations via sinking of warm saline waters (e.g. Brass et al., 1982; Barron and Peterson, 1990).

The consequences of the different modes of deep-ocean circulation could be critical to understanding the global heat balance of the Cretaceous. Some models are unable to replicate the observed meridional gradient with the present understanding of ocean circulation (Poulsen et al., 1999), and latent heat transport via the atmosphere may account for the enhanced polar heat transport (Ufnar et al., 2004). Other models (Barron and Peterson, 1990) invoke the production of deep-water in the low-latitudes to depress tropical temperatures and warm the poles. Still others require doubling oceanic heat transport in conjunction with higher atmospheric CO_2 (Barron et al., 1995). However,

so little is known about modes of ocean circulation during this time that it is difficult to evaluate the various simulations.

Here, we investigate sites from the Atlantic sector of the modern Southern Ocean from the Cenomanian to the Campanian (~70-100 Ma) to reconstruct the evolution of deep-water circulation in the South Atlantic through this time interval.

2. Tectonic Conditions During the mid- to Late Cretaceous

During the Cenomanian (93.5 – 99.6 Ma) plate tectonic boundary conditions were different from the modern (Figure 3-1, Figure 3-2). The deep portions of the South Atlantic basins were not interconnected as they are in the modern. Communication between the South Atlantic and the tropical and North Atlantic did not exist until the opening of the Central Atlantic Gateway sometime between the Turonian and the Campanian (70.6 - 93.5 Ma; e.g. Poulsen et al., 2003; Friedrich and Erbacher, 2006). The Walvis Ridge/Rio Grande Rise complex restricted deep-water connections between the South Atlantic and the Atlantic sector of what would eventually become the Southern Ocean. The India/Madagascar/Kerguelen Plateau terrane bounded the eastern part of the southernmost Atlantic, preventing deep-water flow between the Indian and the Atlantic, and to the west by the connection of South America to Antarctica. Thus the deep South Atlantic consisted of several distinct basins more analogous to the modern Caribbean/Gulf of Mexico basins.

Over the next ~30 Myr, the South Atlantic became wider and deeper and connections between the different basins were formed. South America remained

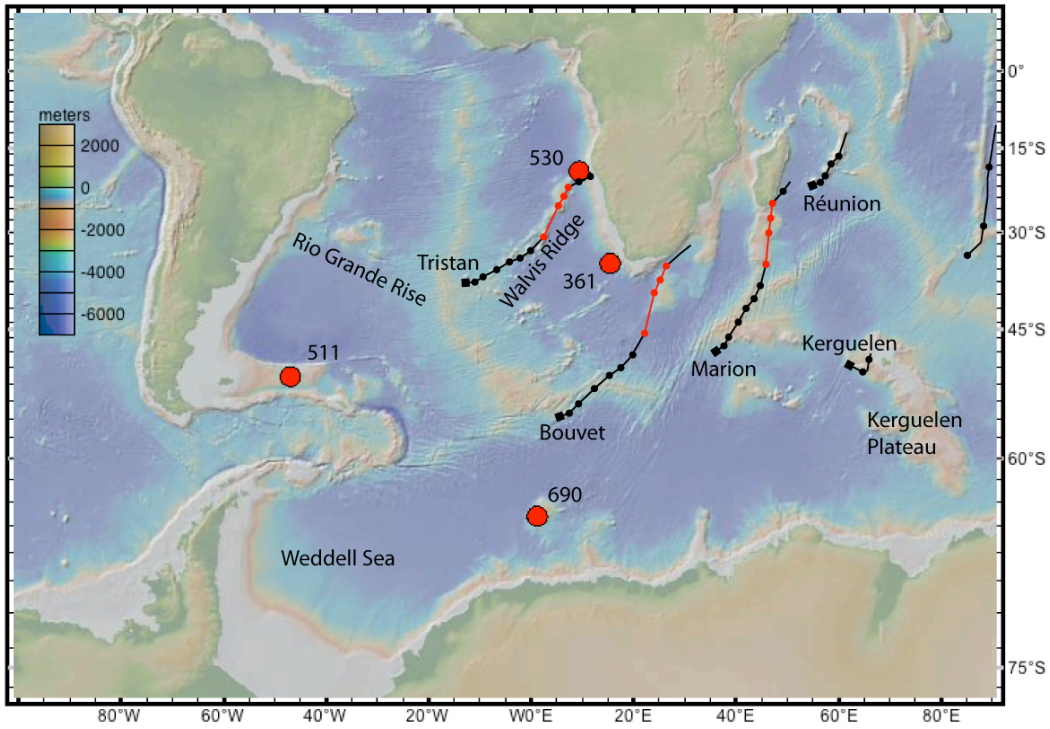

Figure 3-1. Present day location of DSDP Sites 361, 511, 530, and ODP Site 690 as well as relevant geographic features with bathymetry. Hotspot tracks from Duncan (1991). Boxes mark present location of labeled hotspots. Circles mark location every 10 Myr. Red portion of track emplaced during study interval. Map created using GeoMapApp version 2.4.2 (http://www.geomapapp.org/).

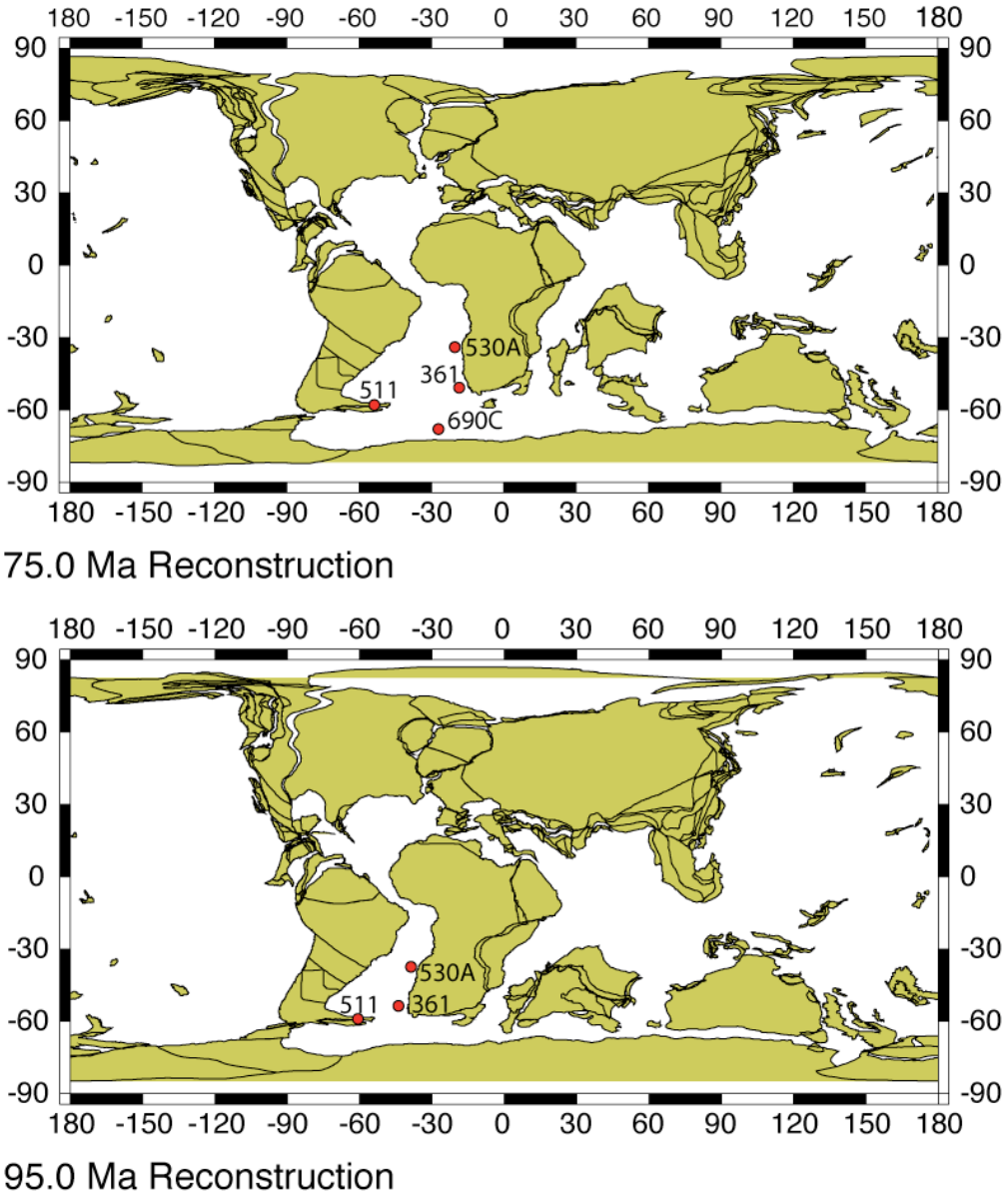

Figure 3-2. Paleogeographic reconstructions (Ocean Drilling Stratigraphic Network; http://www.odsn.de) of the late Campanian (~75Ma) and late Cenomanian (~95Ma) showing locations of Sites 361, 511, 530, and 690. Site 690 is not in the Cenomanian reconstruction as its underlying basement is Campanian in age. Boundaries are continental boundaries, not coastal boundaries.

attached to Antarctica, preventing any deep-water inputs from the Pacific, but the eastern boundary consisting of India, Madagascar, and the Kerguelen Plateau began to break up, no longer forming a continuous land bridge between Antarctica and Africa. While surface- and intermediate-water connections likely existed, there was likely little or no communication between the deep Atlantic and Indian Oceans until the Paleocene (Hay et al., 1999).

3. Methods

3.1 Site selection

We investigated four South Atlantic Deep Sea Drilling Project (DSDP) and Ocean Drilling Program (ODP) sites (Figure 3-1, Figure 3-2, Figure 3-3). Each site occupied a distinct basin during the Cenomanian, and these basins now share a common deep-water source.

DSDP Site 361 is located in the present day Cape Basin and has the deepest water depth through the study interval. During the Late Cretaceous, Site 361 was at a paleolatitude of ~50°S and a paleodepth of ~3500 m. The record from this site tracks the composition of deep-waters formed in the South Atlantic high-latitudes.

DSDP Site 511 (Falkland Plateau) is the southernmost site (paleolatitude ~ 60°S) (Huber et al., 1995). At a shallower paleodepth of ~1500 – 2000 m (Basov and Krasheninnikov, 1983), this site contributes to the reconstruction of water mass stratification.

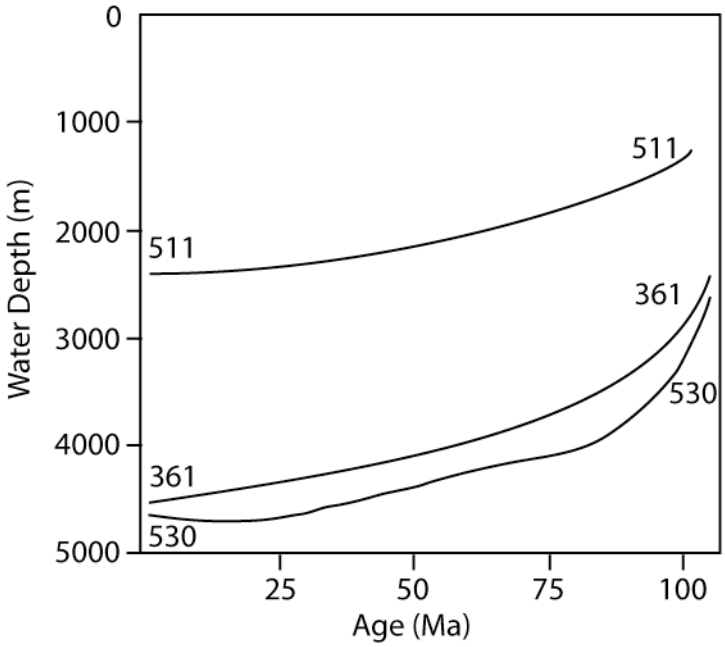

Figure 3-3. Subsidence histories from Sites 361, 511, and 530. After Melguen (1978), Basov and Krashen-innikov (1983), and Dean et al. (1984) respectively.

DSDP Site 530 is located in the present day Angola Basin, just north of Walvis Ridge near the African margin, and is the northernmost site (paleolatitude ~35-40°S) (Dean et al., 1984) in the study. The paleodepth during the Cenomanian was ~3000 m, but the site rapidly subsided throughout the Late Cretaceous, and by the mid-Campanian had a paleodepth of ~4500 m (Dean et al., 1984). The site also moved north less than 5° of latitude from the Cenomanian to the Campanian. This is the only site in this study to undergo significant subsidence through this interval. During the Cenomanian, Site 530 was isolated at depth from the sites further south by the Walvis Ridge/Rio Grande Rise complex. But as the igneous complex subsided, Site 530 provides the ideal location to examine changes in water exchange among the South Atlantic basins as well as between the Angola Basin and the Central Atlantic Gateway. Today, Walvis Ridge prevents Antarctic Bottom Water (AABW) from entering the Angola Basin from the south. Deep water enters the Angola Basin from the north through the Romanche Fracture Zone.

ODP Site 690 (Maud Rise), and during the Late Cretaceous, was located at paleolatitude (~65°S) and paleodepth (~1800 m) (D'Hondt and Arthur, 1996). This site provides a Southern Ocean end-member for comparison to the other intermediate depth sites (511).

We used existing age models for the four sites constructed using biostratigraphic, paleomagnetic, and Sr isotope datums (Table 3-1).

Table 3-1. DSDP and ODP Holes used in this study, as well as sources for age models.

Hole	361	511	530A	690C
Paleolatitude	45°S	60°S	35°S	65°S
Paleodepth	3500 m	1800 m	3000 m	1800 m
Age Model	(Davey, 1978)	(Huber et al., 2002)	(Keating and Herrero-Bervera, 1984)	(Barrera and Savin, 1999)

3.2 Tracing water masses with neodymium isotopes

The neodymium (Nd) isotopic composition of a water mass, expressed as ε_{Nd}, [the $^{143}Nd/^{144}Nd$ value of a geologic sample normalized to the bulk earth (DePaolo and Wasserburg, 1976)] reflects the isotopic composition of the rocks weathering into the water mass source region. Due to the short residence time (~1000 years; e.g. Tachikawa et al., 1999) relative to oceanic mixing (~1500 years), a water mass retains the Nd isotopic composition inherited from its source region with minor predictable changes caused by processes such as boundary exchange (Lacan and Jeandel, 2005b) and mixing. Temporal changes in the Nd isotopic composition at a given location can result from a change in water mass source region or a change in the composition of weathered material delivered to the water mass formation region.

Today, the ε_{Nd} of North Atlantic Deep Water (NADW) is ~ -14 (e.g. Piepgras and Wasserburg, 1987; Jeandel, 1993). NADW is the product of highly unradiogenic waters that convected in the Labrador Sea with relatively radiogenic waters that convected in the Norwegian-Greenland Sea (e.g. Goldstein and Jacobsen, 1987; Lacan and Jeandel, 2005a). In contrast, Antarctic Bottom Water (AABW) is more radiogenic (ε_{Nd} ~ -7 to -9) and reflects a combination of upwelled unradiogenic NADW and

radiogenic (ε_{Nd} ~ 0 to -5) Pacific surface waters (e.g. Piepgras and Wasserburg, 1982). During glacial intervals, when NADW production was reduced, AABW became more radiogenic, reflecting the greater proportion of Pacific surface waters (e.g. Piotrowski et al., 2005; Goldstein et al., 2007). In the Indian Ocean, AABW flows north, carrying the Southern Hemisphere signal with it (Jeandel et al., 1998; Goldstein et al., 2007). Intermediate depths in the Indian Ocean are more radiogenic than AABW as they contain a greater proportion of Pacific surface waters (Jeandel et al., 1998; Amakawa et al., 2000).

Biogenic apatite (fish teeth and bones) record and retain the ε_{Nd} signature of the water at the sediment/water interface where they were deposited (e.g. Staudigel et al., 1985; Reynard et al., 1999). Neodymium is incorporated into the apatite via an early diagenetic process and is resistant to post-depositional alteration.

The Nd isotopic composition of Cretaceous water masses is not well known, as the spatial coverage of available data is limited to only a handful of sites. No Cretaceous age South Atlantic values have been reported prior to this study, though Cenomanian North Atlantic values reported elsewhere (Pucéat et al., 2005; MacLeod et al., 2008) are more radiogenic than Paleogene South Atlantic values (Thomas et al., 2003; Scher and Martin, 2004; Via and Thomas, 2006). As in the Cenozoic, reported Pacific deep-water values are more radiogenic than Atlantic through the Cretaceous (Frank et al., 2005; MacLeod et al., 2008).

3.3 Sampling strategy

Sites 361, 511, and 530 were all sampled from the Cenomanian through the Campanian at an average resolution of ~550 kyr, ~330 kyr, and ~1.1 Myr respectively. Both Sites 361 and 511 have a regional hiatus representing ~3.5 Myr of sedimentation in the lower Campanian, and therefore the records at these sites lack early Campanian samples. The Cretaceous sedimentary sequence at Site 690 is relatively short because the basement age is Campanian, thus the record consists of only 6 samples taken at an average resolution of ~340 kyr.

Fish debris were picked from each sample. Replicate samples were also picked from at least one sample for each site to confirm reproducibility. All samples underwent an oxidative/reductive cleaning stage as described in Boyle (1981) with modifications as in Vance et al. (2004). The rare earth elements were isolated using RE Spec cation exchange chemistry, and then the Nd was separated from the other rare earth elements using methyllactic acid chemistry.

Samples analyzed at UNC-Chapel Hill were run as NdO^+ using a multi-collector VG Sector 54, and at Texas A&M on the Thermo Triton thermal ionization mass spectrometer as Nd^+. The procedural blank is ~15 pg and is considered negligible. Replicate samples analyzed at both UNC-Chapel Hill and Texas A&M University yielded values within error of each other. At UNC-CH, external analytical precision based upon replicate analysis of the international standard JNdi (Tanaka et al., 2000), analyzed as an oxide, yielded 0.512111 ± 11 ppm (n=30) which is calibrated relative to the La Jolla standard (0.511858) as 0.512116. Replicate analysis of the JNd_i standard

(n=28) on the TAMU Thermo Triton is currently 7.0 ppm (2σ) and the value is 0.51210156. Replicate analysis of the La Jolla standard (n=22) on the TAMU Triton yields a value of 0.5118459 at 6.2 ppm (2σ). All values are corrected for age and are presented as $\varepsilon_{Nd(t)}$ values.

4. Results

At the Cape Basin Site 361, $\varepsilon_{Nd(t)}$ values range from -4.7 to -6.9. Samples at the base of the analyzed section (~857 – 865 mbsf) record values that are more than one epsilon unit more radiogenic than the upper part of the record (Appendix 2, Figure 3-2, Figure 3-3). From ~479 – 815 mbsf, $\varepsilon_{Nd(t)}$ values lie consistently between ~-6.0 and -6.9.

DSDP Site 511, the intermediate water site on Falkland Plateau had $\varepsilon_{Nd(t)}$ values range from -4.2 to -6.7, with values decreasing upsection. A densely sampled portion of the record (29 samples over ~145 m; ~225 – 370 mbsf) yields values from -5.4 to -6.7.

The range of $\varepsilon_{Nd(t)}$ values recorded at Site 530 is greater than that from the other three sites. From ~990 – 913 mbsf, $\varepsilon_{Nd(t)}$ values range between -6.3 to -7.8. Over the interval 913 – 828 mbsf, $\varepsilon_{Nd(t)}$ values increase from -6.3 to a peak value of +3.4. From ~828 to 752 mbsf, values decrease to -8.2. The following ~104 m (~752 – 648 mbsf) are marked by a more gradual decrease of ~4 $\varepsilon_{Nd(t)}$ units to -11.1. Site 690 values from ~316 – 291 mbsf are between -9.7 and -10.2 epsilon units (Appendix 2, Figure 3-2, Figure 3-3).

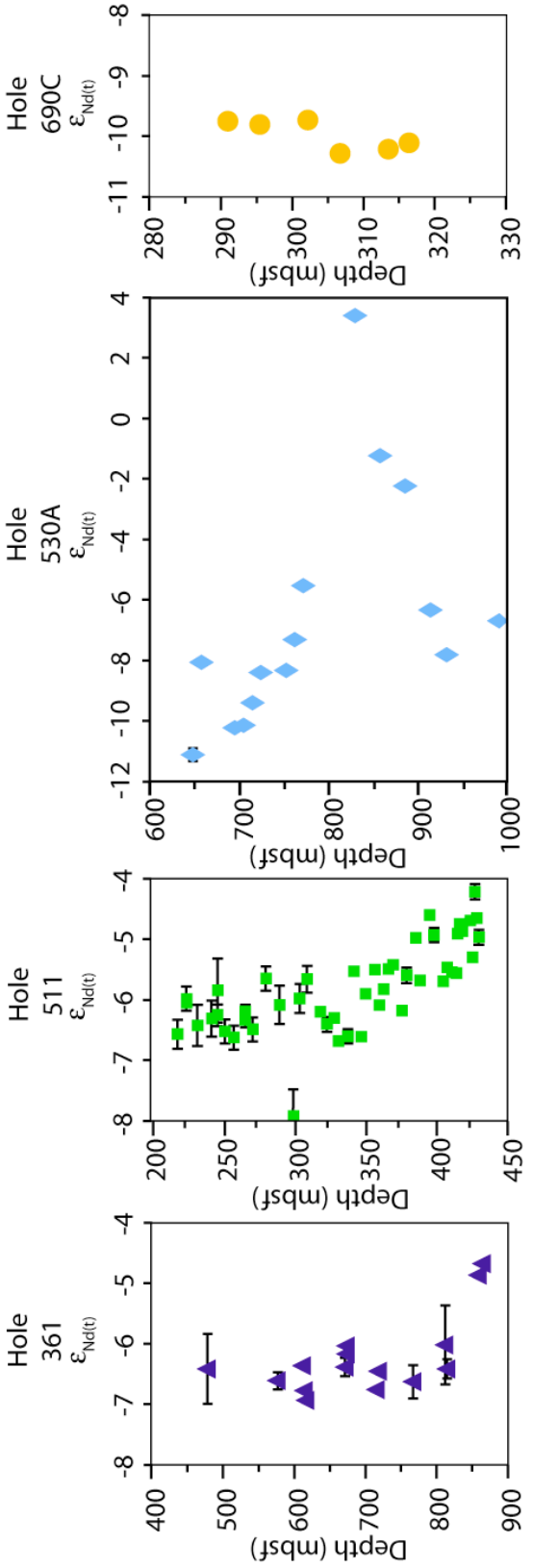

Figure 3-4. Nd isotopic results from Sites 361, 511, 530, and 690 plotted against depth in meters below seafloor.

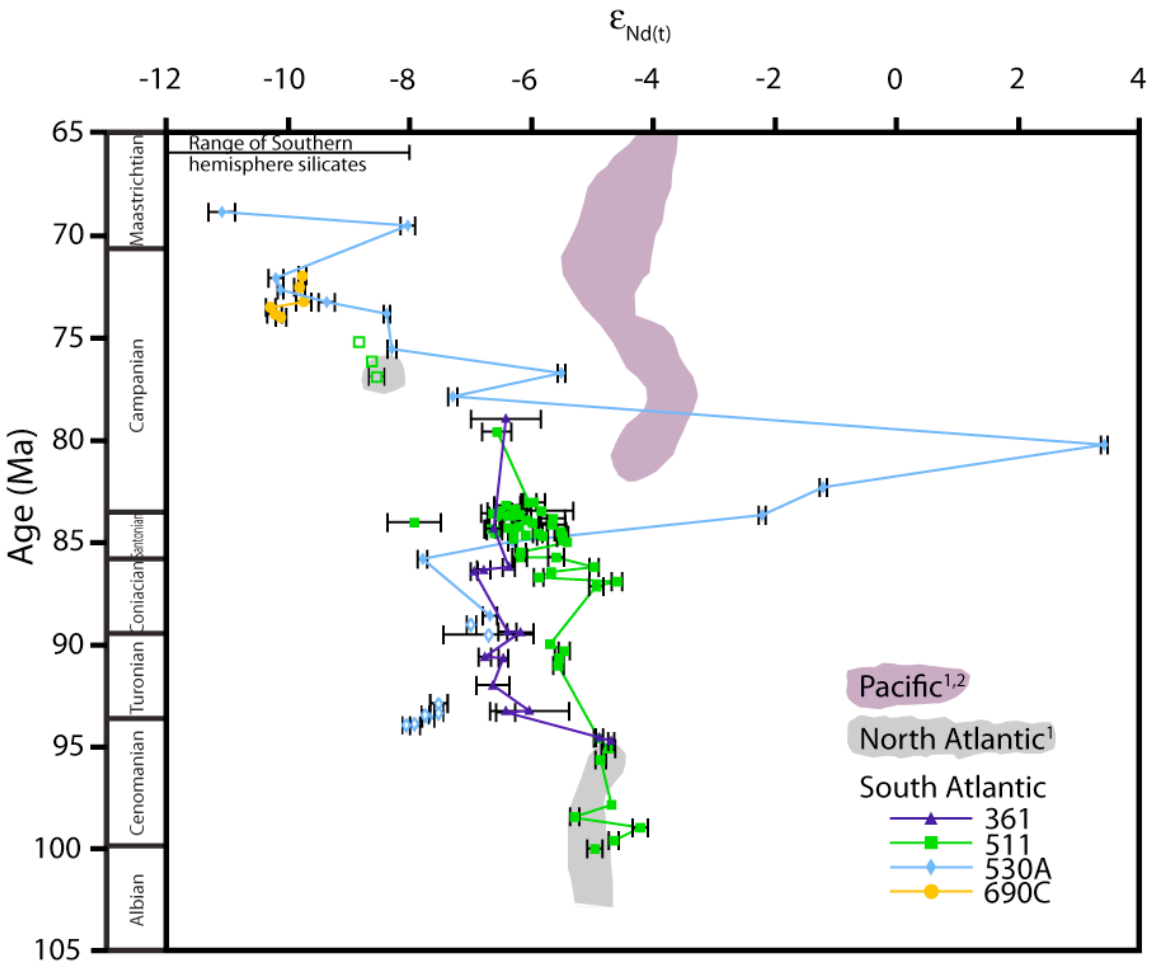

Figure 3-5. Nd isotopic results from Sites 361, 511, 530, and 690 plotted on a common time scale for comparison of trends. Notice the different values during the Cenomanian and the similar values during the Campanian. Hollow symbols for site 511 are from Robinson et al. (*submitted*). Pacific and North Atlantic ranges from: [1]MacLeod et al. 2008, [2]Frank et al. 2005. For information about age models, see Table 3-1.

5. Discussion

5.1. The Angola Basin Santonian – early Campanian excursion

The most prominent feature of the Site 530 record is a large radiogenic excursion of ~9.5 epsilon units beginning in the late Santonian and ending ~10 Myr later in the mid-Campanian. Peak $\varepsilon_{Nd(t)}$ values of +3.4 are the most radiogenic seawater values reported for the Mesozoic or Cenozoic. This excursion does not exist in the Site 361 and 511 records implying the feature may be local to the Angola Basin. However, a significant regional hiatus occurs in Sites 361 and 511 (Wise, 1983; Huber, 1992). Age model uncertainties could place the entirety of the excursion within this hiatus. Thus the excursion may or may not reflect a regional change. However, without evidence that the radiogenic excursion is directly related to the hiatus in Sites 361 and 511, we consider the event unique to Site 530.

Vocaniclastic turbidites found throughout this interval in Site 530 (Stow and Miller, 1980) point to active volcanism at Walvis Ridge. The volcaniclastic sediments in this interval have largely been altered to smectite clays, a process that would result in the leaching of Nd out of the volcanic sediments and into the water column. Sampled Walvis Ridge basalts $\varepsilon_{Nd(t)}$ values range from -1.0 to +1.8 (Richardson et al., 1982), thus the locally sourced volcaniclastic sediments had a Nd isotopic composition commensurate with the values recorded by the fish debris during the excursion (with the exception of the most radiogenic value in the record). However, replacement of the original seawater Nd isotopic signal in bottom waters through sedimentary leaching should only occur in the most extraordinary circumstances, in this case such

circumstances would have consisted of intense leaching of silicates that have isotopic values significantly different from that of seawater and an ocean basin with sluggish circulation. Sites 361, 511, or 690 likely did not experience such conditions, however, the large proportion of altered volcanic glass in Site 530 sediments and the restricted nature of the Angola Basin at this time suggests the excursion could have been generated by the locally derived volcanic Nd. When Angola Basin opened to the flow of southern sourced high-latitude deep waters, circulation in the basin became sufficiently vigorous to prevent leached Nd from dominating the local deep-water signal. The seawater Nd recorded by fish debris returned to "normal" seawater values within a single data point (2.3 Myr). Thus we conclude that the excursion was related to changes in local/regional weathering inputs rather than to any aspect of broader deep-water circulation.

It is also possible that the extremely radiogenic values recorded in Angola Basin reflect the isotopic composition of a locally formed water mass. The Etendeka traps were deposited in Angola by the Tristan hotspot 125 Ma (O'Connor and Duncan, 1990), providing a subaerially exposed source of radiogenic Nd that may have weathered into the region during the excursion. Weathering inputs from these radiogenic rocks would have increased the Nd isotopic composition of the local surface waters. Convection of radiogenic surface waters in the region may have been facilitated by high regional surface water salinities. The surface waters above Angola Basin were among the most saline during the Late Cretaceous (39.5 ppt; Brady et al., 1998). Thus salinity may have been a primary driver of circulation in the restricted Angola Basin during this time.

5.2. Temporal trends in water mass composition

With the four new Nd isotope records we can reconstruct the mid- to Late Cretaceous evolution of the intermediate- and deep-water mass composition in the Atlantic sector of the Southern Ocean (Figure 3-3). Where they overlap, the four records suggest a common long-term trend among the basins/regions of the South Atlantic, that of overall decreasing $\varepsilon_{Nd(t)}$ values from ~100Ma to ~68Ma. However transient differences among the sites (both in trend and absolute composition) may reflect changes in water mass stratification, basin connections, and weathering inputs.

The $\varepsilon_{Nd(t)}$ values at Sites 361, 511, and 530 are several epsilon units more radiogenic than expected based on the $\varepsilon_{Nd(t)}$ values of silicates weathered from any of the Southern Hemisphere continents (~-8 to -13; e.g. Goldstein et al., 1984; Bayon et al., 2004; Jeandel et al., 2007; Roy et al., 2007) during the Cenomanian to mid-Campanian. There are two possible explanations for this that are not necessarily exclusive of each other. The emplacement of numerous Large Igneous Provinces (LIPs) during the Cretaceous may explain this discrepancy. The peak activity of hotspots like Marion (Storey et al., 1995) and Kerguelen (Duncan, 1991) have been dated to this interval. In addition, both the Madagascar Plateau (the location of Marion hot spot during the Late Cretaceous) and Kerguelen Plateau were subaerially exposed during this time (Coffin, 1992; Storey et al., 1995), thus exposing newly deposited basalts to weathering which supplied dissolved radiogenic Nd into the Southern Ocean.

In addition, there may have been shallow, narrow connections between the South Atlantic and Pacific Oceans that permitted circulation of Pacific surface waters over the

Drake Passage into the South Atlantic. The contribution of Pacific Ocean surface waters would have increased the Nd isotopic composition of the South Atlantic surface waters. The weathering of the LIPs in the eastern portion of the South Atlantic Ocean, superimposed upon any contribution of Pacific surface water circulation into the basin, would have led to even more radiogenic surface waters.

Based on the relatively radiogenic composition of deep waters in the southern Atlantic basin, we suggest that deep-water convection occurred in the eastern portion of the Cape Basin (the southeastern segment of the Atlantic sector of the Southern Ocean). Surface waters in the South Atlantic and Southern Ocean during this time would have been more radiogenic to the east, due to close proximity of the proto-Indian Ocean LIPs. Emplacement of the southern portion of Kerguelen Plateau (south of ~54°S today) occurred from ~115 to ~101 Ma (Whitechurch et al., 1992). Subsidence models and the end of shelf deposition limit the time of subaerial exposure of most of the island to between ~11 and 20 million years (Coffin, 1992). Once below sea level, the LIPs would have ceased to contribute weathered Nd to the surface waters. Consequently, radiogenic Nd input from Kerguelen into the South Atlantic surface waters would have gradually decreased from the Cenomanian to the early Campanian. Final subsidence of the southern Kerguelen Plateau did not occur until the Paleocene, but it had become small enough to no longer significantly impact the South Atlantic Nd budget by the early Campanian (Coffin, 1992). Thus the long-term decrease in the composition of waters from $\varepsilon_{Nd(t)}$ values of ~-4 – -6 during the Cenomanian to <-10 in the Campanian suggests diminished input of radiogenic surface waters to the region of deep-water formation.

The Kerguelen hotspot was located under Broken Ridge during the Coniacian interval (Duncan, 1991) and this smaller feature likely only impacted regional Indian Ocean surface values.

The Nd isotope values from the two high latitude sites (Sites 361 and 511) reveal differences in the temporal evolution of the water mass composition (Figure 3-3). Before the Cenomanian/Turonian boundary, the ε_{Nd} values of the two sites are similar (based on two data points). We interpret the similar values as representing a single water mass that originated in the southeastern portion of the Southern Ocean as discussed above. However, near the Cenomanian/Turonian boundary the composition of waters at Site 361 shifted ~1.4 $\varepsilon_{Nd(t)}$ units toward less radiogenic values, and remained relatively constant to the early Campanian. Site 511 values gradually decreased before converging with the values at Site 361 during the Campanian. This difference created a transient offset of approximately one epsilon unit between the two sites spanning ~10 million years.

There are several possible interpretations for the Nd isotopic differences recorded at Sites 361 and 511. The offset may have been geochemical in nature (e.g., changes in local weathering inputs and particle scavenging), rather than oceanographic (e.g., changes in the location of water mass formation). In this case, the water mass at Sites 361 and 511 remained the same throughout the offset, but an increase in local unradiogenic material in the surface waters of the South Atlantic away from the LIPs may have led to more unradiogenic values at depth via particle exchange analogous to the modern North Pacific (e.g. Goldstein and Hemming, 2003). Particle exchange

occurs when Nd scavenged from surface waters bonded to particles is released at depth. This release can occur by respiration of particulate organic matter, or through dissolution of calcite or silica minerals. In theory, this process would have the greatest effect at deeper sites as falling particles have a greater time to dissolve. Thus Site 361 should have been affected more by potential particle exchange processes than Site 511.

Alternatively, the two sites may have experienced different water mass histories throughout the study interval. In this case, each site was situated in a different water mass with the same isotopic composition during the Cenomanian, the shallower Site 511 characterizing an intermediate-water mass and Site 361 a deep-water mass. Both water masses formed in the eastern portion of the high-latitude South Atlantic as discussed above. The westward movement of the deep-water convection site into a region of less radiogenic surface waters (further from the LIPs) near the Cenomanian/Turonian boundary drove the $\varepsilon_{Nd(t)}$ record to less radiogenic values in Site 361. A major reason that we believe deep waters formed in the eastern portion of the South Atlantic is the isolation of the eastern basin to surface water inputs. This remoteness could allow for the waters to become more saline than open ocean waters at the same latitude. However, models (Poulsen et al. 1999) project that with warming, precipitation would increase at the high latitudes. The one epsilon unit decrease occurs at the onset of the Turonian "super greenhouse", and deep-water convection may have shifted to the colder Weddell Sea as the eastern basin became fresher. The Weddell Sea would have still yielded radiogenic values, due to surface currents from the east, in addition to limited input from the Pacific Ocean surface waters, as discussed above. However, the distance from the

LIPs, combined with the contribution of Antarctic weathering inputs into the Weddell Sea would have lead to slightly less radiogenic surface waters than in the east. Eventually, the subsidence of the Kerguelen and Marion hotspots in the South Atlantic drove all surface waters to less radiogenic values (see above), causing the intermediate- and deep-water masses to share a similar composition again.

In order to understand the broader regional history of water mass composition and deep-ocean circulation patterns through the mid- to Late Cretaceous, we must now consider the record from Angola Basin Site 530, which was separated from the other deep site (Site 361) by Walvis Ridge. During the early Coniacian Nd isotope values of Site 530, both from this study and from Robinson et al. (*submitted*), were identical to those recorded at Site 361. However, this brief interval of convergence is likely not evidence of a common water mass based on existing tectonic constraints. The data alone cannot distinguish between water mass sources at Sites 361 and 530, however, despite the similar paleodepths, the Walvis Ridge/Rio Grande Rise Complex was closed below the upper-bathyal zone to ocean circulation prior to the Campanian (Dean et al., 1984; Frank and Arthur, 1999). If the deep Angola Basin were ventilated from southern-sourced water masses overtopping the Rio Grande Rise, the value would be similar to the shallower Site 511, rather than Site 361. It is more likely that the radiogenic surface waters found at the high-latitude South Atlantic was transported north via surface circulation and particle exchange delivering more local Nd to the seafloor, combined with sluggish circulation in the Angola Basin, led to similar values during the Coniacian.

During the late Campanian, $\varepsilon_{Nd(t)}$ values in Site 530 were more unradiogenic than the earlier part of the record. Values in the range of -8 to -10 match those found in Site 690. In addition, mid-Campanian values from Site 511 reported elsewhere (Robinson et al., *submitted*) also fall in this range. This suggests one of two possibilities. The first interpretation is that the intermediate- and deep-waters recorded by each of the sites may have had the same Nd isotopic composition coincidentally. $\varepsilon_{Nd(t)}$ values of the continental margins of Africa, South America, and Antarctica are broadly similar, and deep-water formation off any one of these sites could have yielded similar values (e.g. Goldstein et al., 1984; Bayon et al., 2004; Jeandel et al., 2007; Roy et al., 2007). Alternatively, during the Campanian Sites 361, 511, and 530 began to share a common water mass.

The simplest explanation of the data is the interpretation that all three sites were located in the same water mass by the Campanian. The subduction of the Walvis Ridge/Rio Grande Rise complex through the Late Cretaceous allowed the communication of deep-water between the central South Atlantic and the Southern Ocean sector of the Atlantic. Walvis Ridge likely remained a barrier to deep-ocean circulation, as it is today. However, the subduction of the Rio Grande Rise allowed communication between the Southern Ocean and the western South Atlantic, and deep-waters could have flowed into Angola Basin through a fracture zone. The similarity of the values from 511, 530, and 690 reinforces this idea. The common $\varepsilon_{Nd(t)}$ decrease recorded at all three sites is therefore evidence of a single water mass. In addition, the unradiogenic values recorded by all investigated sites during the Campanian likely

reflect weathering inputs from the southern continents (e.g. Bayon et al., 2004; Roy et al., 2007; Figure 3-3), further confirming the hypothesis of proto-Southern Ocean sourced deep-waters, rather than circulation from the tropics or North Atlantic. The $\varepsilon_{Nd(t)}$ values are more radiogenic than those that would be expected from a North Atlantic source (~-14).

A common water mass began circulating among the basins of the South Atlantic during the Campanian, thus establishing the onset of connected thermohaline circulation based on deep-water formation in the Southern Ocean. We cannot establish a more precise chronology for this event due to a prominent excursion and gaps in the three long-term records. The timing of the water mass convergence at Site 530 is obscured by a radiogenic excursion (see discussion below) over-printing the water mass signal. In addition, Site 690 is too young to identify the timing of the change, and a hiatus in Sites 361 and 511 spans the majority of the transition. However, sometime between ~79 Ma and ~75 Ma Rio Grande Rise no longer impeded deep-water flow among the basins. The timing we have identified based on the new Nd isotope records is earlier than the Maastrichtian age of opening below ~2000 m estimated from stable isotope records (Frank and Arthur, 1999). The common water mass identified at all four sites fills the deep ocean to at least ~1800 m (the paleodepths of Sites 511 and 690). This would allow the deep-water formed in the South Atlantic to flow over the Rio Grande Rise, and sink to depth, analogous to ventilation of the Caribbean basin today. The data presented here capture the early opening of the Rio Grande Rise before fully opening to bottom waters. Deep-water production in the South Atlantic by mechanisms similar today had

been established by the Paleogene (Thomas et al., 2003; Via and Thomas, 2006). The data we present here extend the record of Southern Ocean deep-water formation back to at least the mid- to late-Campanian.

The South Atlantic Ocean data presented here shares broad similarities to the pattern in the North Atlantic Ocean (Figure 3-3), as recorded at Blake Nose (30º06'N 76º14'W; MacLeod et al., 2008). Due to the tectonic barriers during the Cenomanian (Central Atlantic Gateway, Walvis Ridge/Rio Grande Rise), the deep waters in the North Atlantic Ocean were probably not the same as those in the South Atlantic Ocean. We believe the values are coincident, and reflect an input of Pacific sourced surface waters to the area of deep-water formation that filled the North Atlantic Ocean at this time. However, by the Campanian both tectonic barriers separating deep-water flow from the South Atlantic Ocean to the North have subsided, thus the similar values likely reflect a common water mass sourced in the high-latitude South Atlantic Ocean.

5.3. Orbital variations in ocean circulation

Nd isotope variations from the densely sampled portion of Site 511 suggest the possibility of 800 kyr variations in the composition of waters in the western South Atlantic (Figure 3-4). From ~84.9 to ~84.5 Ma, $\varepsilon_{Nd(t)}$ values are ~ -5.6. At ~84.5 Ma, a sudden shift to less radiogenic values of ~1.0 $\varepsilon_{Nd(t)}$ units establishes a new stable state at ~ -6.6, then returns to ~ -5.6 at ~84.1 Ma. This same trend and timing also appears to characterize the record from ~84.1 to ~83 Ma, however, the greater internal error on those samples complicates the interpretation of low amplitude variations. Orbitally-paced changes in deep-water mass composition are known from other intervals of

geologic time, notably the late Pleistocene. During the glacial-interglacial 100 kyr cycles of the late Pleistocene, the deep-water composition of the Cape Basin fluctuated by up to 2.5 epsilon units (Piotrowski et al., 2005), reflecting changes in the relative proportions of NADW and AABW. The ~1 epsilon unit changes in deep-water composition during the Santonian portion of our record is paleoceanographically significant (e.g., the amplitude of change may reflect changes in water mass composition). However, the connection to orbital parameters is unclear. Regardless, Site 511 features one epsilon unit variations on an 800 kyr period, that may be orbitally induced.

6. Conclusions

1. Deep-water formation in the high-latitude South Atlantic occurred throughout the Late Cretaceous, but the presence of a number of boundaries to deep-water circulation did not permit widespread circulation of this water mass.

2. The subsidence of the Kerguelen Plateau caused the gradual shift in $\varepsilon_{Nd(t)}$ values to less radiogenic values.

3. The opening of the Rio Grande Rise to deep water circulation allowed this water mass to flow north into the rest of the South Atlantic basin between ~75-79 Ma.

4. Deep-water circulation may have been impacted by orbital cycles, as seen in Site 511.

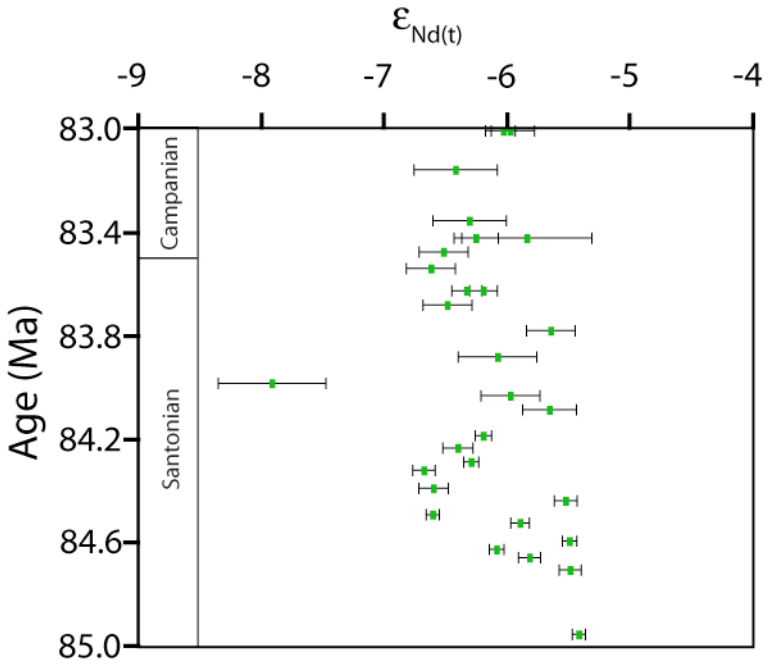

Figure 3-6. Expanded Nd isotopic results for Site 511 from ~83-85 Ma. Notice the periodic changes of approximately one epsilon unit. These changes are on the order of half the glacial/interglacial change in the South Atlantic today and may be reflecting orbitally induced changes in deep-ocean circulation.

CHAPTER IV

DEEP-WATER CONNECTIONS BETWEEN THE PACIFIC AND INDIAN OCEANS

Little is known about ocean circulation during the greenhouse climate of the Cretaceous. Different oceanographic and tectonic boundary conditions during the Cretaceous prevent a direct comparison to modern oceanic circulation, which modulates climate by the sinking of cold, dense waters in the North Atlantic and Southern Ocean. However, during the Cretaceous, the northern basins of the North Atlantic did not yet exist. In addition, the South Atlantic Ocean basin was not connected to the other oceans at depth, preventing the formation of a global deep-ocean circulation scheme. Thus to begin to reconstruct the evolution of the deep-ocean system we must examine each major ocean basin separately. Here we use new Nd isotope data from a depth transect of three sites on the western Australian margin to reconstruct ocean circulation in the proto-Indian Ocean. Our data suggest that during the Cenomanian, deep water formed in the Southern Indian Ocean, and by the late Cenomanian Pacific-sourced deep waters reached the deep sites, joined by intermediate waters ~5 My later. This new circulation regime persisted for ~20 Myr. Deep-water formation resumed in the Southern Indian Ocean during the mid Campanian.

1. Introduction

One of the biggest question marks in climate science today is how the planet will respond to a greenhouse gas forcing several times higher than today, as projected for the next century in the IPCC reports (IPCC, 2007). During the Late Cretaceous,

atmospheric carbon dioxide levels were estimated to have been 2-5 times higher than modern levels (e.g. Royer et al., 2004; Berner, 2006). The early part of the Late Cretaceous was also the warmest interval of the last 100 Myr with sea surface temperatures ranging from 36°C in the tropics (e.g. Pearson et al., 2001; Norris et al., 2002; Wilson et al., 2002) to 20°C in the southern high latitudes (Huber et al., 1995). The resulting diminished meridional temperature gradient is a characteristic of greenhouse climates, yet it is unclear how greenhouse climate dynamics produce and maintain such low gradients.

As discussed in Chapter I, ocean circulation plays an important role in the redistribution of captured incoming solar radiation, and our goal is to understand the relative importance of deep-ocean circulation in the climate dynamics of greenhouse intervals. Because so little is known about the manner in which the deep oceans operated during the Late Cretaceous, we must determine the composition of intermediate- and deep-water masses as a necessary first step in reconstructing the pattern of deep-ocean circulation. Only after we have established where and how deep waters formed, and how they circulated, can we begin to assess the relative importance of such circulation in greenhouse climate dynamics.

To that end, we have reconstructed the history of individual ocean basins using Nd isotopes. Here, we investigate three sites from the Indian Ocean during the mid Late Cretaceous (Cenomanian – Campanian; ~100 – 70 Ma) to reconstruct changes in deep-water circulation within the Indian Ocean.

1.1. Mid to Late Cretaceous boundary conditions of the proto-Indian Ocean

The paleogeography of the Cenomanian (93.5 – 99.6 Ma) proto-Indian Ocean differed from the present boundary conditions (Figure 4-1, Figure 4-2). The northern portion of the basin, the Tethys Sea, was open to the Atlantic. A landmass that consisted of India, Madagascar, Kerguelen Plateau, Broken Ridge, Mascarene Plateau, and the early Ninetyeast Ridge bounded the southern portion of the proto-Indian Ocean to the south and west (Hay et al., 1999), isolating the southern region from the Atlantic sector of the Southern Ocean. The eastern boundary of the southern basin was partially blocked by Australia, which was still connected to Antarctica, to the south and southeast Asia to the north. Between these two partial barriers lay the eastern Tethys with an opening into the Pacific greater than 3,000 km wide.

The breakup of the India/Madagascar/Kerguelen landmass over the following ~30 Myr created a more complex system of basins within the proto-Indian Ocean. Rifting and seafloor spreading created several marginal basins, such as that between Kerguelen and India and between India and Africa. This tectonic activity also moved the Indian sub-continent north several thousand kilometers as the northern portion of the Indian plate subducted beneath Asia. While surface- and intermediate-water connections likely existed, there was likely little to no communication between the deep Atlantic and Indian Oceans until the Paleocene (Hay et al., 1999).

1.2. Tracing water masses with neodymium isotopes

Today, the ε_{Nd} of North Atlantic Deep Water is ~ -14 (e.g. Piepgras and Wasserburg, 1987; Jeandel, 1993). NADW is the product of highly unradiogenic waters

convected in the Labrador Sea with relatively radiogenic waters convected in the Norwegian-Greenland Sea (e.g. Goldstein and Jacobsen, 1987; Lacan and Jeandel, 2005a). In contrast, Antarctic Bottom Water is more radiogenic (ε_{Nd} ~ -7 to -9) and reflects a combination of upwelled unradiogenic NADW and radiogenic Pacific surface waters (Piepgras and Wasserburg, 1982). In the Indian Ocean, AABW flows north, carrying the Southern Hemisphere signal with it (Jeandel et al., 1998; Goldstein et al., 2007). Intermediate depths in the Indian Ocean are more radiogenic than AABW as they contain a greater proportion of Pacific surface waters (Jeandel et al., 1998; Amakawa et al., 2000).

Biogenic apatite (fish teeth and bones) record and retain the ε_{Nd} signature of the water at the sediment/water interface where they were deposited (e.g. Staudigel et al., 1985; Reynard et al., 1999). Neodymium is incorporated into the apatite via an early diagenetic process and is resistant to post-depositional alteration (Person et al., 1995; Martin and Scher, 2004).

The Nd isotopic composition of Cretaceous water masses is not well known, as the spatial coverage of available data is limited to a handful of sites. Only four Cretaceous age South Atlantic records exist (see Chapter III). South Atlantic $\varepsilon_{Nd(t)}$ values at the beginning of the Late Cretaceous were more radiogenic than during the Paleogene, but subsequently became more unradiogenic and representative of a common southern high-latitude deep-water mass (Thomas et al., 2003; Scher and Martin, 2004; Via and Thomas, 2006). Cenomanian North Atlantic values (Pucéat et al., 2005; MacLeod et al., 2008) were more radiogenic than contemporaneous South Atlantic

values. The opening of gateways (Central Atlantic Gateway and Rio Grande Rise) allowed deep-waters sourced in the South Atlantic high latitudes to reach the North Atlantic, producing lower $\varepsilon_{Nd(t)}$ values during the Campanian (Chapter III). Pacific values were more radiogenic than Atlantic through the Cretaceous (Frank et al., 2005; MacLeod et al., 2008).

The data we present in this chapter represents the first mid to Late Cretaceous Nd isotope data from the proto-Indian Ocean. Prior to this study, the record of proto-Indian Ocean water mass composition extended only back into the early Paleogene, with Indian Ocean $\varepsilon_{Nd(t)}$ values similar to those from the South and North Atlantic, but less radiogenic than the Pacific (Thomas et al., 2003).

2. Methods

2.1. Site selection

We investigated three Ocean Drilling Program (ODP) sites that form a depth transect on the western margin of Australia (Figure 4-1, Figure 4-2). Site 763 (Exmouth Plateau; 45°S paleolatitude, 1000 m paleodepth) (Haq et al., 1992) sat at intermediate depths during the Cretaceous. Bathyal and abyssal depths characterize Sites 766 and 765 (paleolatitudes: 45°S and 40°S; paleodepths: 3000 m and 4000m), (Gradstein, 1992; Gradstein et al., 1990) from Exmouth Plateau and Argo Abyssal Plain. We determined ages by linearly interpolating sedimentation rates between biostratigraphic datums for all three sites (Table 4-1).

2.2. Sampling strategy

We sampled the Cenomanian through the Campanian time interval at Sites 763, 765, and 766. Sampling resolution was approximately one sample every ~7.8 meters (~1 Myr), ~3.6 meters (~2.5 Myr), and ~2 meters (~1 Myr) respectively.

Fish debris were picked from each sample. Replicate samples were also picked from one sample from Site 765 and five samples from Site 766 to confirm reproducibility. All samples underwent an oxidative/reductive cleaning stage as described in Boyle (1981) with modifications as in Vance et al. (2004). The rare earth elements were isolated using RE Spec cation exchange chemistry, and then the Nd was separated from the other rare earth elements using methyllactic acid chemistry.

Samples at UNC-Chapel Hill were run as NdO^+ using a multi-collector VG Sector 54, and at Texas A&M on the Thermo Triton thermal ionization mass spectrometer as Nd^+. The procedural blank is ~15 pg and is considered negligible. Replicate samples analyzed at both UNC-Chapel Hill and Texas A&M University yielded values within error of each other. At UNC-CH, external analytical precision based upon replicate analysis of the international standard JNdi (Tanaka et al., 2000), analyzed as an oxide, yielded 0.512111 ± 11 ppm (n=30). Replicate analysis of the JNd_i standard (n=28) on the TAMU Thermo Triton is currently 7.0 ppm (2σ) and the value is 0.51210156. Replicate analysis of the La Jolla standard (n=22) on the TAMU Triton yields a value of 0.5118459 at 6.2 ppm (2σ). All values are corrected for age and are presented as $\varepsilon_{Nd(t)}$ values.

Table 4-1. DSDP and ODP Holes used in this study, as well as sources for age models.

Hole	763B	765C	766A
Paleolatitude	45°S	40°S	45°S
Paleodepth	1000 m	4000 m	3000 m
Age Model	(Clarke and Jenkyns, 1999)	(Kaminski et al., 1992; Lees, 2002)	(Clarke and Jenkyns, 1999; Robinson et al., *submitted*)

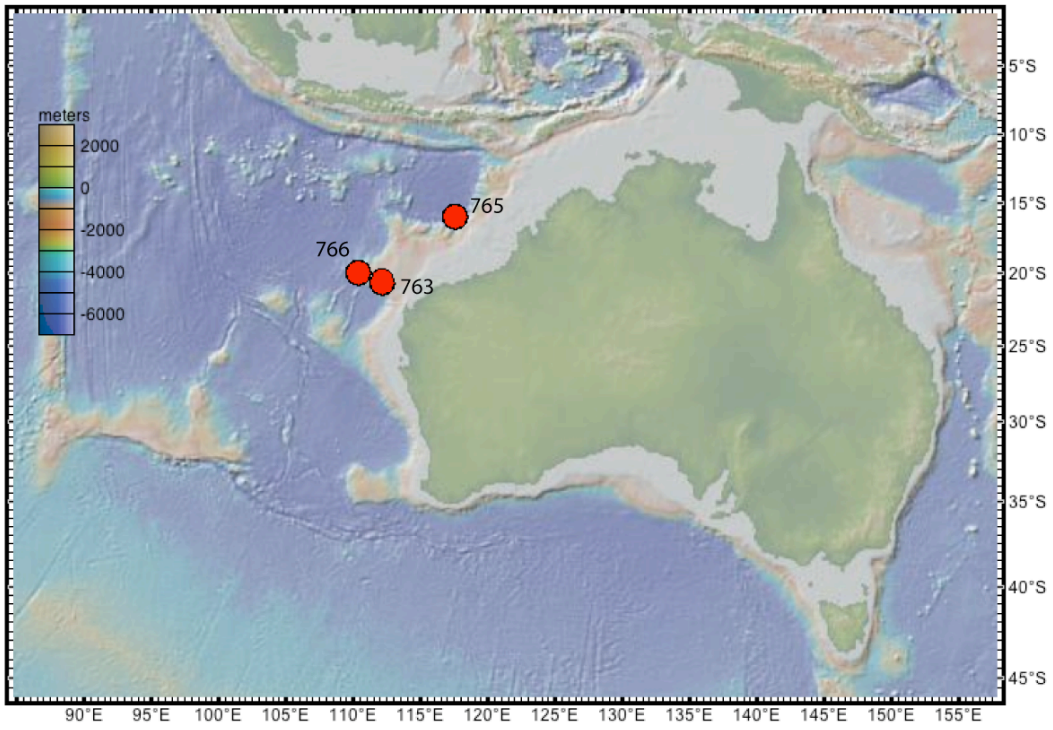

Figure 4-1. Present day locations of Ocean Drilling Sites 763, 765, and 766 with bathymetry. Map created with GeoMapApp version 2.4.2 (http://www.geomapapp.org/)

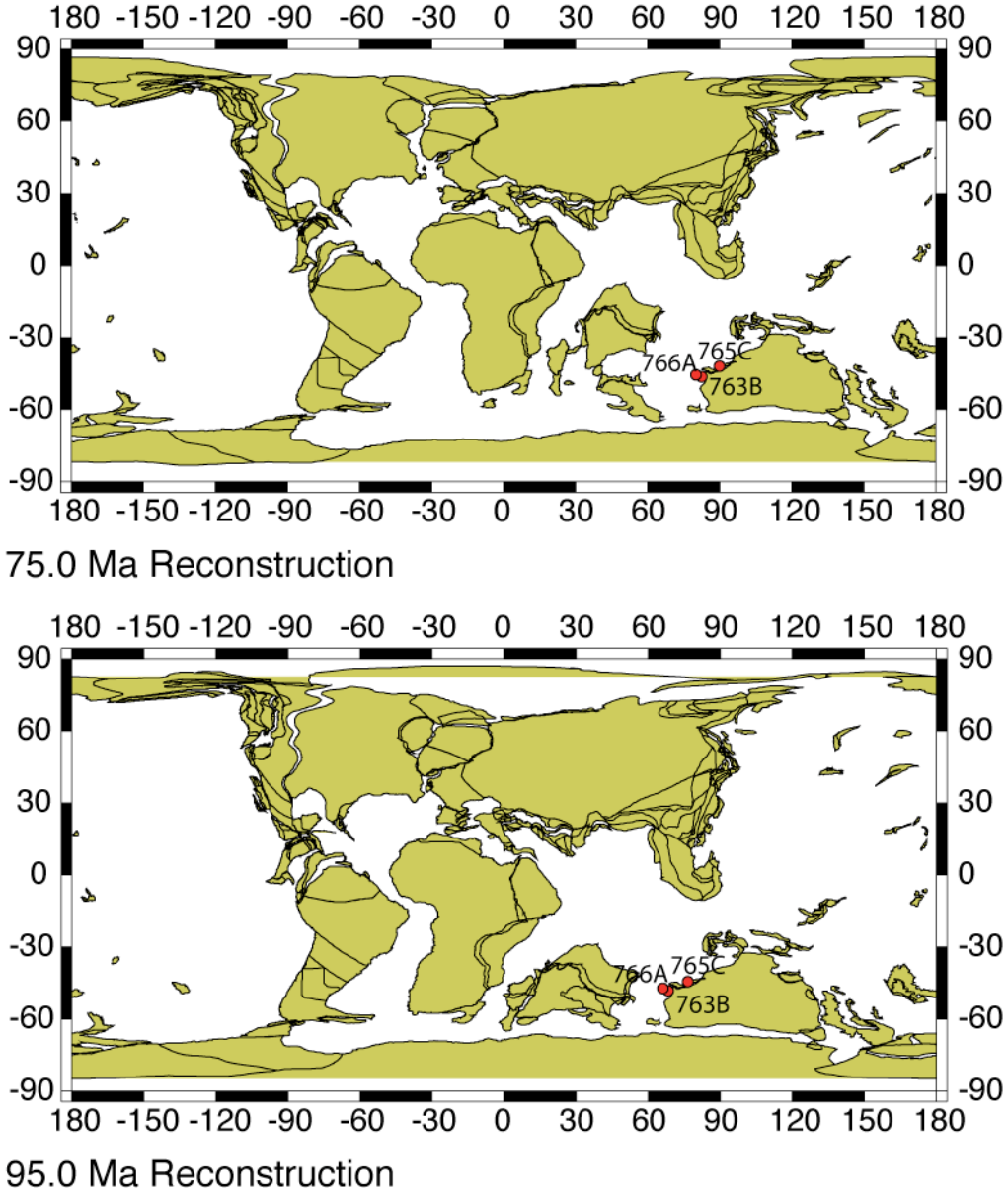

Figure 4-2. Paleogeographic reconstructions (Ocean Drilling Stratigraphic Network; http://www.odsn.de) of the late Campanian (~75Ma) and late Cenomanian (~95Ma) showing locations of Sites 763, 765, and 766. Boundaries are continental boundaries, not coastal boundaries.

3. Results

Site 763 $\varepsilon_{Nd(t)}$ values range from -7.2 to -11.3 (Appendix 3; Figure 4-3, Figure 4-4). Over the interval 405.4 to 323.9 mbsf, $\varepsilon_{Nd(t)}$ values increase by ~3.4 epsilon units, peaking at ~-7.7. Superimposed on this long-term increase is a radiogenic excursion to ~-7.2 epsilon units at 362.7 mbsf. From 323.9 to the top of the record at 257.4 mbsf $\varepsilon_{Nd(t)}$ values decrease to ~-11.3.

Nd isotope data from ODP Site 765 range from ~-7.3 to -10.3 (Appendix 3; Figure 4-3, Figure 4-4). From ~594.2 to ~590.7 mbsf $\varepsilon_{Nd(t)}$ values are stable from ~ -8.4 to -8.2. Values become more radiogenic upsection from 590.7 to 585.4 mbsf, peaking at -7.3 epsilon units. From 585.4 to 565.8 mbsf (the top of the analyzed section), $\varepsilon_{Nd(t)}$ values generally decrease to -10.3.

$\varepsilon_{Nd(t)}$ values recorded at ODP Site 766 vary from ~ -10.1 to ~ -5.3 (Appendix 3; Figure 4-3, Figure 4-4). Values at the base of the analyzed section (~ 150.6 – 138.8 mbsf) are relatively constant between ~ -7.8 to -8.5. Between 138.8 mbsf and 126.0 mbsf, $\varepsilon_{Nd(t)}$ values generally increase to ~ -5.3. From 126.0 to 105.9 mbsf, values decrease to ~-10 and remain constant to the top of the analyzed section at 97.4 mbsf.

4. Discussion

4.1. Evolution of proto-Indian Ocean water mass composition

Comparison of the trends and values recorded at the three sites enables us to reconstruct the history of both the intermediate and deep waters in the eastern portion of the Cretaceous Indian Ocean. Site 763 was located at ~1000m water depth, while Sites 765 and 766 were situated at ~3000m and 4000m, respectively, throughout the

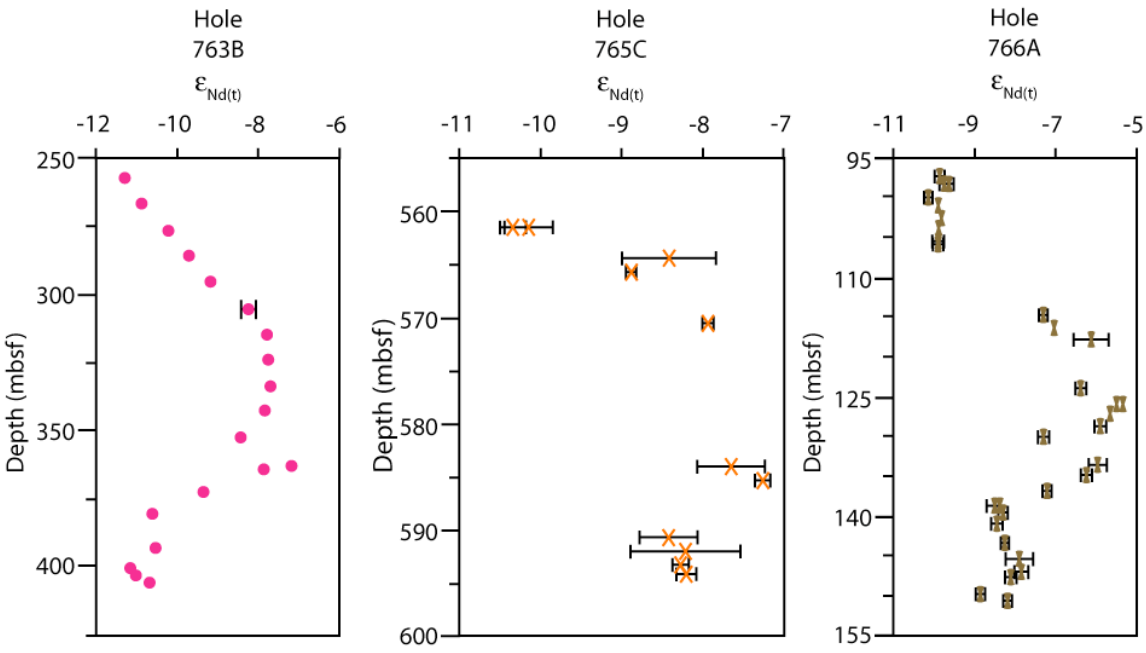

Figure 4-3. Nd isotopic results from Sites 763, 765, and 766 plotted against depth in meters below seafloor.

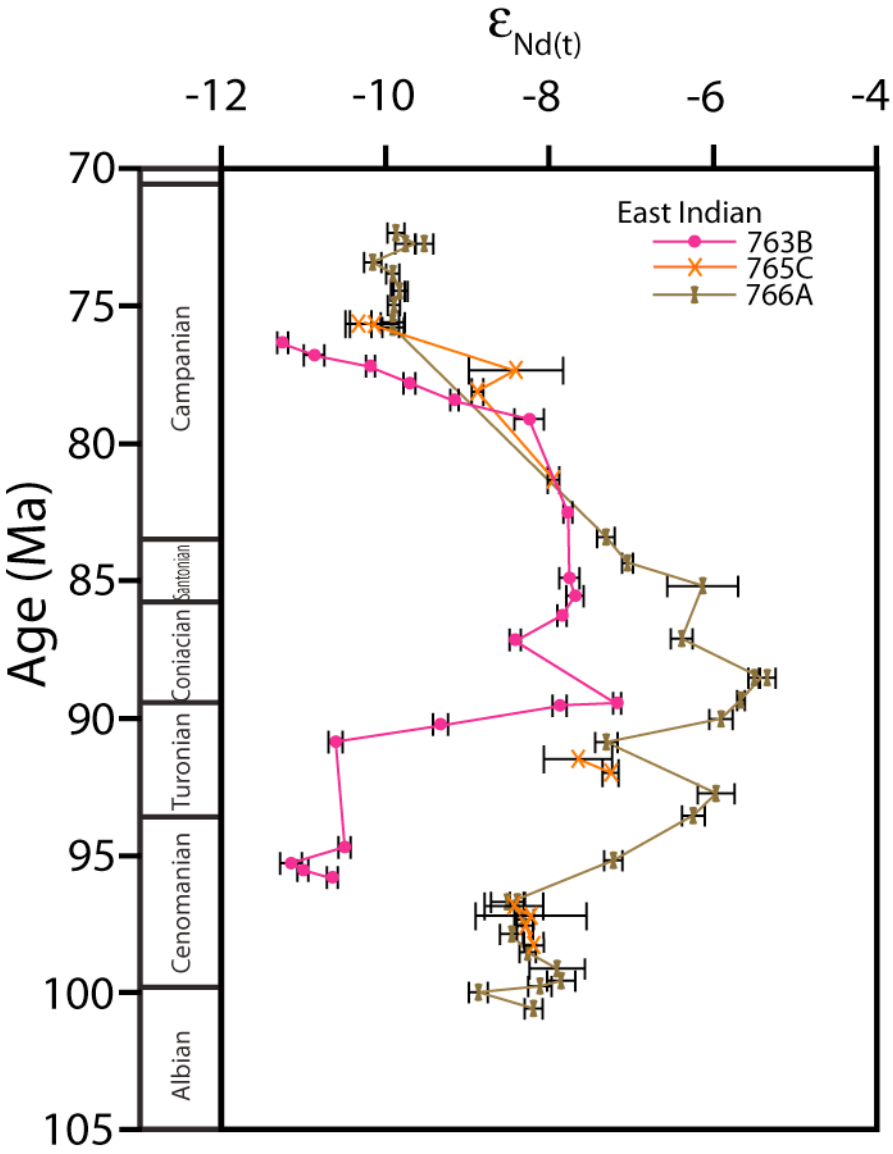

Figure 4-4. Nd isotopic results from Sites 763, 765, and 766 plotted versus age. Notice the similar values during the Cenomanian and the Campanian in Sites 765 and 766 and similarity in the size of the radiogenic shift in 763 and 766. For information about age models, see Table 4-1.

Cretaceous. In spite of the significant depth range encompassed by the three sites, the Nd isotope trends recorded have similar shapes, although the values recorded at the deeper sites were more radiogenic than the shallow site.

The most striking feature of the combined records is the shift in Nd isotopic composition to more radiogenic values during the first half of the study interval, followed by a shift back to lower, more unradiogenic values during the younger portion of the records. While the initial portion of the radiogenic shift is not evident in the Site 765 record, this is likely due to the gaps in the stratigraphy – the portions of the records that are contemporaneous with Site 766 samples are identical thus there is no reason to suspect that the missing portion of the Site 765 record was different from Site 766. Site 763 records the same radiogenic shift, but the Nd isotope values are less radiogenic. It is interesting to note that the onset of the radiogenic shift appears to have occurred earlier in the deep waters, however closer inspection of the records suggests that the corresponding time interval in the Site 763 record may be missing. Again, the similarity in trends exhibited by the portions of the records that cover the same time interval suggests that all three sites experienced the same changes in Nd isotope composition. Thus, in spite of the Nd isotope differences between Sites 763 and 765/766, we interpret the data to reflect a common history of the water mass(es) for the three sites encompassing the depth range of at least 1000 to 4000m.

During the younger portion of the record (Santonian to early Campanian), Nd isotope values at all three sites decreased. While the earlier radiogenic shifts in Sites 763 and 766 are of similar magnitude (~3.2 epsilon units), the unradiogenic shift that

began during the Santonian is smaller in Site 763 (~3.5 epsilon units to ~3.8 epsilon units). However, the records from Sites 763 and 765 do not extend through the latter portion of the Campanian, and therefore those records may not reflect the entirety of the Nd isotope decrease that was recorded at Site 766 which indicates a consistent isotopic composition during the late Campanian of ~-10. Since our record does not reach a consistent value in Site 763 as in Site 766, we believe that the entire unradiogenic shift is not present in our record, and late Campanian $\varepsilon_{Nd(t)}$ values at Site 763 are closer to -11.6, an offset of ~1.7 epsilon units from Site 765 and 766 late Campanian values. Our interpretation of this offset is discussed below.

The similar trends recorded by all three sites in the eastern proto-Indian Ocean suggest a common water mass, however Nd isotope values at the shallowest location, Site 763, are consistently ~2 epsilon units lower than the two deeper sites. This may be due in large part to the fact that Site 763 recorded much higher rates of terrestrial input from the unradiogenic Australian continent (Elburg et al., 2002). Because the water depth at Site 763 was relatively shallow (~1000m), the water mass at that depth may have been impacted by vertical mixing with a shallower water mass that had lower Nd isotope values due to weathering inputs from the Australian continent; similar to the susceptibility of NADW to isotopic imprints from waters above (von Blanckenburg, 1999). Alternatively, the source of the intermediate depth water at Site 763 was different from that of the deep water at Sites 765 and 766, and that water mass had a less radiogenic signature. The common trends among the sites suggest that one process produced the trends in the Nd isotopic values at each site. The most straightforward

explanation for such a process would have been that both water masses originated in the same general region (i.e. the same marginal sea), even though they may have experienced different formation histories. Thus any change to the Nd weathering inputs or delivery of surface water Nd to that region would have impacted both water masses proportionally. However, because the two potential water masses formed in the same region, they will be treated as one water mass for the purposes of circulation, ventilation, and heat transport for the rest of this paper. No data constraining the regional surface water Nd isotopic composition or circulation patterns exist yet to distinguish between these two possibilities.

It is important to note that correlations among the three sites depend on the age model used for each site. For example, both Clarke and Jenkyns (1999) and Robinson et al. (*submitted*) developed age models for Site 766. The Clarke and Jenkyns (1999) age model places the two major isotopic shifts ~1.5 Myr and ~3.6 Myr later than the model used by Robinson et al. (*submitted*). We used the age model developed in Robinson et al. (*submitted*) for our discussion, however, correlation of the smaller-scale features among the three Nd isotope records sensitive to changes in the age model.

While the correlation of smaller-scale features may be hindered by the selection of the age model, the first order features demonstrated by the three records indicate a change from relatively unradiogenic values, to radiogenic values, and then back to relatively unradiogenic values. This pattern suggests a fundamental change in the mode of deep-ocean circulation.

4.2. Implications for regional and global deep-ocean circulation

The temporal and spatial patterns of Nd isotope values in the eastern Indian Ocean are best explained by a change in the composition of intermediate and deep waters that circulated in the region. The unradiogenic values that characterize the Cenomanian portion of the record are likely derived from water mass formation in the high-latitude southern portion of the Indian Ocean, possibly in the marginal sea between Kerguelen and Australia (Figure 4-2). The $\varepsilon_{Nd(t)}$ values during this time are similar to those predicted from Indian/Australian/Antarctic margin silicates (Colin et al., 1999; Elburg et al., 2002; Roy et al., 2007). The western side of Australia was a more likely region of deep-water formation than the eastern side based on hydrographic and geochemical constraints. While the temperature gradients on either side of the continent were likely similar, the marginal sea on the western margin could have been more saline seasonally or permanently than the open ocean sites on the eastern margin. Second, while the ε_{Nd} values of the rivers that drained into the South Pacific from Australia and Antarctica would have been similar to those on the other side of Australia, there would have been significant contribution of radiogenic Nd from the North Pacific in the surface waters to the east of Australia.

The radiogenic Nd isotope values that characterize the late Cenomanian through Santonian interval may have resulted from increased weathering of radiogenic Nd into the south Indian Ocean from nearby Large Igneous Provinces (LIPs), without a concomitant change in the source of deep waters. During the Late Cretaceous, the Kerguelen Plateau was subaerially exposed (Duncan, 1991; Coffin, 1992). Data from

the South Atlantic suggests that radiogenic Nd from LIP weathering impacted the surface waters of the South Atlantic (see Chapter III). Thus increased weathering of the eastern portions of the LIPs may have delivered more radiogenic Nd to the surface waters in the region of convection, thereby generating more radiogenic deep-water compositions. Eastern Indian Ocean intermediate and deep-water Nd isotope compositions began to decrease during the Santonian, coincident with the gradual subsidence of the LIPs (Coffin, 1992). Once these sources of radiogenic Nd were submerged, seawater values decreased.

Alternatively, beginning in the late Cenomanian (manifested first in the Site 766 record), the more radiogenic Nd isotopic composition of deep waters in the eastern proto-Indian basin suggests a contribution of deep waters from the more radiogenic Pacific Ocean (Frank et al., 2005; MacLeod et al., 2008). While no Pacific data spanning the study interval exist, reconstructions of deep-water composition prior to the late Cenomanian as well as data from the Campanian to Paleogene data show $\varepsilon_{Nd(t)}$ values of ~-4 to -5 (Frank et al., 2005; MacLeod et al., 2008; Robinson et al., *submitted*); only one epsilon unit higher than the radiogenic values recorded in Site 766 (Figure 4-4). Then by the Santonian, Pacific deep-water influence in the Indian waned (or convection in the southern Indian Ocean recommenced), as seen in the return to unradiogenic $\varepsilon_{Nd(t)}$ values over the following ~10 Myr.

Several studies hypothesize about formation of deep waters in the Pacific during the Cretaceous (e.g. Barron and Peterson, 1990; Barron et al., 1995; Brady et al., 1998), but no previous investigation reported evidence for a contribution of Pacific deep waters

within the other two oceanic basins. Our data indicates that the influence of a Pacific deep-water mass in the Indian Ocean began during the peak warming of the Cretaceous (e.g. Huber et al., 1995; Clarke and Jenkyns, 1999; Pearson et al., 2001; Huber et al., 2002). The cessation or reduction of Indian Ocean deep-water formation was probably due to changes in the hydrologic cycle inferred to have occurred during the peak of Cretaceous sea surface warmth in the Turonian to Santonian (e.g. Huber et al., 2002; Wilson et al., 2002; Forster et al., 2007). Warming during the Cretaceous likely increased precipitation rates in the high latitudes (e.g. Poulsen et al., 1999). In a large open ocean basin such as the Pacific, an increase in precipitation would have little effect on surface ocean densities. However, in a restricted basin, such as that between India and Australia where Indian Ocean deep waters likely convected during the Cretaceous, an increase in precipitation could have decreased the density of surface water, impeding deep convection. In addition, the surface waters likely warmed during this time interval, further decreasing their density. Upon global cooling through the Campanian, salinity values in the south Indian Ocean could rise, and sea surface temperatures decrease, enough to reinitiate deep-water production. Interestingly, while deep-water temperatures in the Indian Ocean exhibit a monotonic decrease from the peak Turonian warmth to the Campanian (e.g. Wilson et al., 2002), sea surface temperatures are constant from the Turonian to Santonian (Huber et al., 1995; Huber et al., 2002; Forster et al., 2007). This may reflect changes occurring in the high-latitude Pacific surface waters that are decoupled from the Atlantic, where deep-water temperatures are warm through the Santonian (e.g. Huber et al., 2002).

The decrease of the Nd isotopic composition of Indian Ocean intermediate and deep waters to unradiogenic values (~-10) coincides with the convergence to unradiogenic values within the South Atlantic (Chapter III). It is unlikely that the similar values in the Atlantic and Indian Oceans represented a common water mass, given the tectonic restrictions on deep-water flow at this time. Instead we suggest that deep waters convected in both regions acquired similar signatures due to similar weathering products derived from the southern continents. The common timing between the Indian and Atlantic Oceans likely was related to global cooling (Huber et al., 2002; Wilson et al., 2002; Forster et al., 2007) and the associated precipitation change (e.g. Poulsen et al., 1999) in the Campanian. Global cooling initiated the production of deep water in the Indian Ocean, and may have caused a westward movement of deep-water production in the South Atlantic to more unradiogenic surface waters away from the Marion, Kerguelen, and Reunion hotspots.

The similar values in the Atlantic and Indian Oceans may also reflect shared surface water values. By the Campanian, there was open communication of surface to upper-bathyal waters between the two ocean basins. If the locations of intermediate- to deep-water formation in the high latitudes were located off either coast of Kerguelen Plateau, the surface waters may have shared a similar history and Nd value. Open communication between the basins would also have decreased the residence time of surface waters in the previously marginal seas, decreasing the potential impact of Kerguelen and Marion hotspots on the surface water ε_{Nd} values, driving more unradiogenic signatures.

5. Conclusions

1. Intermediate- and deep-water formation in the high-latitude southern Indian Ocean during the Cenomanian and Campanian was sufficiently vigorous to impact abyssal to upper-bathyal depths.

2. Deep-water production in the Indian Ocean diminished or ceased during the late Cenomanian. The deep Indian basin was influenced by a water mass sourced in the Pacific until the mid-Campanian. Alternatively, the warm interval spanning the Turonian to Santonian may have altered weathering of subaerially exposed LIPs into the source region of deep-water production, imparting a more radiogenic, "Pacific-like" signal without a concomitant change in deep water provenance.

3. Indian Ocean sourced deep waters dominated the Indian Ocean again by the mid Campanian.

4. The coincident timing of the advent of deep-water production in the Indian and South Atlantic (Chapter III) probably shares a common cause, most likely global cooling during the Campanian.

CHAPTER V

SUMMARY

In this dissertation I employed the Nd isotopic composition of ancient seawater recorded in biogenic apatite and benthic foraminiferal calcite to reconstruct water mass composition and circulation patterns during the late Pleistocene and the Late Cretaceous. While biogenic apatite is widely accepted as a robust recorded of the seawater Nd isotopic composition, the signal recorded by benthic foraminifera had not been previously tested. Data presented in Chapter II confirms the utility of benthic foraminifera regardless of species or life habitat.

Neodymium isotope data generated for two locations along the Southern California margin indicate that the source of the water mass bathing the margin did not vary on millennial time scales within Marine Isotope Stage 3. The data suggest a constant southern-sourced intermediate water mass for the region. Changes in seafloor oxygenation on millennial time scales resulted from changes in local sea surface productivity. Increased upwelling during interstadials led to an increase in nutrient availability in the surface waters. The increased nutrients stimulated greater phytoplankton productivity, which rained to depth and consumed dissolved oxygen via the metabolism of organic carbon.

The tectonic evolution of the ocean basins exerted a first order control on the nature of deep-ocean circulation during the mid- to Late Cretaceous time interval. During the early part of the study interval, the South Atlantic was segmented into multiple basins likely isolated from each other with respect to deep-water flow. Nd

isotope data suggest that convection of deep waters occurred in the eastern portion of the South Atlantic near the large igneous provinces (LIPs) of the eastern Southern Ocean. Weathering of the subaerially exposed portions of the LIPs imparted a radiogenic isotopic signature to the deep-water mass(es) sinking in the region. Subsidence of the LIPs during the latter portion of the study interval led to a decrease in the amount of radiogenic Nd weathered into the basin, which caused a gradual shift to more unradiogenic values in the water mass(es) that formed in the region. During the early Campanian, subsidence of the Walvis Ridge/Rio Grande Rise complex permitted circulation of deep waters between the high-latitude South Atlantic and Angola Basin, effectively ending the period of deep basin segmentation.

The mid- to Late Cretaceous Indian Ocean was ventilated by different water masses than the South Atlantic. During the early portion of the study interval, convection occurred in the marginal sea between India and Australia during the Cenomanian. However, during the late Cenomanian, the source of deep waters in the Indian Ocean switched to deep waters that sank in the Pacific Ocean based on a shift toward more radiogenic Nd isotope values along the western Australian margin. This new circulation regime lasted through the peak Cretaceous warming into the Santonian. A shift back to less radiogenic values during the early Campanian to unradiogenic Nd isotopic values suggests resumption of deep-water formation in the Indian Ocean. These early Campanian Indian Ocean Nd isotope values are similar to those in the South Atlantic. However the similar values likely do not reflect a common water mass, but instead the open exchange of surface waters over the recently subducted Kerguelen

Plateau between the two ocean basins. This open communication of surface waters led to a uniform southern hemisphere surface water Nd isotope value which subsequently led to similar deep water values as the surface waters convected in both the South Atlantic and the Indian Oceans.

REFERENCES

Albarède, F., Goldstein, S.L., 1992. World map of Nd isotopes in sea-floor ferromanganese deposits. Geology 20, 761-763.

Amakawa, H., Alibo, D.S., Nozaki, Y., 2000. Nd isotopic composition and REE pattern in the surface waters of the eastern Indian Ocean and its adjacent seas. Geochimica et Cosmochimica Acta 64, 1715-1727.

Amakawa, H., Nozaki, Y., Alibo, D.S., Zhang, J., Fukugawa, K., Nagai, H., 2004. Neodymium isotopic variations in Northwest Pacific waters. Geochimica et Cosmochimica Acta 68, 715-727.

Amakawa, H., Sasaki, K., Ebihara, M., 2009. Nd isotopic composition in the central North Pacific. Geochimica et Cosmochimica Acta 73, 4705-4719.

Andreasen, D.H., Ravelo, A.C., Broccoli, A.J., 2001. Remote forcing at the Last Glacial Maximum in the Tropical Pacific Ocean. Journal of Geophysical Research 106, 879-897.

Armstrong, H.A., Pearson, D.G., Griselin, M., 2001. Thermal effects on rare earth element and strontium isotope chemistry in single conodont elements. Geochimica et Cosmochimica Acta 65, 435-441.

Arsouze, T., Dutay, J.C., Lacan, F., Jeandel, C., 2007. Modeling the neodymium isotopic composition with a global ocean circulation model. Chemical Geology 239, 165-177.

Arz, H.W., Lamy, F., Ganopolski, A., Nowaczyk, N., Pätzold, J., 2007. Dominant Northern Hemisphere climate control over millennial-scale glacial sea-level variability. Quaternary Science Reviews 26, 312-321.

Barrera, E., Savin, S.M., 1999. Evolution of late Campanian-Maastrichtian marine climates and oceans. In: Barrera, E. and Johnson, C.C. (Eds), Evolution of the Cretaceous Ocean-Climate System, Special Paper 332, Geological Society of America, pp. 245-282.

Barron, E.J., Fawcett, P.J., Peterson, W.H., Pollard, D., Thompson, S.L., 1995. A "simulation" of mid-Cretaceous climate. Paleoceanography 10, 953-962.

Barron, E.J., Harrison, C.G., Sloan, J.L., Hay, W.W., 1981. Paleogeography, 180 million years ago to the present. Eclogae Geologicae Helvetiae 74, 443-470.

Barron, E.J., Peterson, W.H., 1990. Mid-Cretaceous ocean circulation: Results from model sensitivity studies. Paleoceanography 5, 319-337.

Basov, I.A., Krasheninnikov, V.A., 1983. Bentic foraminifers in Mesozoic and Cenozoic sediments of the southwestern Atlantic as an indicator of paleoenvironment, Deep Sea Drilling Project Leg 71. In: Ludwig, W.J. and Krasheninnikov, V.A. (Eds), Initial Reports of the Deep Sea Drilling Project, 71, U.S. Government Printing Office, pp. 739-787.

Bayon, G., German, C.R., Burton, K.W., Nesbitt, R.W., Rogers, N., 2004. Sedimentary Fe-Mn oxyhydroxides as paleoceanographic archives and the role of aeolian flux in regulating oceanic dissolved REE. Earth and Planetary Science Letters 224, 477-492.

Behl, R.J., Kennett, J.P., 1996. Brief interstadial events in the Santa Barbara basin, NE Pacific, during the past 60 kyr. Nature 379, 243-246.

Berner, R.A., 2006. GEOCARBSULF: A combined model for Phanerozoic atmospheric O_2 and CO_2. Geochimica et Cosmochimica Acta 70, 5653-5664.

Bograd, S.J., Schwing, F.B., Castro, C.G., Timothy, D.A., 2002. Bottom water renewal in the Santa Barbara Basin. Journal of Geophysical Research 107, doi:10.1029/2001JC001291.

Boyle, E.A., 1981. Cadmium, zinc, copper, and barium in foraminifera tests. Earth and Planetary Science Letters 53, 11-35.

Boyle, E.A., 1992. Cadmium and _^{13}C paleochemical ocean distributions during the Stage-2 Glacial Maximum. Annual Review of Earth and Planetary Sciences 20, 245-287.

Brady, E.C., DeConto, R.M., Thompson, S.L., 1998. Deep water formation and poleward ocean heat transport in the warm climate extreme of the Cretaceous (80 Ma). Geophysical Research Letters 25, 4205-4208.

Brass, G.W., Southam, J.R., Peterson, W.H., 1982. Warm saline bottom water in the ancient ocean. Nature 296, 620-623.

Burton, K.W., Vance, D., 2000. Glacial-interglacial variations in the neodymium isotope composition of seawater in the Bay of Bengal recorded by planktonic foraminifera. Earth and Planetary Science Letters 176, 425-441.

Cannariato, K.G., Kennett, J.P., 1999. Climatically related millennial-scale fluctuations in strength of California margin oxygen-minimum zone during the past 60 k.y. Geology 27, 975-978.

Cannariato, K.G., Kennett, J.P., Behl, R.J., 1999. Biotic response to late Quaternary rapid climate switches in Santa Barbara Basin: Ecological and evolutionary implications. Geology 27, 63-66.

Carissimo, B.C., Oort, A.H., Vonder Haar, T.H., 1985. Estimating the meridional energy transports in the atmosphere and ocean. Journal of Physical Oceanography 15, 82-91.

Carter, P., Vance, D., Schmidt, D.N., 2007. Benthic foraminifera as a novel substrate for deep-water Nd isotopes. Geochimica et Cosmochimica Acta 71, A148-A148.

Charles, C.D., Lynch-Stieglitz, J., Ninnemann, U.S., Fairbanks, R.G., 1996. Climate connections between the hemisphere revealed by deep sea sediment core ice core correlations. Earth and Planetary Science Letters 142, 19-27.

Clarke, L.J., Jenkyns, H.C., 1999. New oxygen isotope evidence for long-term Cretaceous climatic change in the Southern Hemisphere. Geology 27, 699-702.

Coffin, M.F., 1992. Emplacement and subsidence of Indian Ocean plateaus and submarine ridges. In: Duncan, R.A. (Eds), Synthesis of Results from Scientific Drilling in the Indian Ocean, Geophysical Monograph 70, American Geophysical Union, pp. 115-125.

Colin, C., Turpin, L., Bertaux, J., Desprairies, A., Kissel, C., 1999. Erosional history of the Himalayan and Burman ranges during the last two glacial-interglacial cycles. Earth and Planetary Science Letters 171, 647-660.

Curry, W.B., Lohmann, G.P., 1982. Carbon isotopic changes in benthic foraminifera from the western South-Atlantic - Reconstruction of glacial abyssal circulation patterns. Quaternary Research 18, 218-235.

D'Hondt, S., Arthur, M.A., 1996. Late Cretaceous oceans and the cool tropic paradox. Science 271, 1838-1841.

Dansgaard, W., Johnsen, S.J., Clausen, H.B., Dahljensen, D., Gundestrup, N.S., Hammer, C.U., Hvidberg, C.S., Steffensen, J.P., Sveinbjornsdottir, A.E., Jouzel, J., Bond, G., 1993. Evidence for general instability of past climate from a 250-Kyr ice-core record. Nature 364, 218-220.

Davey, R.J., 1978. Marine Cretaceous palynology of Site 361, DSDP Leg 40, off Southwestern Africa. In: Bolli, H.M. and Ryan, W.B.F. (Eds), Initial Reports of the Deep Sea Drilling Project, 40, US Government Printing Office, pp. 883-913.

De Pol-Holz, R., Ulloa, O., Lamy, F., Dezileau, L., Sabatier, P., Hebbeln, D., 2007. Late Quaternary variability of sedimentary nitrogen isotopes in the eastern South Pacific Ocean. Paleoceanography 22, PA2207, doi:10.1029/2006PA001308.

Dean, W.E., 2007. Sediment geochemical records of productivity and oxygen depletion along the margin of western North America during the past 60,000 years: teleconnections with Greenland Ice and the Cariaco Basin. Quaternary Science Reviews 26, 98-114.

Dean, W.E., Hay, W.W., Sibuet, J.-C., 1984. Geologic evolution, sedimentation, and paleoenvironments of the Angola Basin and adjacent Walvis Ridge: Synthesis of results of Deep Sea Drilling Project Leg 75. In: Hay, W.W. and Sibuet, J.-C.e.a. (Eds), Initial Reports of the Deep Sea Drilling Project, 75, US Govt. Printing Office, pp. 509-544.

DePaolo, D.J., Wasserburg, G.J., 1976. Nd isotopic variations and petrogenetic models. Geophysical Research Letters 3, 249-252.

Duncan, R.A., 1991. Age distribution of volcanism along aseismic ridges in the Eastern Indian Ocean. In: Weissel, J., Peirce, J., Taylor, E. and Alt, J. (Eds), Proceedings of the Ocean Drilling Program, Scientific Results, 121, Ocean Drilling Program, pp. 507-517.

Ekart, D.D., Cerling, T.E., Montañez, I.P., Tabor, N.J., 1999. A 400 million year carbon isotope record of pedogenic carbonate; implications for paleoatomospheric carbon dioxide. American Journal of Science 299, 805-827.

Elburg, M.A., van Bergen, M., Hoogewerff, J., Foden, J., Vroon, P., Zulkarnain, I., Nasution, A., 2002. Geochemical trends across an arc-continent collision zone: magma sources and slab-wedge transfer processes below the Pantar Strait volcanoes, Indonesia. Geochimica et Cosmochimica Acta 66, 2771-2789.

Emery, K.O., Uchupi, E., 1984. The Geology of the Atlantic Ocean. Springer-Verlag, New York. 1050 pp.

Fiedler, P.C., Talley, L.D., 2006. Hydrography of the eastern tropical Pacific: A review. Progress In Oceanography 69, 143-180.

Forster, A., Schouten, S., Baas, M., Sinninghe Damsté, J.S., 2007. Mid-Cretaceous (Albian-Santonian) sea surface temperature record of the tropical Atlantic Ocean. Geology 35, 919-922.

Frank, T.D., Arthur, M.A., 1999. Tectonic forcings of Maastrichtian ocean-climate evolution. Paleoceanography 14, 103-117.

Frank, T.D., Thomas, D.J., Leckie, R.M., Arthur, M.A., Bown, P.R., Jones, K., Lees, J.A., 2005. The Maastrichtian record from Shatsky Rise (northwest Pacific): A tropical perspective on global ecological and oceanographic changes. Paleoceanography 20, PA1008, doi:10.1029/2004PA001052.

Freeman, K.H., Hayes, J.M., 1992. Fractionation of carbon isotopes by phytoplankton and estimates of ancient CO_2 levels. Global Biogeochemical Cycles 6, 185-198.

Friedrich, O., Erbacher, J., 2006. Benthic foraminiferal assemblages from Demerara Rise (ODP Leg 207, western tropical Atlantic): Possible evidence for a progressive opening of the Equatorial Atlantic Gateway. Cretaceous Research 27, 377-397.

Ganeshram, R.S., Pedersen, T.F., Calvert, S.E., McNeill, G.W., Fontugne, M.R., 2000. Glacial-interglacial variability in denitrification in the world's oceans: Causes and consequences. Paleoceanography 15, 361-376.

Goldstein, S.J., Jacobsen, S.B., 1987. The Nd and Sr isotopic systematics of river-water dissolved material: Implications for the sources of Nd and Sr in seawater. Chemical Geology: Isotope Geoscience section 66, 245-272.

Goldstein, S.J., Jacobsen, S.B., 1988. Nd and Sr isotopic systematics of river water suspended material: implications for crustal evolution. Earth and Planetary Science Letters 87, 249-265.

Goldstein, S.L., Hemming, S.R., 2003. Long-lived isotopic tracers in oceanography, paleoceanography, and ice-sheet dynamics. In: Heinrich, D.H. and Karl, K.T. (Eds), Treatise on Geochemistry, Pergamon, pp. 453-489.

Goldstein, S.L., O'Nions, R.K., Hamilton, P.J., 1984. A Sm-Nd isotopic study of atmospheric dusts and particulates from major river systems. Earth and Planetary Science Letters 70, 221-236.

Goldstein, S.L., Zylberberg, D., Pahnke, K., Hemming, S.R., van de Flierdt, T., 2007. Quantifying changes in the global thermohaline circulation: A circum-Antarctic perspective. US Geological Surveys and The National Acadamies USGS OF-2007-2047, Extended Abstract 209.

Gradstein, F.M., 1992. Legs 122 and 123, Northwestern Australian margin - A stratigraphic and paleogeographic summary. In: Gradstein, F.M. and Ludden, J.N. (Eds), Proceedings of the Ocean Drilling Program, Scientific Results, 123, Ocean Drilling Program, pp. 801-816.

Gradstein, F.M., Kaminski, M.A., Agterberg, F.P., 1999. Biostratigraphy and paleoceanography of the Cretaceous seaway between Norway and Greenland. Earth-Science Reviews 46, 27-98.

Gradstein, F.M., Ludden, J.N., and Shipboard Scientific Party, 1990. Background and introduction. In: Ludden, J.N. and Gradstein, F.M. (Eds), Proceedings of the Ocean Drilling Program, Initial Repots, 123, Ocean Drilling Program, pp. 3-12.

Grootes, P.M., Stuiver, M., White, J.W.C., Johnsen, S.J., Jouzel, J., 1993. Comparison of oxygen isotope records from the GISP2 and GRIP Greenland ice cores. Nature 366, 552-554.

Haley, B.A., Klinkhammer, G.P., McManus, J., 2004. Rare earth elements in pore waters of marine sediments. Geochimica et Cosmochimica Acta 68, 1265-1279.

Haq, B.U., Boyd, R.L., Exon, N.F., von Rad, U., 1992. Evolution of the Central Exmouth Plateau: A post-drilling perspective. In: von Rad, U. and Haq, B., U. (Eds), Proceedings of the Ocean Drilling Program, Scientific Results, 122, Ocean Drilling Program, pp. 801-816.

Hay, W.W., DeConto, R.M., 1999. Comparison of modern and Late Cretaceous meridional energy transport and oceanology. In: Barrera, E. and Johnson, C.C. (Eds), Evolution of the Cretaceous Ocean-Climate System, Special Paper 332, Geological Society of America, pp. 283-300.

Hay, W.W., DeConto, R.M., Wold, C.N., Wilson, K.M., Voigt, S., Schulz, M., Wold-Rossby, A., Dullo, W.-C., Ronov, A.B., Balukhovsky, A.N., Söding, E., 1999. Alternative global Cretaceous paleogeography. In: Barrera, E. and Johnson, C.C. (Eds), Evolution of the Cretaceous Ocean-Climate System, Special Paper 332, Geological Society of America, pp. 1-47.

Hay, W.W., Migdisov, A., Balukhovsky, A.N., Wold, C.N., Flögel, S., Söding, E., 2006. Evaporites and the salinity of the ocean during the Phanerozoic: Implications for climate, ocean circulation and life. Palaeogeography, Palaeoclimatology, Palaeoecology 240, 3-46.

Hendy, I.L., Kennett, J.P., 1999. Latest Quaternary North Pacific surface-water responses imply atmosphere-driven climate instability. Geology 27, 291-294.

Hendy, I.L., Kennett, J.P., 2003. Tropical forcing of North Pacific intermediate water distribution during Late Quaternary rapid climate change? Quaternary Science Reviews 22, 673-689.

Hendy, I.L., Kennett, J.P., Roark, E.B., Ingram, B.L., 2002. Apparent synchroneity of submillennial scale climate events between Greenland and Santa Barbara Basin, California from 30-10 ka. Quaternary Science Reviews 21, 1167-1184.

Hendy, I.L., Pedersen, T.F., 2005. Is pore water oxygen content decoupled from productivity on the California Margin? Trace element results from Ocean Drilling Program Hole 1017E, San Lucia slope, California. Paleoceanography 20, PA4026, doi:10.1029/2004PA001123.

Hendy, I.L., Pedersen, T.F., 2006. Oxygen minimum zone expansion in the eastern tropical North Pacific during deglaciation. Geophysical Research Letters 33, L20602, doi:10.1029/2006GL025975.

Hendy, I.L., Pedersen, T.F., Kennett, J.P., Tada, R., 2004. Intermittent existence of a southern Californian upwelling cell during submillennial climate change of the last 60 kyr. Paleoceanography 19, PA3007, doi:10.1029/2003PA000965.

Huber, B.T., 1992. Upper Cretaceous planktic foraminiferal biozonation for the austra realm. Marine Micropaleontology 20, 107-128.

Huber, B.T., Hodell, D.A., 1996. Middle-Late Cretaceous climate of the southern high latitudes: Stable isotopic evidence for minimal equator-to-pole thermal gradients: Discussion and reply. Geological Society of America Bulletin 108, 1192-1196.

Huber, B.T., Hodell, D.A., Hamilton, C.P., 1995. Middle-Late Cretaceous climate of the southern high latitudes: Stable isotopic evidence for minimal equator-to-pole thermal gradients. Geological Society of America Bulletin 107, 1164-1191.

Huber, B.T., Norris, R.D., MacLeod, K.G., 2002. Deep-sea paleotemperature record of extreme warmth during the Cretaceous. Geology 30, 123-126.

Hughen, K.A., Overpeck, J.T., Peterson, L.C., Trumbore, S., 1996. Rapid climate changes in the tropical Atlantic region during the last deglaciation. Nature 380, 51-54.

IPCC, 2007. Climate Change 2007: The Physical Science Basis. Contribution of Working Group I to the Fourth Assessment Report of the Intergovernmental Panel on Climate Change. Cambridge University Press, Cambridge, United Kingdom and New York, NY, USA. 1009 pp.

Jeandel, C., 1993. Concentration and isotopic composition of Nd in the South Atlantic Ocean. Earth and Planetary Science Letters 117, 581-591.

Jeandel, C., Arsouze, T., Lacan, F., Techine, P., Dutay, J.C., 2007. Isotopic Nd compositions and concentrations of the lithogenic inputs into the ocean: A compilation, with an emphasis on the margins. Chemical Geology 239, 156-164.

Jeandel, C., Thouron, D., Fieux, M., 1998. Concentrations and isotopic compositions of neodymium in the eastern Indian Ocean and Indonesian straits. Geochimica et Cosmochimica Acta 62, 2597-2607.

Kaiho, K., 1994. Benthic foraminiferal dissolved-oxygen index and dissolved-oxygen levels in the modern ocean. Geology 22, 719-722.

Kaminski, M.A., Baumgartner, P.O., Bown, P.R., Haig, D.W., McMinn, A., Moran, M., Mutterlose, J., Ogg, J.G., 1992. Magnetobiostratigraphic synthesis of Leg 123: Sites 765 and 766 (Argo Abyssal Plain and lower Exmouth Plateau). In: Gradstein, F.M. and Ludden, J.N. (Eds), Proceedings of the Ocean Drilling Program, Scientific Results, 123, Ocean Drilling Program, pp. 717-737.

Keating, B.H., Herrero-Bervera, E., 1984. Magnetostratigraphy of Cretaceous and early Cenozoic sediments of Deep Sea Drilling Project Site 530, Angola Basin. In: Hay, W.W. and Sibuet, J.-C. (Eds), Initial Reports of the Deep Sea Drilling Project, 75, US Government Printing Office, pp. 1211-1218.

Kennett, J.P., Roark, E.B., Cannariato, K.G., Ingram, B.L., Tada, R., 2000. Latest Quaternary paleoclimatic and radiocarbon chronology, Hole 1017E, southern California margin. In: Lyle, M., Koizumi, I., Richter, C. and Moore, T.C.J. (Eds), Proceedings of the Ocean Drilling Program, Scientific Results, 167, Ocean Drilling Program, pp. 249-254.

Kennett, J.P., Venz, K., 1995. Late Quaternary climatically related planktonic foraminiferal assemblage changes: Hole 893A, Santa Barbara Basin, California.

In: Kennett, J.P., Baldauf, J.G. and Lyle, M.W. (Eds), Proceedings of the Ocean Drilling Program, Scientific Results, 146, Ocean Drilling Program, pp. 281-293.

Kienast, S.S., Calvert, S.E., Pedersen, T.F., 2002. Nitrogen isotope and productivity variations along the northeast Pacific margin over the last 120 kyr: Surface and subsurface paleoceanography. Paleoceanography 17, doi:10.1029/2001PA000650.

Klevenz, V., Vance, D., Schmidt, D.N., Mezger, K., 2008. Neodymium isotopes in benthic foraminifera: Core-top systematics and a down-core record from the Neogene south Atlantic. Earth and Planetary Science Letters 265, 571-587.

Lacan, F., Jeandel, C., 2001. Tracing Papua New Guinea imprint on the central Equatorial Pacific Ocean using neodymium isotopic compositions and Rare Earth Element patterns. Earth and Planetary Science Letters 186, 497-512.

Lacan, F., Jeandel, C., 2005a. Acquisition of the neodymium isotopic composition of the North Atlantic Deep Water. Geochemistry Geophysics Geosystems 6, Q12008, doi:10.1029/2005GC000956.

Lacan, F., Jeandel, C., 2005b. Neodymium isotopes as a new tool for quantifying exchange fluxes at the continent-ocean interface. Earth and Planetary Science Letters 232, 245-257.

Lees, J.A., 2002. Calcareous nannofossil biogeography illustrates palaeoclimate change in the Late Cretaceous Indian Ocean. Cretaceous Research 23, 537-634.

Linsley, B.K., 1996. Oxygen-isotope record of sea level and climate variations in the Sulu Sea over the past 150,000 years. Nature 380, 234-237.

MacLeod, K.G., Martin, E.E., Blair, S.W., 2008. Nd isotopic excursion across Cretaceous ocean anoxic event 2 (Cenomanian-Turonian) in the tropical North Atlantic. Geology 36, 811-814.

Mangelsdorf, K., Guntner, U., Rullkotter, J., 2000. Climatic and oceanographic variations on the California continental margin during the last 160 kyr. Organic Geochemistry 31, 829-846.

Martin, E.E., Scher, H.D., 2004. Preservation of seawater Sr and Nd isotopes in fossil fish teeth: Bad news and good news. Earth and Planetary Science Letters 220, 25-39.

Martin, J.E., Patrick, D., Kihm, A.J., Foit, F.F., Grandstaff, D.E., 2005. Lithostratigraphy, tephrochronology, and rare earth element geochemistry of fossils at the classical Pleistocene Fossil Lake area, south central Oregon. Journal of Geology 113, 139-155.

McLennan, S.M., Taylor, S.R., McCulloch, M.T., Maynard, J.B., 1990. Geochemical and Nd-Sr isotopic composition of deep-sea turbidites: Crustal evolution and plate tectonic associations. Geochimica et Cosmochimica Acta 54, 2015-2050.

Murphy, D.P., Thomas, D.J., *submitted*. The role of intermediate water circulation in stadial-interstadial oxygenation variations along the Southern California margin. Quaternary Science Reviews

Mutterlose, J., Brumsack, H., Flögel, S., Hay, W.W., Klein, C., Langrock, U., Lipinski, M., Ricken, W., Söding, E., Stein, R., Swientek, O., 2003. The Greenland-Norwegian Seaway: A key area for understanding Late Jurassic to Early

Cretaceous paleoenvironments. Paleoceanography 18, 1010, doi:10.1029/2001PA000625.

Nederbragt, A.J., Thurow, J.W., Bown, P.R., 2008. Paleoproductivity, ventilation, and organic carbon burial in the Santa Barbara Basin (ODP Site 893, off California) since the last glacial. Paleoceanography 23, PA1211, doi:10.1029/2007PA001501.

Norris, R.D., Bice, K.L., Magno, E.A., Wilson, P.A., 2002. Jiggling the tropical thermostat in the Cretaceous hothouse. Geology 30, 299-302.

O'Connor, J.M., Duncan, R.A., 1990. Evolution of the Walvis Ridge and Rio Grande Rise hotspot system: Implications for African and South American plate motions over hotspots. Journal Geophysical Research 95, 17475-17502.

O'Nions, R.K., Carter, S.R., Cohen, R.S., Evensen, N.M., Hamilton, P.J., 1978. Pb, Nd and Sr isotopes in oceanic ferromanganese deposits and ocean floor basalts. Nature 273, 435-438.

Ortiz, J.D., O'Connell, S.B., DelViscio, J., Dean, W.E., Carriquiry, J.D., Marchitto, T., Zheng, Y., van Geen, A., 2004. Enhanced marine productivity off western North America during warm climate intervals of the past 52 ky. Geology 32, 521-524.

Palmer, M.R., 1985. Rare earth elements in foraminifera tests. Earth and Planetary Science Letters 73, 285-298.

Pearson, P.N., Ditchfield, P.W., Singano, J., Harcourt-Brown, K.G., Nicholas, C.J., Olsson, R.K., Shackleton, N.J., Hall, M.A., 2001. Warm tropical sea surface temperatures in the Late Cretaceous and Eocene epochs. Nature 413, 481-487.

Person, A., Bocherens, H., Saliège, J.-F., Paris, F., Zeitoun, V., Gérard, M., 1995. Early Diagenetic Evolution of Bone Phosphate: An X-Ray-Diffractometry Analysis. Journal of Archaeological Science 22, 211-221.

Piepgras, D.J., Jacobsen, S.B., 1988. The isotopic composition of neodymium in the North Pacific. Geochimica et Cosmochimica Acta 52, 1373-1381.

Piepgras, D.J., Wasserburg, G.J., 1980. Neodymium isotopic variations in seawater. Earth and Planetary Science Letters 50, 128-138.

Piepgras, D.J., Wasserburg, G.J., 1982. Isotopic composition of neodymium in waters from the Drake Passage. Science 217, 207-214.

Piepgras, D.J., Wasserburg, G.J., 1987. Rare-Earth Element transport in the western North-Atlantic inferred from Nd isotopic observations. Geochimica et Cosmochimica Acta 51, 1257-1271.

Piepgras, D.J., Wasserburg, G.J., Dasch, E.J., 1979. Isotopic composition of Nd in different ocean masses. Earth and Planetary Science Letters 45, 223-236.

Piotrowski, A.M., Goldstein, S.L., Hemming, S.R., Fairbanks, R.G., 2005. Temporal relationships of carbon cycling and ocean circulation at glacial boundaries. Science 307, 1933-1938.

Pospelova, V., Pedersen, T.F., de Vernal, A., 2006. Dinoflagellate cysts as indicators of climatic and oceanographic changes during the past 40 kyr in the Santa Barbara Basin, southern California. Paleoceanography 21, PA2010, doi:10.1029/2005PA001251.

Poulsen, C.J., Barron, E.J., Johnson, C.C., Fawcett, P., 1999. Links between major climatic factors and regional oceanic circulation in the mid-Cretaceous. In: Barrera, E. and Johnson, C.C. (Eds), Evolution of the Cretaceous Ocean-Climate System, Special Paper 332, Geological Society of America, pp. 73-90.

Poulsen, C.J., Gendaszek, A.S., Jacob, R.L., 2003. Did the rifting of the Atlantic Ocean cause the Cretaceous thermal maximum? Geology 31, 115-118.

Price, G.D., Sellwood, B.W., Pirrie, D., 1996. Middle-Late Cretaceous climate of the southern high latitudes: Stable isotopic evidence for minimal equator-to-pole thermal gradients: Discussion and reply. Geological Society of America Bulletin 108, 1192-1196.

Pucéat, E., Lécuyer, C., Reisberg, L., 2005. Neodymium isotope evolution of NW Tethyan upper ocean waters throughout the Cretaceous. Earth and Planetary Science Letters 236, 705-720.

Reid, J.L., 1965. Intermediate Waters of the Pacific Ocean. The Johns Hopkins Press, Baltimore, MD. 85 pp.

Reynard, B., Lècuyer, C., Grandjean, P., 1999. Crystal-chemical controls on rare-earth element concentrations in fossil biogenic apatites and implications for paleoenvironmental reconstructions. Chemical Geology 155, 233-241.

Richardson, S.H., Erlank, A.J., Duncan, A.R., Reid, D.L., 1982. Correlated Nd, Sr and Pb isotope variation in Walvis Ridge basalts and implications for the evolution of their mantle source. Earth and Planetary Science Letters 59, 327-342.

Roberts, N.L., Piotrowski, A.M., McManus, J.F., Keigwin, L.D., 2010. Synchronous deglacial overturning and water mass source changes. Science 327, 75-78.

Robinson, S.A., Murphy, D.P., Vance, D., Thomas, D.J., *submitted*. Formation of 'Southern Component Water' in the Late Cretaceous: Evidence from Nd-isotopes. Geology

Rohling, E.J., Grant, K., Hemleben, C., Kucera, M., Roberts, A.P., Schmeltzer, I., Schulz, H., Siccha, M., Siddall, M., Trommer, G., 2008. New constraints on the timing of sea level fluctuations during early to middle marine isotope stage 3. Paleoceanography 23, PA3219, doi:10.1029/2008PA001617.

Roy, M., van de Flierdt, T., Hemming, S.R., Goldstein, S.L., 2007. $^{40}Ar/^{39}Ar$ ages of hornblende grains and bulk Sm/Nd isotopes of circum-Antarctic glacio-marine sediments: Implications for sediment provenance in the southern ocean. Chemical Geology 244, 507-519.

Royer, D.L., Berner, R.A., Montanez, I.P., Tabor, N.J., Beerling, D.J., 2004. CO_2 as a primary driver of Phanerozoic climate. GSA Today 14, doi: 10.1130/1052-5173.

Rutberg, R.L., Peacock, S.L., 2006. High-latitude forcing of interior ocean _^{13}C. Paleoceanography 21, PA2012, doi:10.1029/2005PA001226.

Scher, H.D., Martin, E.E., 2004. Circulation in the Southern Ocean during the Paleogene inferred from neodymium isotopes. Earth and Planetary Science Letters 228, 391-405.

Scotese, C.R., 1991. Jurassic and Cretaceous plate tectonic reconstructions. Palaeogeography, Palaeoclimatology, Palaeoecology 87, 493-501.

Soutar, A., Crill, P.A., 1977. Sedimentation and climatic patterns in the Santa Barbara Basin during the 19th and 20th centuries. Geological Society of America Bulletin 88, 1161-1172.

Staudigel, H., Doyle, P., Zindler, A., 1985. Sr and Nd isotope systematics in fish teeth. Earth and Planetary Science Letters 76, 45-56.

Stordal, M.C., Wasserburg, G.J., 1986. Neodymium isotopic study of Baffin Bay water: sources of REE from very old terranes. Earth and Planetary Science Letters 77, 259-272.

Storey, M., Mahoney, J.J., Saunders, A.D., Duncan, R.A., Kelley, S.P., Coffin, M.F., 1995. Timing of hot spot-related volcanism and the breakup of Madagascar and India. Science 267, 852-855.

Stott, L.D., Berelson, W., Douglas, R., Gorsline, D., 2000. Increased dissolved oxygen in Pacific intermediate waters due to lower rates of carbon oxidation in sediments. Nature 407, 367-370.

Stow, D.A.V., Miller, J., 1980. Minerology, petrology, and diagenesis of sediments at Site 530, southeast Angola Basin. In: Hay, W.W. and Sibuet, J.-C. (Eds), Initial Reports of the Deep Sea Drilling Program, 75, US Government Printing Office, pp. 857-873.

Tachikawa, K., Jeandel, C., Roy-Barman, M., 1999. A new approach to the Nd residence time in the ocean: The role of atmospheric inputs. Earth and Planetary Science Letters 170, 433-446.

Tanaka, T., Togashi, S., Kamioka, H., Amakawa, H., Kagami, H., Hamamoto, T., Yuhara, M., Orihashi, Y., Yoneda, S., Shimizu, H., Kunimaru, T., Takahashi, K., Yanagi, T., Nakano, T., Fujimaki, H., Shinjo, R., Asahara, Y., Tanimizu, M., Dragusanu, C., 2000. JNdi-1: A neodymium isotopic reference in consistency with LaJolla neodymium. Chemical Geology 168, 279-281.

Thomas, D.J., Bralower, T.J., Jones, C.E., 2003. Neodymium isotopic reconstruction of late Paleocene-early Eocene thermohaline circulation. Earth and Planetary Science Letters 209, 309-322.

Torres, M.E., Mix, A.C., Kinports, K., Haley, B., Klinkhammer, G.P., McManus, J., de Angelis, M.A., 2003. Is methane venting at the seafloor recorded by _^{13}C of benthic foraminifera shells? Paleoceanography 18, 1062, doi:10.1029/2002PA000824.

Trenberth, K.E., Caron, J.M., 2001. Estimates of meridional atmosphere and ocean heat transports. Journal of Climate 14, 3433-3443.

Tsuchiya, M., 1981. The origin of the Pacific Equatorial 13°C Water. Journal of Physical Oceanography 11, 794-812.

Tucholke, B.E., Sibuet, J.-C., 2007. Leg 210 synthesis: Tectonic, magmatic, and sedimentary evolution of the Newfoundland-Iberia rift. In: Tucholke, B.E., Sibuet, J.-C. and Klaus, A. (Eds), Proceedings of the Ocean Drilling Program, Scientific Results, 210, Ocean Drilling Program, pp. 1-56.

Ufnar, D.F., González, L.A., Ludvigson, G.A., Brenner, R.L., Witzke, B.J., 2004. Evidence for increased latent heat transport during the Cretaceous (Albian) greenhouse warming. Geology 32, 1049-1052.

Vance, D., Scrivner, A.E., Beney, P., Staubwasser, M., Henderson, G.M., Slowey, N.C., 2004. The use of foraminifera as a record of the past neodymium isotope composition of seawater. Paleoceanography 19, PA2009, doi:10.1029/2003PA000957.

Veizer, J., Godderis, Y., Francois, L.M., 2000. Evidence for decoupling of atmospheric CO_2 and global climate during the Phanerozoic eon. Nature 408, 698-701.

Via, R.K., Thomas, D.J., 2006. Evolution of Atlantic thermohaline circulation: Early Oligocene onset of deep-water production in the North Atlantic. Geology 34, 441-444.

von Blanckenburg, F., 1999. Perspectives: Paleoceanography - Tracing past ocean circulation? Science 286, 1862-1863.

Waelbroeck, C., Labeyrie, L., Michel, E., Duplessy, J.C., McManus, J.F., Lambeck, K., Balbon, E., Labracherie, M., 2002. Sea-level and deep water temperature changes derived from benthic foraminifera isotopic records. Quaternary Science Reviews 21, 295-305.

Wang, Y.J., Cheng, H., Edwards, R.L., An, Z.S., Wu, J.Y., Shen, C.C., Dorale, J.A., 2001. A high-resolution absolute-dated Late Pleistocene monsoon record from Hulu Cave, China. Science 294, 2345-2348.

Whitechurch, H., Montigny, R., Sevigny, J.H., Storey, M., Salters, V.J.M., 1992. K-Ar and $^{40}Ar/^{39}Ar$ ages of central Kerguelen Plateau basalts. In: Wise, S.W., Jr., Schlich, R., Palmer-Julson, A. and Thomas, E. (Eds), Proceedings of the Ocean Drilling Program, Scientific Results, 120, Ocean Drilling Program, pp. 71-77.

Wilson, P.A., Norris, R.D., Cooper, M.J., 2002. Testing the Cretaceous greenhouse hypothesis using glassy foraminiferal calcite from the core of the Turonian tropics on Demerara Rise. Geology 30, 607-610.

Wise, S.W., Jr., 1983. Mesozoic and Cenozoic calcareous Nannofossils recovered by Deep Sea Drilling Project Leg 71 in the Falkland Plateau region, southwest Atlantic Ocean. In: Ludwig, W.J. and Krasheninnikov, V.A. (Eds), Initial Reports of the Deep Sea Drilling Project, 71, U.S. Govt. Printing Office, pp. 481-550.

Zhang, Y., Lacan, F., Jeandel, C., 2008. Dissolved rare earth elements tracing lithogenic inputs over the Kerguelen Plateau (Southern Ocean). Deep Sea Research Part II: Topical Studies in Oceanography 55, 638-652.

Zimmerman, H.B., Boersma, A., McCoy, F.W., 1987. Carbonaceous sediments and palaeoenvironment of the Cretaceous South Atlantic Ocean. Geological Society, London, Special Publications 26, 271-286.

APPENDIX 1

Table 2-1a. Site 893 Nd data generated for this study. Errors reported are 2σ standard errors. TAMU = Texas A&M University, UNC-CH = University of North Carolina Chapel Hill.

Hole 893A Depth (mbsf)	Age (kyr)	$^{143}Nd/^{144}Nd$	ε_{Nd}	Substrate	Lab
53.93	36.317	0.5121704 ± 0.0013	-9.1 ± 0.3	Fish Debris	TAMU
54.39	37.212	0.5121842 ± 0.0010	-8.9 ± 0.2	Fish Debris	UNC-CH
55.8	38.801	0.5121860 ± 0.0008	-8.8 ± 0.2	Fish Debris	TAMU
57.24	39.515	0.5122006 ± 0.0014	-8.5 ± 0.3	Forams + Fish	TAMU
58.26	40.03	0.5122040 ± 0.0007	-8.5 ± 0.2	Fish Debris	TAMU
58.91	40.259	0.5122422 ± 0.0011	-7.7 ± 0.2	Fish Debris	TAMU
59.91	40.568	0.5122017 ± 0.0011	-8.5 ± 0.2	Fish Debris	UNC-CH
60.62	40.789	0.5121794 ± 0.0009	-8.8 ± 0.2	Fish Debris	TAMU
60.85	40.938	0.5121815 ± 0.0018	-8.9 ± 0.4	Fish Debris	UNC-CH
62.16	41.841	0.5121791 ± 0.0014	-9.0 ± 0.3	Fish Debris	UNC-CH
62.46	42.048	0.5121759 ± 0.0010	-9.0 ± 0.2	Fish Debris	UNC-CH
64.12	42.84	0.5121865 ± 0.0010	-8.8 ± 0.2	Forams + Fish	TAMU
65.01	43.138	0.5121840 ± 0.0005	-8.9 ± 0.1	Fish Debris	TAMU
66.32	43.951	0.5121696 ± 0.0013	-9.1 ± 0.3	Fish Debris	UNC-CH
67.35	44.649	0.5121741 ± 0.0010	-9.1 ± 0.2	Fish Debris	UNC-CH
67.66	44.858	0.5121886 ± 0.0012	-8.8 ± 0.2	Fish Debris	UNC-CH
68.09	45.15	0.5122048 ± 0.0009	-8.5 ± 0.2	Fish Debris	UNC-CH
68.98	45.609	0.5122328 ± 0.0010	-7.9 ± 0.2	Fish Debris	UNC-CH
71.05	46.518	0.5121616 ± 0.0010	-9.3 ± 0.2	Fish Debris	UNC-CH
71.94	47.832	0.5121845 ± 0.0016	-8.9 ± 0.3	Fish Debris	UNC-CH
72.88	49.204	0.5122170 ± 0.0010	-8.2 ± 0.2	Fish Debris	UNC-CH
73.47	50.075	0.5121750 ± 0.0014	-9.0 ± 0.3	Fish Debris	UNC-CH
74.05	50.931	0.5122046 ± 0.0014	-8.5 ± 0.3	Fish Debris	UNC-CH

Table 2-1b. Site 1017 Nd data generated for this study. Errors reported are 2σ standard errors. TAMU = Texas A&M University, UNC-CH = University of North Carolina Chapel Hill.

Hole 1017E

Depth (mbsf)	Age (kyr)	$^{143}Nd/^{144}Nd$	ε_{Nd}	Substrate	Lab
2.145	9.756	0.5123200 ± 0.0011	-6.2 ± 0.2	Fish Debris	TAMU
2.255	10.411	0.5123199 ± 0.0008	-6.2 ± 0.2	Fish Debris	TAMU
7.535	35.07	0.5122787 ± 0.0011	-7.0 ± 0.2	Fish Debris	UNC-CH
7.665	37.776	0.5122997 ± 0.0011	-6.6 ± 0.2	Forams	UNC-CH
7.85	38.948	0.5122926 ± 0.0011	-6.7 ± 0.2	Fish Debris	UNC-CH
8.135	40.007	0.5122773 ± 0.0010	-7.0 ± 0.2	Forams + Fish	UNC-CH
8.275	40.518	0.5122900 ± 0.0012	-6.8 ± 0.2	Fish Debris	UNC-CH
8.435	41.103	0.5122838 ± 0.0011	-6.9 ± 0.2	Fish Debris	UNC-CH
8.685	42.016	0.5122843 ± 0.0017	-6.9 ± 0.3	Forams	UNC-CH
8.795	42.417	0.5122799 ± 0.0013	-7.0 ± 0.3	Fish Debris	UNC-CH
9.095	43.546	0.5122877 ± 0.0012	-6.8 ± 0.2	Fish Debris	UNC-CH
9.425	44.795	0.5122800 ± 0.0011	-7.0 ± 0.2	Forams	UNC-CH
9.615	45.573	0.5123050 ± 0.0017	-6.5 ± 0.3	Forams + Fish	UNC-CH
9.695	46.034	0.5122979 ± 0.0010	-6.6 ± 0.2	Forams + Fish	UNC-CH
9.74	46.294	0.5123000 ± 0.0010	-6.6 ± 0.2	Forams	UNC-CH
9.885	47.129	0.5122822 ± 0.0012	-6.9 ± 0.2	Forams	UNC-CH
9.965	47.59	0.5122727 ± 0.0018	-7.1 ± 0.4	Forams	UNC-CH
10.025	47.936	0.5122908 ± 0.0010	-6.8 ± 0.2	Forams	UNC-CH
10.185	48.858	0.5122836 ± 0.0012	-6.9 ± 0.2	Fish Debris	UNC-CH
10.465	50.471	0.5121739 ± 0.0014	-9.1 ± 0.3	Forams + Fish	UNC-CH

APPENDIX 2

Table 3-2a. Site 361 Nd data generated for this study. Errors reported are 2σ standard errors. TAMU = Texas A&M University, UNC-CH = University of North Carolina Chapel Hill.

Hole 361 Depth (mbsf)	Age (Ma)	$^{143}Nd/^{144}Nd$	$\varepsilon_{Nd(t)}$	Lab
479.91	79.016	0.51227511 ± 0.0029	-6.42 ± 0.58	TAMU
577.98	84.378	0.51226257 ± 0.0007	-6.62 ± 0.14	TAMU
612.50	86.265	0.51227454 ± 0.0005	-6.37 ± 0.10	TAMU
614.54	86.377	0.51225316 ± 0.0006	-6.78 ± 0.11	TAMU
615.98	86.456	0.51224500 ± 0.0003	-6.94 ± 0.06	TAMU
671.48	89.396	0.51227207 ± 0.0008	-6.39 ± 0.15	TAMU
672.73	89.431	0.51228311 ± 0.0011	-6.17 ± 0.22	TAMU
672.73	89.431	0.51228991 ± 0.0007	-6.04 ± 0.14	TAMU
716.00	90.626	0.51225218 ± 0.0005	-6.77 ± 0.10	TAMU
719.00	90.709	0.51226800 ± 0.0004	-6.46 ± 0.08	TAMU
766.71	92.028	0.51225847 ± 0.0014	-6.63 ± 0.28	TAMU
811.74	93.272	0.51228921 ± 0.0033	-6.02 ± 0.66	TAMU
814.50	93.348	0.51226880 ± 0.0008	-6.42 ± 0.16	TAMU
858.99	94.577	0.51234800 ± 0.0003	-4.87 ± 0.06	TAMU
864.74	94.736	0.51235799 ± 0.0003	-4.67 ± 0.05	TAMU

Table 3-2b. Site 511 Nd data generated for this study. Errors reported are 2σ standard errors. TAMU = Texas A&M University, UNC-CH = University of North Carolina Chapel Hill.

Hole 511 Depth (mbsf)	Age (Ma)	$^{143}Nd/^{144}Nd$	$\varepsilon_{Nd(t)}$	Lab
219.51	79.567	0.51226770 ± 0.0012	-6.56 ± 0.24	UNC-CH
225.51	83.010	0.51229630 ± 0.0010	-5.97 ± 0.20	UNC-CH
225.51	83.010	0.51229346 ± 0.0005	-6.03 ± 0.10	TAMU
233.16	83.163	0.51227350 ± 0.0017	-6.41 ± 0.34	UNC-CH
243.01	83.360	0.51227920 ± 0.0015	-6.30 ± 0.30	UNC-CH
247.50	83.427	0.51230310 ± 0.0012	-5.83 ± 0.53	UNC-CH
247.50	83.427	0.51228190 ± 0.0009	-6.25 ± 0.18	UNC-CH
252.50	83.481	0.51226830 ± 0.0010	-6.51 ± 0.20	UNC-CH
258.50	83.545	0.51226300 ± 0.0010	-6.62 ± 0.20	UNC-CH
266.64	83.632	0.51228486 ± 0.0006	-6.19 ± 0.11	TAMU
266.64	83.632	0.51227793 ± 0.0006	-6.32 ± 0.12	TAMU
271.76	83.688	0.51226980 ± 0.0010	-6.48 ± 0.20	UNC-CH
281.01	83.787	0.51231300 ± 0.0010	-5.64 ± 0.20	UNC-CH
290.52	83.889	0.51229070 ± 0.0016	-6.07 ± 0.32	UNC-CH
300.01	83.991	0.51219640 ± 0.0022	-7.91 ± 0.44	UNC-CH
304.51	84.039	0.51229600 ± 0.0012	-5.97 ± 0.24	UNC-CH
309.51	84.093	0.51231230 ± 0.0011	-5.65 ± 0.22	UNC-CH
319.01	84.195	0.51228462 ± 0.0003	-6.19 ± 0.07	TAMU
323.51	84.243	0.51227401 ± 0.0006	-6.40 ± 0.12	TAMU
328.51	84.297	0.51227947 ± 0.0003	-6.29 ± 0.06	TAMU
331.51	84.329	0.51225972 ± 0.0005	-6.67 ± 0.09	TAMU
338.01	84.399	0.51226374 ± 0.0006	-6.59 ± 0.12	TAMU
342.51	84.448	0.51231891 ± 0.0005	-5.52 ± 0.09	TAMU
347.51	84.501	0.51226335 ± 0.0003	-6.60 ± 0.05	TAMU
350.51	84.534	0.51229980 ± 0.0004	-5.89 ± 0.08	TAMU
357.11	84.604	0.51232045 ± 0.0003	-5.49 ± 0.06	TAMU
360.01	84.636	0.51229000 ± 0.0003	-6.08 ± 0.06	TAMU
363.04	84.668	0.51230370 ± 0.0004	-5.81 ± 0.09	TAMU
366.22	84.717	0.51232067 ± 0.0005	-5.48 ± 0.09	TAMU
369.51	84.966	0.51232420 ± 0.0003	-5.41 ± 0.05	TAMU

Table 3-b. continued

Hole 511 Depth (mbsf)	Age (Ma)	$^{143}Nd/^{144}Nd$	$\varepsilon_{Nd(t)}$	Lab
376.03	85.460	0.51228509 ± 0.0004	-6.17 ± 0.08	TAMU
379.01	85.686	0.51231491 ± 0.0006	-5.59 ± 0.13	TAMU
385.46	86.174	0.51234661 ± 0.0004	-4.96 ± 0.08	TAMU
388.48	86.403	0.51231015 ± 0.0003	-5.67 ± 0.07	TAMU
395.03	86.899	0.51236563 ± 0.0004	-4.59 ± 0.09	TAMU
398.01	87.125	0.51234826 ± 0.0006	-4.92 ± 0.12	TAMU
404.53	89.927	0.51230809 ± 0.0003	-5.68 ± 0.06	TAMU
407.51	90.264	0.51231964 ± 0.0004	-5.45 ± 0.09	TAMU
410.51	90.604	0.51231550 ± 0.0003	-5.53 ± 0.07	TAMU
413.75	90.972	0.51231453 ± 0.0004	-5.55 ± 0.08	TAMU
414.61	94.541	0.51234670 ± 0.0003	-4.89 ± 0.07	TAMU
416.04	95.069	0.51235470 ± 0.0006	-4.73 ± 0.11	TAMU
417.47	95.597	0.51234826 ± 0.0004	-4.85 ± 0.08	TAMU
423.47	97.812	0.51235629 ± 0.0003	-4.68 ± 0.05	TAMU
425.03	98.388	0.51232492 ± 0.0004	-5.28 ± 0.07	TAMU
426.47	98.920	0.51238020 ± 0.0006	-4.20 ± 0.12	TAMU
428.12	99.529	0.51235754 ± 0.0004	-4.64 ± 0.08	TAMU
429.25	99.946	0.51234118 ± 0.0006	-4.95 ± 0.12	TAMU

Table 3-2c. Site 530 Nd data generated for this study. Errors reported are 2σ standard errors. TAMU = Texas A&M University, UNC-CH = University of North Carolina Chapel Hill.

Hole 530A Depth (mbsf)	Age (Ma)	$^{143}Nd/^{144}Nd$	$\varepsilon_{Nd(t)}$	Lab
647.90	68.887	0.51204030 ± 0.0011	-11.08 ± 0.22	TAMU
657.39	69.554	0.51219680 ± 0.0006	-8.02 ± 0.12	TAMU
695.43	72.107	0.51208427 ± 0.0006	-10.20 ± 0.12	TAMU
704.89	72.687	0.51208800 ± 0.0002	-10.12 ± 0.05	TAMU
714.54	73.277	0.51212677 ± 0.0007	-9.36 ± 0.13	TAMU
723.87	73.848	0.51217733 ± 0.0002	-8.37 ± 0.05	TAMU
752.24	75.584	0.51218078 ± 0.0004	-8.29 ± 0.07	TAMU
761.91	77.897	0.51223110 ± 0.0004	-7.29 ± 0.08	TAMU
771.43	76.759	0.51232300 ± 0.0003	-5.50 ± 0.06	TAMU
828.40	80.247	0.51277933 ± 0.0003	3.43 ± 0.06	TAMU
856.75	82.339	0.51254140 ± 0.0003	-1.19 ± 0.06	TAMU
885.30	83.676	0.51248942 ± 0.0003	-2.20 ± 0.06	TAMU
913.29	84.987	0.51227804 ± 0.0004	-6.31 ± 0.07	TAMU
931.30	85.830	0.51220210 ± 0.0004	-7.79 ± 0.08	TAMU
990.25	88.591	0.51225788 ± 0.0006	-6.67 ± 0.12	TAMU

Table 3-2d. Site 690 Nd data generated for this study. Errors reported are 2σ standard errors. TAMU = Texas A&M University, UNC-CH = University of North Carolina Chapel Hill.

Hole 690C Depth (mbsf)	Age (Ma)	$^{143}Nd/^{144}Nd$	$\varepsilon_{Nd(t)}$	Lab
291.00	71.971	0.51210739 ± 0.0003	-9.75 ± 0.06	TAMU
295.50	72.554	0.51210472 ± 0.0004	-9.80 ± 0.09	TAMU
302.10	73.273	0.51210792 ± 0.0006	-9.73 ± 0.12	TAMU
306.60	73.552	0.51208000 ± 0.0004	-10.27 ± 0.08	TAMU
313.30	73.870	0.51208307 ± 0.0006	-10.21 ± 0.12	TAMU
316.30	74.014	0.51208841 ± 0.0004	-10.10 ± 0.09	TAMU

APPENDIX 3

Table 4-2a. Site 763 Nd data generated for this study. Errors reported are 2σ standard errors. TAMU = Texas A&M University, UNC-CH = University of North Carolina Chapel Hill.

Hole 763B Depth (mbsf)	Age (Ma)	$^{143}Nd/^{144}Nd$	$\varepsilon_{Nd(t)}$	Lab
257.43	76.307	0.51202687 ± 0.0003	-11.28 ± 0.07	TAMU
266.71	76.714	0.51204830 ± 0.0006	-10.86 ± 0.12	TAMU
276.66	77.176	0.51208191 ± 0.0003	-10.20 ± 0.06	TAMU
285.80	77.775	0.51210752 ± 0.0004	-9.70 ± 0.07	TAMU
295.37	78.403	0.51213428 ± 0.0003	-9.17 ± 0.05	TAMU
305.32	79.055	0.51218208 ± 0.0009	-8.23 ± 0.18	TAMU
314.66	82.477	0.51220388 ± 0.0003	-7.78 ± 0.06	TAMU
323.92	84.864	0.51220486 ± 0.0006	-7.74 ± 0.12	TAMU
333.67	85.547	0.51220711 ± 0.0005	-7.69 ± 0.11	TAMU
342.43	86.249	0.51219976 ± 0.0003	-7.83 ± 0.06	TAMU
352.37	87.119	0.51216874 ± 0.0003	-8.43 ± 0.07	TAMU
362.74	89.441	0.51223200 ± 0.0003	-7.17 ± 0.05	TAMU
363.99	89.542	0.51219695 ± 0.0004	-7.85 ± 0.09	TAMU
372.26	90.212	0.51212041 ± 0.0005	-9.34 ± 0.09	TAMU
380.18	90.853	0.51205566 ± 0.0004	-10.60 ± 0.08	TAMU
392.66	94.672	0.51205813 ± 0.0004	-10.52 ± 0.07	TAMU
400.16	95.319	0.51202592 ± 0.0007	-11.14 ± 0.13	TAMU
402.82	95.549	0.51203292 ± 0.0003	-11.00 ± 0.07	TAMU
405.37	95.768	0.51205000 ± 0.0003	-10.67 ± 0.07	TAMU

Table 4-2b. Site 765 Nd data generated for this study. Errors reported are 2σ standard errors. TAMU = Texas A&M University, UNC-CH = University of North Carolina Chapel Hill.

Hole 765C Depth (mbsf)	Age (Ma)	$^{143}Nd/^{144}Nd$	$\varepsilon_{Nd(t)}$	Lab
561.55	75.71	0.51207540 ± 0.0008	-10.34 ± 0.16	UNC-CH
561.55	75.71	0.51208540 ± 0.0015	-10.15 ± 0.30	UNC-CH
564.43	77.39	0.51217361 ± 0.0029	-8.41 ± 0.58	TAMU
565.75	78.15	0.51214929 ± 0.0003	-8.88 ± 0.06	TAMU
570.58	81.37	0.51219654 ± 0.0003	-7.93 ± 0.07	TAMU
584.03	91.58	0.51220680 ± 0.0021	-7.65 ± 0.42	UNC-CH
585.37	92.06	0.51222667 ± 0.0005	-7.25 ± 0.10	TAMU
590.70	96.86	0.51216500 ± 0.0018	-8.42 ± 0.36	UNC-CH
592.02	97.21	0.51217550 ± 0.0034	-8.21 ± 0.68	UNC-CH
593.30	97.44	0.51217230 ± 0.0005	-8.27 ± 0.10	TAMU
594.17	98.27	0.51217564 ± 0.0006	-8.20 ± 0.12	TAMU

Table 4-2c. Site 766 Nd data generated for this study. Errors reported are 2σ standard errors. TAMU = Texas A&M University, UNC-CH = University of North Carolina Chapel Hill.

Hole 766A Depth (mbsf)	Age (Ma)	$^{143}Nd/^{144}Nd$	$\varepsilon_{Nd(t)}$	Lab
97.38	72.403	0.51210152 ± 0.0006	-9.86 ± 0.12	TAMU
98.31	72.777	0.51210733 ± 0.0006	-9.74 ± 0.12	TAMU
98.31	72.777	0.51211328 ± 0.0006	-9.63 ± 0.11	TAMU
100.00	73.460	0.51208651 ± 0.0005	-10.14 ± 0.10	TAMU
101.04	73.877	0.51209904 ± 0.0004	-9.90 ± 0.08	TAMU
102.61	74.509	0.51210271 ± 0.0005	-9.82 ± 0.10	TAMU
102.61	74.509	0.51210289 ± 0.0003	-9.82 ± 0.07	TAMU
103.92	75.037	0.51209913 ± 0.0004	-9.88 ± 0.08	TAMU
105.50	75.674	0.51209790 ± 0.0007	-9.90 ± 0.15	TAMU
105.91	75.839	0.51209807 ± 0.0007	-9.90 ± 0.13	TAMU
114.78	83.475	0.51222829 ± 0.0005	-7.29 ± 0.11	TAMU
116.39	84.401	0.51224152 ± 0.0003	-7.03 ± 0.07	TAMU
117.88	85.258	0.51228824 ± 0.0016	-6.11 ± 0.43	TAMU
123.96	87.165	0.51227415 ± 0.0007	-6.37 ± 0.13	TAMU
125.98	88.590	0.51231904 ± 0.0004	-5.48 ± 0.07	TAMU
125.98	88.590	0.51232717 ± 0.0005	-5.32 ± 0.10	TAMU
127.17	89.416	0.51231034 ± 0.0002	-5.64 ± 0.05	TAMU
128.77	90.259	0.51229768 ± 0.0007	-5.88 ± 0.14	TAMU
130.06	90.939	0.51222529 ± 0.0007	-7.29 ± 0.14	TAMU
133.59	92.799	0.51229330 ± 0.0011	-5.95 ± 0.23	TAMU
134.88	93.629	0.51227857 ± 0.0007	-6.23 ± 0.14	TAMU
136.88	95.246	0.51222807 ± 0.0006	-7.20 ± 0.11	TAMU
138.75	96.759	0.51216090 ± 0.0010	-8.50 ± 0.20	UNC-CH
138.75	96.759	0.51216720 ± 0.0005	-8.37 ± 0.09	TAMU
139.55	97.406	0.51217111 ± 0.0006	-8.29 ± 0.12	TAMU
140.96	97.929	0.51216306 ± 0.0007	-8.45 ± 0.14	TAMU
143.38	98.610	0.51217281 ± 0.0005	-8.25 ± 0.10	TAMU
145.38	99.172	0.51219100 ± 0.0017	-7.89 ± 0.34	TAMU
147.04	99.639	0.51219342 ± 0.0009	-7.84 ± 0.17	TAMU
147.70	99.824	0.51217988 ± 0.0007	-8.10 ± 0.14	TAMU
149.77	100.406	0.51214100 ± 0.0006	-8.86 ± 0.11	TAMU
150.63	100.648	0.51217555 ± 0.0006	-8.18 ± 0.11	TAMU

VITA

Daniel Patrick Murphy received his Bachelor of Science degree in Marine Biology from Hawai'i Pacific University in 2002. After a one-year stint substitute teaching high school, he attended the University of California at Santa Barbara, from which he earned his Master of Science degree in March 2006. From there, he traveled east to the Department of Oceanography at Texas A&M University and received his Doctor of Philosophy in Oceanography in May 2010. His research interests include changes in ocean circulation in the geologic past, controls on pelagic sedimentation, abrupt climate change, and the role of greenhouse gases in the past ~3 million years.

Dr. Murphy can be reached at: Department of Oceanography, Texas A&M University, 3146 TAMU, College Station, TX 77843-3146 or via email at: dmurphy@neo.tamu.edu.